Dear Participants
of 16th Conference: INTEGRATED OPTICS - Sensors, Sensing Structures and Methods, IOS'2022

Organizers welcome All of You very cordially in Szczyrk, in the beautiful scenery of the Beskidy Mountains.

We wish all Participants of the Conference IOS'2022 plenty of scientific satisfactions and many professional and social impressions.

Organizers

President of the Conference:	Prof. T. Pustelny
Secretary of the Conference:	Dr S. Drewniak
Treasurer of the Conference:	Dr A. Olszewska
Members:	Dr hab. P. Struk
	Dr B. Pustelny
	Dr M. Procek
	Dr hab. K. Barczak

This book includes the Program of IOS'2022 and Abstracts of presentations and posters sent by their Authors

PROGRAMME
of the *IOS'2022 Conference -*
Integrated Optics - Sensors, Sensing Structures and Methods
Szczyrk, 28 February – 04 March 2022

28.02.2022 Monday	
14.00	***Lunch***
16.00-16.10	**OPENING CEREMONY of the Conferences** **50th Jubilee WSW&QA** **49th WSEA&V** **16th IOS'2022**
16.10-16.45	**Jubilee Session**
16.10-16.30	*Plenary lecture:* **The Golden Jubilee of the 50th WINTER SCHOOL ON WAVE AND QUANTUM ACOUSTICS - historical reminiscences** T. PUSTELNY, R. BUKOWSKI
16.30-16.35	*Address by the Chairman of the Honorary Committee:* A.ŚLIWIŃSKI, (online)
16.35-16.45	*Other speeches*
16.45-17.30	***Coffee Break***
17.30-18.15	**"ALTRA VOLTA" - MUSIC GLANCE**
18.30	***Supper***
20.00	**50 YEARS HAVE GONE BY - AN EVENING OF REMEMBRANCE** 50 LAT MINĘŁO…- WIECZÓR WSPOMNIEŃ

01.03.2022 Tuesday	
8.00	***Breakfast***
13.00	***Lunch***
14.00 – 14.30	*Plenary lecture:* **Actphast4R and PhotonHub Europe the efficient mechanisms for deep technology support in photonics** M. KUJAWIŃSKA
14.30 – 18.20	**High Technologies for Photonics - IMiO, CEZAMATand VIGO alliance Session**
14.30 – 15.00	**Integrated photonics – present capabilities and future challenges** R. PIRAMIDOWICZ, S. STOPIŃSKI, K. ANDERS, A. JUSZA, M. SŁOWIKOWSKI, A. PAŚNIKOWSKA, M. LELIT, A. POŁATYŃSKI, A. KAŹMIERCZAK, M. A. BUTT
15.00 – 15.20	**Spatial division multiplexing fiber optic systems – key components and performance parameters** K.ANDERS, A. PAŚNIKOWSKA P. BORTNOWSKI S. STOPIŃSKI, M. SŁOWIKOWSKI, P.MAZUREK, J.P. TURKIEWICZ, P. MERGO, K. MARKIEWICZ, M. NAPIERAŁA, T. NASIŁOWSKI, R. PIRAMIDOWICZ
15.20 – 15.40	**Silica-Titania Integrated Photonic Structures for Multiparameter Sensors Applications** M. A. BUTT, A. KAŹMIERCZAK, A. JUSZA, C. TYSZKIEWICZ, P. KARASIŃSKI, R. PIRAMIDOWICZ
15.40 – 16.00	**Integrated multi-channel transmitters for WDM-PON systems – design and development** A. PAŚNIKOWSKA, S. STOPIŃSKI, A. KAŹMIERCZAK, R. PIRAMIDOWICZ
16.00 – 16.15	**Miniature mid-IR spectrometer – concept, implementation and perspectives** F. ŁABAJ, J. KALWAS, A. GÓRSKI, P. LESZCZ, R. PIRAMIDOWICZ
16.15 – 16.30	**Single-frequency integrated ring lasers with hybrid intra-cavity wavelength filtering** S. STOPIŃSKI, R. PIRAMIDOWICZ
16.30 – 17.00	***Coffee Break***

01.03.2022 Tuesday	
17.00 – 17.20	**Non-invasive patient's breath monitoring during MRI diagnosis with the use of integrated photonic interrogator** M. SŁOWIKOWSKI, A. KAŹMIERCZAK, M. BIENIEK, S. SZOSTAK, S. STOPIŃSKI, R. PIRAMIDOWICZ
17.20 – 17.40	**Advances in development of SiN-based integrated photonic platform for visible spectral range** M. LELIT, M. SŁOWIKOWSKI, M. GOLAS, M. FILIPIAK, M. JUCHNIEWICZ, B. STONIO, B. MICHALAK, K. PAVŁOV, M. MYŚLIWIEC, P. WIŚNIEWSKI, A. KAŹMIERCZAK, K. ANDERS, S. STOPIŃSKI, R. B. BECK, R. PIRAMIDOWICZ
17.40 – 18.00	**Grey-tone mask aligner lithography optimization for micro-optics applications** K. PAVŁOV, M. FILIPIAK, M. JUCHNIEWICZ, B. MICHALAK, M. MYŚLIWIEC, M. SŁOWIKOWSKI, B. STONIO, P. WIŚNIEWSKI, R. BECK
18.00 – 18.20	**Thermal reflow study in fabrication of microlens array** M. FILIPIAK, M. MYŚLIWIEC, M. SŁOWIKOWSKI
18.20 – 19.00	**Optical Coherence Tomography Session**
18.20 – 18.40	**Mathematical Aspects of Backscattering Cross-Section Estimation of Nanoparticles by Optical Coherence Tomography** J. PLUCIŃSKI, M. R. STRĄKOWSKI
18.40 – 19.00	**The optical coherence tomography for thin-film profiling enhanced by spectroscopic analysis** M. R. STRĄKOWSKI, J. PLUCIŃSKI, A. M. KAMIŃSKA, P. STRĄKOWSKA
20.00	***Festive Supper (Banquet)*** ***in the initial part, the performance of the jazz band "CSW Trio"***

02.03.2022 Wednesday	
8.00	***Breakfast***
13.00	***Lunch***
14.00 – 18.20	**National Laboratory for Photonics and Quantum Technologies NLPQT Session**
14.00 – 14.20	**NLPQT – concept and general information** C. RADZEWICZ
14.20 – 14.40	**Ultrastable frequency for metrology network in Poland** M. BOBER, K. TURZA, A. BINCZEWSKI, W. BOGACKI, Ł. ŚLIWCZYŃSKI, P. KREHLIK, M. NAROŻNIK M. ZAWADA
14.40 – 15.00	**Accurate metrology of simple molecules for studying fundamental physics** P. WCISŁO
15.00 – 15.20	**Dual-comb generation in a single laser cavity for sensing applications** Ł. A. STERCZEWSKI, M. KOWALCZYK, J. SOTOR
15.20 – 15.40	**Large-area plasmonic nanostructures for SERS applications** M. SUSTER, A.SZYMAŃSKA, A. KRÓLIKOWSKA, P. WRÓBEL
15.40 – 16.00	**Possibilities of using optical fibers sensors in climate change** A. PAŹDZIOR
16.00 – 16.15	**Photonic sensing of gases and volatiles needs, technologies and solutions for science and business** K. BARCZAK, E. MACIAK
16.15 – 16.30	**Novel ultrafast dynamics of double-frequency breathing-like dissipative solitons** K. KRUPA, T. M. KARDAS, Y. STEPANENKO
16.30 – 17.00	***Coffee Break***

02.03.2022 Wednesday	
17.00 -17.20	**Ultrafast fiber lasers for ophthalmic imaging applications** J. BOGUSŁAWSKI, D. STACHOWIAK, Z. ŁASZCZYCH, A. HUDZIKOWSKI, A. GŁUSZEK, M. WOJTKOWSKI, G. SOBOŃ
17.20 – 17.40	**Correlation of human two photon vision and optical coherence tomography imaging for in vivo identification of retinal layer containing photopigments** I. GORCZYŃSKA, M.M. BARTUZEL, P. STREMPLEWSKI, A. CONSEJO, M. SYLWESTRZAK
17.40 – 18.00	**Towards two-photon bio-imaging with GRIN lenses and image guide** P. SZCZYPKOWSKI
18.00 – 18.20	**Towards on-chip multidimensional quantum key distribution** M. KARPIŃSKI
18.20 – 19.00	**Quantum Cryptography Session**
18.20 – 18.40	**Quantum Hacking in the Age of Quantum Cryptography – practical issues** M.ŻYCZKOWSKI, P. MARKOWSKI
18.40 – 19.00	**Automatic detection of defects in composite structures by the TDS method** K. KAMIŃSKI, N. PAŁKA, P. SYNASZKO, E. CZERWIŃSKA, K. DRAGAN
19.00	***Supper***
20.00	**Poster Session**

03.03.2022 Thursday	
8.00	***Breakfast***
13.00	***Lunch***
13.30 – 13.50	*Plenary lecture* **The trials of digital data improvement continuously recording by rotational seismometer** L. R. JAROSZEWICZ
13.50 – 15.50	**Detection of quantum effects in glass – diamond photonic systems QUNNA Session**
13.50 – 14.10	**Nanodiamonds for sensing of magnetic fields, and more…** A.M. WOJCIECHOWSKI, M. MRÓZEK, M. JANI, T. KOŁODZIEJ, A. EBRAHIMI, S. SENGOTTUVEL, P. CZARNECKA, Z. ORZECHOWSKA, W. GAWLIK
14.10 – 14.30	**Opto-magnetic fiber probes and magnetic field sensing based on negatively charged nitrogen-vacancy centers in nanodiamonds** A. FILIPKOWSKI, M. MRÓZEK, G. STĘPNIEWSKI, T. KARPATE, M. GŁOWACKI, M. FICEK, W. GAWLIK, R. BUCZYŃSKI, A. WOJCIECHOWSKI, R. BOGDANOWICZ, M. KLIMCZAK
14.30 – 14.50	**Implementation of nanodiamonds to enhance the sensing properties of fiber optic sensors** M. JANIK, M. FICEK, M. SAWCZAK, M. ŚMIETANA, R. BOGDANOWICZ
14.50 – 15.10	**Silicon nitride as a new mirror in fiber optic sensors** S. PAWŁOWSKA
15.10 – 15.30	**Boron-doped carbon nanowalls for sensing application** M. FICEK, K.J. SANKARAN, P. NIEDZIAŁKOWSKI, M. PIERPAOLI, P. JAKÓBCZYK, R. BOGDANOWICZ
15.30 – 15.50	**High-performance optical frequency comb sources** A. M. HEIDT, P. HÄNZI, B. SIERRO, D. SPANGENBERG, A. RAMPUR
15.50 – 16.10	*Plenary lecture* **Optical beaming of electrical discharges** W. KRÓLIKOWSKI
16.10 – 19.00	**Photonic Structures**
16.10 – 16.30	**Machine learning for resolution increase of refractive index measurements** M. SZCZERSKA, P. RUDNICKI, M. KOSOWSKA, A. DRABIK-KRUCZKOWSKA, M. KRUCZKOWSKI
16.30 – 17.00	***Coffee Break***

03.03.2022 Thursday	
17.00 – 17.20	**Electrically-driven LC PDMS microstructures for integrated optics applications** K.A. RUTKOWSKA, P. SOBOTKA, SZ. BACZYŃSKI, M. GROM, A. DYBKO, K. MARCHLEWICZ, M. JUCHNIEWICZ
17.20 – 17.40	**Optimizing up-conversion emission in the fluoroindate glasses for biomedical applications** G. L. JIMÉNEZ, B. STARZYK, M. LESNIAK, M. KOCHANOWICZ, D. DOROSZ
17.40 – 18.00	**Nanocomposite glasses and optical fibers for optical sensing applications** K.CZAJKOWSKI, K. SADOWSKA, M. LEŚNIAK, D. DOROSZ, J. DOROSZ, M.KOCHANOWICZ, P. MILUSKI, J. ŻMOJDA
18.00 – 18.15	**Investigation of the luminescent properties of nanophosphors co-doped with lanthanide ions for biological sensing** K. SADOWSKA, P. AWRAMIUK, K. GRYKO, M. KALINOWSKA, J. ŻMOJDA
18.15 – 18.30	**Polarization maintaining nanostructured single-mode optical fiber with artificial anisotropy** A. ANUSZKIEWICZ, M. BOUET, D. MICHALIK, G. STEPNIEWSKI, R. KASZTELANIC, A. FILIPKOWSKI, D. PYSZ, A. CASSEZ, M. KLIMCZAK, G. BOUWMANS, A. MUSSOT, R. BUCZYNSKI
18.30 – 18.45	**Nanostructured few-mode fiber for mode-division-multiplexed systems** R.KASZTELANIC, D. MICHALIK, A. ANUSZKIEWICZ, R. BUCZYŃSKI
18.45 – 19.00	**Light depolarization by dual-frequency nematic liquid crystals** P. MARĆ, N. BENNIS, A. PAKUŁA, E. PAWLIKOWSKA, A.SPADŁO, K. GARBAT, R. WĘGŁOWSKI, L. R. JAROSZEWICZ
19.00	***Supper***

03.03.2022 Thursday	
20.00 – 21.00	**Optoelectronic Engineering**
20.00 – 20.15	**The SS-OCT imaging probe based on MOEMS/MEMS Mirau micro-interferometer and 2-axis electrothermal microscanner for endomicroscopic application** P. STRUK, S. BARGIEL, B. MIRECKI, M. JÓŹWIK, Q. TANGUY, R. CHUTANI, N. PASSILLY, P. LUT, H. XIE3, F. E. GRACIA-RAMIREZ, M. WOJTKOWSKI, C. GORECKI
20.15 – 20.30	**Rib waveguide homogeneous sensitivity with regard to single mode propagation conditio** C. TYSZKIEWICZ, A. KAŻMIERCZAK, M.A. BUTT, P. KARASIŃSKI
20.30 – 20.45	**Measurements of the spectral interferogram for single-mode waveguide layers** K. GUT
20.45 – 21.00	**PPB-level NO_2 concentrations sensing by nanostructured ZnO – graft copolymer composites** P. KAŁUŻYNSKI, M. PROCEK, A. STOLARCZYK, T. JAROSZ, E. MACIAK
21.00	**Closing of the IOS'2022 Conference**

04.03.2022 Friday	
8.00	***Breakfast***

POSTERS

1. Nonlinearity enhancement in thermally poled glasses with high alkali content
A. ANUSZKIEWICZ, A. FILIPKOWSKI, R. KASZTELANIC, D. PYSZ, R. STĘPIEŃ, R. BUCZYNSKI

2. Optoelectronic system for detecting short-circuits in low voltage networks
K. BARCZAK, J. JURASZEK

3. Compact Optical Gyroscope for Aerospace Applications
S.BILICKI, D. BRAUDA, A.LEDZIŃSKI,W. LEWOCZKO-ADAMCZYK, S. LENZKY, S. MARX, J. NAWROCKI, P. NOGAŚ, R. URBANIAK, H. SCHROEDER

4. Numerical analysis of the broadband interferometric sensor in the planar gradient-step index configuration
M. BŁAHUT

5. Highly birefringent large mode area fibers with artificially anisotropic silica glass core
R. BUCZYNSKI, D. MICHALIK, A. ANUSZKIEWICZ, A. FILIPKOWSKI, G. STĘPNIEWSKI, D. PYSZ, K. HARAŚNY, I. KUJAWA, R. KASZTELANIC

6. Spectral properties of photonic crystal fibers infiltrated with ferroelectric liquid crystals doped with nanoparticles
D. BUDASZEWSKI, D.P. SINGH, T.R. WOLIŃSKI

7. Photopolymerization of AuNP-doped liquid crystals
M.S. CHYCHŁOWSKI, M. KAJKOWSKA, P. LESIAK, T.R. WOLIŃSKI

8. Statistical analysis of Raman spectra of reduced graphene oxide obtained using various graphite precursor and various oxidation method
Ł. DREWNIAK, S. DREWNIAK, M. SAJDAK, R. MUZYKA

9. The influence of the graphite precursor and the oxidation method on the number of graphene layers in reduced graphene oxide- statistical approach
S. DREWNIAK, Ł. DREWNIAK, M. SAJDAK, R. MUZYKA

10. Simulations of micromachined side-hole optical fiber for refractive index sensing based on optical losses
M. DUDEK, K. KÖLLŐ, P. MARĆ, L. R. JAROSZEWICZ

11. Laser stabilization using acousto-optic modulator for ion cooling purpose in ion trap based quantum computer – basic setup examination
SZ. FIDERKIEWICZ, M. ŻYCZKOWSKI

12. Variability of fluorescence of nitrogen-vacancy centers in nanodiamonds
M. J. GŁOWACKI, M. FICEK, M. SAWCZAK, R. BOGDANOWICZ

13. Numerical analysis of silicon nitride planar Bragg gratings
M. GOLAS, M. LELIT, M. SŁOWIKOWSKI, K. PAVŁOV, B. STONIO, M. FILIPIAK, M. JUCHNIEWICZ, P. WIŚNIEWSKI, R.B. BECK

14. Fabrication of nonlinear chirped fiber Bragg gratings
A. GOLESTANI, R. H.S. BANNERMAN, J. C. GATES, P. G. R. SMITH, M. KARPIŃSKI

15. Luminescent temperature sensor based on glass and glass-ceramic optical fiber
P. GOLONKO, J. ŻMOJDA

16. High-efficiency transmission gratings obtained using azobenzene poly(etherimide) and holographic method
A. HERNIK, D. SZMIGIEL, J. KONIECZKOWSKA, E. SCHAB-BALCERZAK, A. KOZANECKA-SZMIGIEL

17. Magnetically-sensitive nanodiamond thin-films on glass fibers
M. JANI, P. CZARNECKA, S. SENGOTTUVEL, M. MRÓZEK, P. DĄBCZYŃSKI, A. FILIPKOWSKI, I. KUJAWA, D. PYSZ, W. GAWLIK, A. M. WOJCIECHOWSKI

18. Broadband eye-safe emission in germanate double-core optical fiber
M. KOCHANOWICZ, K. SADOWSKA, J. ŻMOJDA, P. MILUSKI, A. BARANOWSKA, T. RAGIN, M. KUWIK, W. A. PISARSKI, J. PISARSKA, M. LEŚNIAK, J. DOROSZ, D. DOROSZ

19. A novel non-pathogenic method for testing virus filtration ability of protective masks using the fluorescence phenomenon
D. KOGUT, P. KAŁUŻYNSKI, M. SKONIECZNA, I. ŚLĘZAK-PROCHAZKA, A. KAZEK-KĘSIK

20. Thermal properties of polymers containing QD CdSe produced in high and low boiling organic solvents
A. KICZOR, P. MERGO

21. Analysis of planar waveguides with a high index overlayer and nonlinear cladding
J. M. KUBICA

22. Growth of B/N co-doped CVD grown homoepitaxial diamond films: optical and electrical properties
S. KUNUKU, M. FICEK, A. WIELOSZYNSKA, M. TAMULEWICZ-SZWAJKOWSKA, K. GAJEWSKI, M. SAWCZAK, A. LEWKOWICZ, J. RYL, T. GOTSZALK, R. BOGDANOWICZ

23. A historical perspective of the fibre-optic seismographs and their field application: the past, present and exciting future
A.T. KURZYCH, L.R. JAROSZEWICZ, M. DUDEK, P. MARĆ, J.K. KOWALSKI

24. 3D-printed mechanical transmission element with a Fiber Bragg Grating sensor in a replaceable measuring head
P. LESIAK, K. POGORZELEC, A. BOCHENEK, P. SOBOTKA, K. BEDNARSKA, A. ANUSZKIEWICZ, T. OSUCH, M. SIENKIEWICZ, P. MAREK, T. WOLIŃSKI

25. Microsphere-based fiber-optic temperature sensor for galvanic electric cells
P. LISTEWNIK

26. Type – II superlattice interband quantum cascade detectors - future higher operating temperature sensors
P. MARTYNIUK

27. Thermo-optical properties of hybrid structure based on tapered optical fiber and mixture of alkanes with nanoparticles of ZnS:Mn
J. E. MOŚ, K. A. STASIEWICZ, L. R. JAROSZEWICZ

28. Monocrystalline free-standing blue phase crystals for photonic applications
E. OTÓN-MARTINEZ, W. PIECEK, P. MORAWIAK, M. MUSZYŃSKI, J. SZCZYTKO

29. Long-range swept-source optical coherence system for in-vivo assessment of intraocular scattering
S. PANEZAI, A. GUPTA, A. JIMENEZ-VILLAR, E. MĄCZYŃSKA-WALKOWIAK, G. GONDEK, D. RUMIŃSKI, I. GRULKOWSKI

30. Monitoring the polarization state in a phase-modulated QKD system to protect against eavesdropping.
E. PAWLIKOWSKA, M. ŻYCZKOWSKI

31. Sensor probes for distributed measurement of temperature profile in soils
A. PAŹDZIOR, J. KOPEĆ, P. MERGO

32. Ultrafast all-polarization-maintaining Yb-doped fiber laser oscillator working at negative net cavity dispersion
M. PIELACH, A. JAMROZIK, J. SZCZEPANEK, K. KRUPA, Y. STEPANENKO

33. Evaluation of eye accommodation distance in a two-track optical system using a vision-based method
M. PISZCZEK, A. KUCHARCZYK, K. SUCHECKI, M. MACIEJEWSKI, M. POMIANEK, L. JODŁOWSKI, P. KRUKOWSKI

34. Implementation of basic refractive defects into the optoelectronic eye
M. PISZCZEK, A. KUCHARCZYK, K. SUCHECKI, M. MACIEJEWSKI, M. POMIANEK, L. JODŁOWSKI, P. KRUKOWSKI

35. Field-of-view correction in a VR HMD display with varifocal optics
M. PISZCZEK, K. SUCHECKI, A. KUCHARCZYK, M. POMIANEK,
M. MACIEJEWSKI, L. JODŁOWSKI, P. KRUKOWSKI

36. Room temperature hydrogen sensor based on electropolymerized polycarbazole layers on platinum electrodes
M. PROCEK, K. GŁOSZ, A. STOLARCZYK, T.JAROSZ

37. The simulation insight into properties of modified nanodiamonds surfaces
K. PYRCHLA

38. Wide-field vector magnetometry using nitrogen-vacancy centers in arbitrarily oriented diamond crystals
S. SENGOTTUVEL, M. MRÓZEK, M. SAWCZAK, M. GŁOWACKI, M FICEK,
W. GAWLIK, A. WOJCIECHOWSKI

39. Er-doped fluoroindate glasses for sensing applications
B. STARZYK, G. L. JIMÉNEZ, M. LEŚNIAK, M. KOCHANOWICZ, M. KUWIK, J. ŻMOJDA, P. MILUSKI, A. BARANOWSKA, J. DOROSZ, W. PISARSKI,
J. PISARSKA, D. DOROSZ

40. Measuring the refractive index of egg white and yolk according to temperature: a preliminary study
P.SOKOŁOWSKI

41. SPR effect controlled by electric field in the optical fiber device with low refractive index nematic liquid crystal
K. A. STASIEWICZ, J. KOREC, K. GARBAT, L. R. JAROSZEWICZ

42. Reduction of nonlinearities by nanodiamond incorporation into glass
G. STĘPNIEWSKI, M. KLIMCZAK, T. KARPATE, M. FICEK, M. GŁOWACKI,
A. HEIDT, R. BOGDANOWICZ, R. BUCZYŃSKI

43. Integrated photonics structure for sensor applications
P. STRUK

44. ZnO thin films prepared by sol-gel method and dip-coating technique - optical properties
K. WOJTASIK, M. ZIĘBA, C. TYSZKIEWICZ, P. KARASIŃSKI

45. Time-resolved spectroscopy of nitrogen implanted GaAs
G.WRZESINSKI, K. SWITKOWSKI

46. Optical properties of erbium-doped TiO_2 films
M.ZIĘBA, K. WOJTASIK, C.TYSZKIEWICZ, P.KARASIŃSKI

LECTURES

Integrated photonics – present capabilities and future challenges

R. PIRAMIDOWICZ[1,3], S. STOPIŃSKI[1,3], K. ANDERS[1,3], A. JUSZA[1], M. SŁOWIKOWSKI[1,2], A. PAŚNIKOWSKA[1], M. LELIT[1,2], A. POŁATYŃSKI[1], A. KAŹMIERCZAK[1], M. A. BUTT[1]

[1]Warsaw University of Technology, Institute of Microelectronics and Optoelectronics, Koszykowa 75, 00-662 Warsaw, Poland
[2]Warsaw University of Technology, Centre for Advanced Materials and Technologies, CEZAMAT, Poleczki 19, 02-822 Warsaw, Poland
[3]VIGO Photonics, Poznańska 129/133, 05-850 Ożarów Mazowiecki
e-mail address: ryszard.piramidowicz@pw.edu.pl

The contemporary world is, in an obvious way, shaped by and heavily dependent on integrated electronic technologies. Microprocessors of various kinds have become omnipresent in our nearest neighborhood, assisting practically every aspect of human activity – communicating, learning, working, shopping, entertaining, exercising, health monitoring etc. Since the beginning of the XXI century, integrated electronic solutions started to be complemented with their counterparts operating in the optical domain – photonic integrated circuits (PICs). Nowadays, these are playing an increasingly important role in an impressively wide application area, covering telecommunication, datacom, sensing, medicine, environmental protection, agriculture, automotive and many others.

In this work, the fundamental issues and the most significant achievements of contemporary integrated photonics will be discussed, with specific emphasis on the Polish perspective and national potential in the field. An overview of the

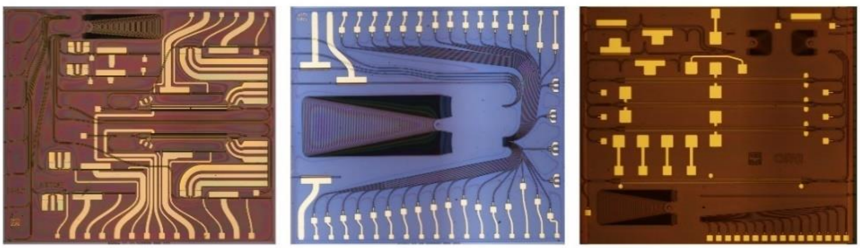

Fig. 1. Microscope pictures of ASPICs developed at WUT (from the left side): a multi-channel transmitter for a WDM-PON system; an integrated interrogator of fiber Bragg gratings; a multi-channel transmitter for hybrid integration with an electronic integrated circuit.

state-of-the-art technologies will be presented with a particular focus on the most promising and sufficiently mature platforms (silicon and silicon-based, indium phosphide), followed by the introduction to the generic concept and analysis of the main application fields of PIC-based devices and systems. These will be illustrated by emerging and commercially available solutions, and application-specific photonic integrated circuits (ASPICs), designed and developed by the research team of Warsaw University of Technology (Fig. 1). The major factors limiting progress in technology development will be discussed together with the perspectives and challenges faced by integrated photonics.

Finally, a new photonic integration platform that is currently being developed in Poland will be announced. It is tailored for operation in the midIR spectral range. The potential applications will be discussed, and the first technological results will be presented.

Acknowledgments:
This work has received support from the National Centre for Research and Development through projects MIRPIC (TECHMATSTRATEG-III/0026/2019-00), NIPPON (PBS3/A3/21/2015), OPTO-SPARE (PBS3/B9/41/2015), and NMKM+ (TECHMATSTRATEG/1348438/ 16/NCBR/2018).

Spatial division multiplexing fiber optic systems – key components and performance parameters

K.ANDERS[1], A. PAŚNIKOWSKA[1], P. BORTNOWSKI[1], S. STOPIŃSKI[1], M. SŁOWIKOWSKI[1,2], P.MAZUREK[3], J.P. TURKIEWICZ[3], P. MERGO[4], K. MARKIEWICZ[5], M. NAPIERAŁA[5], T. NASIŁOWSKI[5], R. PIRAMIDOWICZ[1]

[1]Warsaw University of Technology, Institute of Microelectronics and Optoelectronics, Koszykowa 75, 00-662 Warsaw, Poland
[2]Warsaw University of Technology, Centre for Advanced Materials and Technologies, CEZAMAT, Poleczki 19, 02-822 Warsaw, Poland
[3]Warsaw University of Technology, Institute of Telecommunications, Nowowiejska 15/19, 00-665 Warsaw, Poland
[4]Maria Curie-Skłodowska University, Faculty of Chemistry, Marii Curie-Skłodowskiej Sq. 3, 20-031 Lublin, Poland
[5]InPhoTech sp. z o.o. , Poznańska 400, 05-850 Ołtarzew, Poland
e-mail address: krzysztof.anders@pw.edu.pl

Along with the growing demand for the bandwidth of the optical network, caused, among others, by remote learning, high-definition VOD services, cloud gaming etc., the communication infrastructure reaches the limits of its capacity. The most natural solution – simply multiplying the number of fiber optic cables – is inefficient in terms of costs and workload required. Therefore, the alternative methods, enabling more efficient utilization of the existing infrastructure or deployment of transmission media of significantly higher data capacity, are a subject of intensive research. One of the promising methods to increase the information capacity of a single optical fiber is to use Space Division Mulitiplexing (SDM) technique. Two main approaches dominate among SDM solutions – the use of multicore fiber (MCF) or transmission on multiple modes in a few-mode optical fiber (FMF).

In this work, we demonstrate the results of research and development works on the key components of the system for data transmission with the use of FMFs. In particular, both passive and active few-mode fibers and (de)multiplexing elements have been developed and carefully characterized with respect to their transmission properties. Moreover, the photonic integrated transmitter dedicated to FMF-based optical networks, which allows transmission on different modes using a single wavelength has been designed, manufactured in a generic InP technology, and characterized with respect to its applicability in the FMF system.

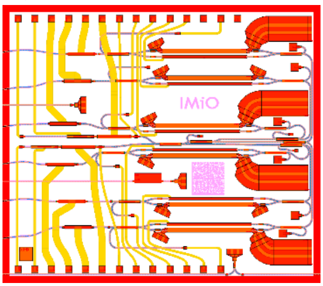

Fig. 1. The topography of the PIC for FMF-based optical networks

Acknowledgments: This work has received support from the National Centre for Research and Development through project NMKM+ (TECHMATSTRATEG1/ /348438/16/NCBR/2018)

Silica-Titania Integrated Photonic Structures for Multiparameter Sensors Applications

M. A. BUTT[1], A. KAŹMIERCZAK[1], A. JUSZA[1], C. TYSZKIEWICZ[2], P. KARASIŃSKI[2], R. PIRAMIDOWICZ[1,3],

[1] Warsaw University of Technology, Institute of Microelectronics and Optoelectronics, Koszykowa 75, 00-662 Warszawa, Poland
[2] Silesian University of Technology, Department of Optoelectronics, Krzywoustego 2, 44-100 Gliwice, Poland
[3] VIGO Photonics, ul. Poznańska 129/133, 05-850, Ożarów Mazowiecki
e-mail address: ali.butt@pw.edu.pl

In two recent decades, the tremendous development of Photonic Integrated Circuits (PICs) has been observed. These waveguide-based structures incorporating several optical functionalities in a single photonic chip (analogous to the electronic ICs) have been developed by numerous research centers worldwide. Three PIC technologies have eventually reached technological maturity and have formed the mainstream, namely: indium phosphide (InP), silicon-on-insulator (SOI), and silicon nitride (SiN). Each of these technologies has its fundamental advantages, including the possibility of direct integration of active optoelectronic components (InP), very dense component integration (SOI), or availability of operation not only in typical near-infrared (NIR) range but also in visible (VIS) one (SiN). Unfortunately, the PICs fabrication using the above-mentioned technologies is complex and requires sophisticated equipment for gaseous phase film deposition waveguides, electron-beam or deep UV lithography, and plasma etching. Consequently, it is difficult for small and medium enterprises (SMEs) or research centers to adopt these technologies. Therefore, only a few of them can afford to have these technologies in-house.

To overcome this limit, an alternative, less equipment-demanding PIC technology would be necessary. The development of such alternative technology is the primary goal of the HYPHA project funded by the Foundation for Polish Science in the framework of the Team-NET program. The project consortium (PORT Wroclaw research center, Silesian Univ. of Technology, Wroclaw Univ. of Technology Warsaw Univ. of Technology) aims to develop SiO_2:TiO_2 sol-gel derived waveguides technology. This should eventually lead to establishing a substitute for PIC mainstream technologies in some niche applications. The concept originates from sol-gel derived waveguide films technology, the group of prof. Karasiński has mastered [1]. The project aims to develop efficient patterning technology and, if possible, reduce the number of necessary fabrication steps (e.g., replacing a classical lithography & etching process in single-step direct nanoimprint). Further, the consortium has the ambition to develop a database of waveguide components that could be used as generic building blocks for developing more sophisticated PICs. Keeping in mind the beneficial properties of SiO_2:TiO_2 waveguides, including the possibility of operating in both VIS and NIR wavelength range and high chemical durability, this technology seems to be an excellent candidate for sensor applications.

In this work, we present and discuss the results of designing the optical resonator structures for sensing applications. For this purpose, waveguide structures, including optical ring resonators [2] and photonic crystal cavities, have been proposed, illustrated in Fig. 1.

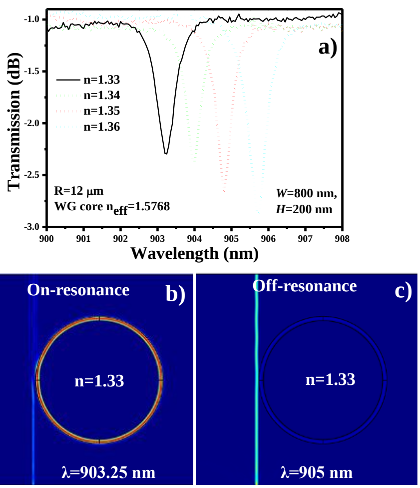

Fig. 1. a) Transmission spectrum of ring resonator in the presence of different ambient refractive indices, b) On-resonance state at λ=903.25 nm, c) Off-resonance state at λ=905 nm.

Fig. 1a shows an exemplary illustration of the numerical simulations of the optical ring resonator and the shift of its transmission spectrum due to ambient refractive index (RI) variation. Moreover, the E-field distribution at the on-resonance and off-resonance states are also shown in fig. 1b and fig.1 c, respectively.

A ring resonator for refractive index sensing application offers sensitivity in the range of 82 nm/RIU to 232 nm/RIU, based on the geometric parameters of the waveguide.

Further work on optimizing the proposed design taking into account the latest consortium achievements on waveguide patterning technology, is still ongoing. Our ambition is to develop a fully operational demonstrator of a multichannel optical sensor system by the end of the project.

Acknowledgments: The work was funded with the project "Hybrid sensor platforms of integrated photonic systems based on ceramic and polymer materials" carried out within the TEAM-NET program of the Foundation for Polish Science financed by the European Union under the European Regional Development Fund, POIR.04.04.00-00-14D6/18-01.

References:

[1] P. Karasiński, A. Kaźmierczak, M. Zięba, C. Tyszkiewicz, K. Wojtasik, P. Kielan, “Highly Sensitive Sensor Structure Based on Sol-Gel Waveguide Films and Grating Couplers”, Electronics 21, 1389, 2021

[2] M. A. Butt, A. Kaźmierczak, C. Tyszkiewicz, P. Karasiński, R. Piramidowicz, “Mode sensitivity exploration of silica-titania waveguide for refractive index sensing applications”, Sensors 21, 7452, 2021.

Integrated multi-channel transmitters for WDM-PON systems – design and development

A. PAŚNIKOWSKA[1], S. STOPIŃSKI[1,2], A. KAŹMIERCZAK[1]
AND R. PIRAMIDOWICZ[1,2]

[1]Warsaw University of Technology, Institute of Microelectronics and Optoelectronics, Koszykowa 75, 00-662 Warszawa, Poland
2VIGO Photonics, Poznańska 129/133, 05-850 Ożarów Mazowiecki
e-mail address: aleksandra.pasnikowska@pw.edu.pl

In the last two decades, technologies of optical communication systems have developed tremendously. This significant progress was possible thanks to the positive feedback between the increasing availability of technical resources, e.g., rapid progress in fiber-optic elements and semiconductor light sources technology, and constantly increasing clients' demands. Recently, the latter effect has been even more boosted due to the COVID-19 pandemic and the disrupting need for broadband services enabling efficient remote work. One of the possible ways to provide sufficient bandwidth to multiple users in access networks is Wavelength Division Multiplexing-Passive Optical Network (WDM-PON) technology. In its basic form, an access system based on PON technology consists of an optical line terminal (OLT) unit at the central office and multiple optical network units (ONUs) at local premises. The WDM-PON extends the potential of the PON system by providing a multi-channel operation and, therefore, a significant increase of the bandwidth. In a natural way, WDM-PON can find application in optical data networks and 5G communication systems thanks to possible low cost, simple operation, and optical transparency. One of the very promising implementations of WDM-PON is the use of photonic integrated circuits (PICs) to exploit their advantages such as compactness, durability, and reliability, combined with relatively low cost of mass production.

In this work, we summarize our research on multi-channel integrated transmitters for application in access networks and datacom systems. Two variants of the transmitters were developed for operation in the C and L bands, differing in the design and manufactured in two different integrated photonic foundries. The circuits use DBR lasers as CW light sources combined with external Mach-Zehnder or electro-absorption modulators. An 8×8 arrayed waveguide grating (AWG) was used as the output multiplexer. The cyclic configuration of the AWG provides redundancy minimizing the risk of potential misalignment of the wavelengths of the signals generated by the lasers with the multiplexer passband, which was an effect observed and discussed in our previous works [1–3].

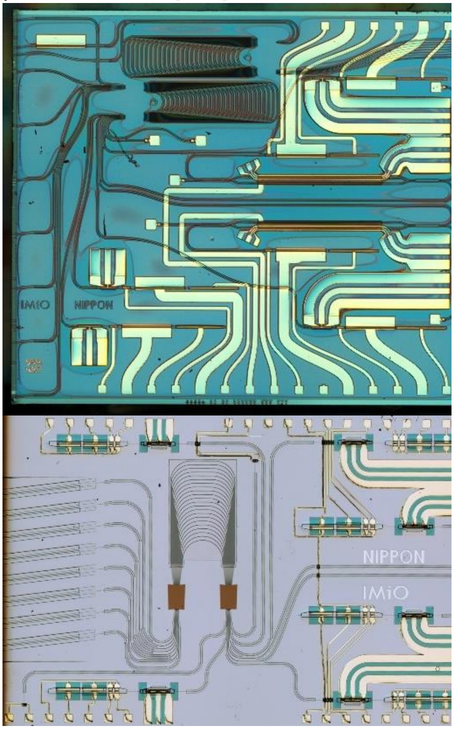

Fig. 1. Microscope picture of multi-channel transmitters manufactured by MSART Photonics (up) and Fraunhofer Heinrich-Hertz-Institut (down)

Microscope pictures of the fabricated devices are presented in Fig 1.

The measurement results confirmed the output fiber-coupled power of the on-chip lasers of ca. 0.6 mW and single-frequency operation with a side mode suppression ratio over 40 dB. The threshold current is relatively low – ca. 28 mA. The most significant characterization results, i.e., multi-channel operation and error-free transmission of digital signals with a bit-rate of 10 Gb/s, prove the suitability of implementing these devices in novel fiber-optic communication systems and integrated datacom solutions.

Acknowledgments: This work was supported by the National Centre for Research and Development (project NIPPON of the 3rd Applied Research Programme, grant agreement PBS3/A3/21/2015).

References:

[1] A. Paśnikowska, S. Stopiński, K. Anders, A. Jusza, R. Piramidowicz, and M. Tomkiewicz, “Integrated transceivers for WDM-PON access systems,” URSI 2018 - Balt. URSI Symp., pp. 31–32, 2018, doi: 10.23919/URSI.2018.8406763.

[2] A. Golba et al., “Monolithically integrated multi-channel transmitters for application in WDM-PON systems,” Proc. SPIE - Int. Soc. Opt. Eng., vol. 10325, p. 103250Y, Feb. 2017, doi: 10.1117/12.2271090.

[3] A. Paśnikowska et al., “Development of InP-based multi-channel transmitters for application in WDM access systems,” in Semiconductor Lasers and Laser Dynamics VIII, May 2018, vol. 10682, p. 79, doi: 10.1117/12.2307641.

Miniature mid-IR spectrometer – concept, implementation and perspectives

F. ŁABAJ[1,2], J. KALWAS[2], A. GÓRSKI[2], P. LESZCZ[2], R. PIRAMIDOWICZ[1, 2]

[1] Warsaw University of Technology, plac Politechniki 1, 00-661, Warsaw, Poland
[2] VIGO Photonics, ul. Poznańska 129/133, 05-850, Ożarów Mazowiecki, Poland
e-mail address: filip.labaj.dokt@pw.edu.pl

Spectral analysis of light affected by the presence of chemical substances, which interact with photons of specific wavelengths (e.g., by absorbing or scattering them), is a technique widely used in scientific research and various industrial applications. Since most substances possess characteristic and discernible spectral signatures (specifically in the mid-IR spectral range), optical spectroscopy can provide a highly accurate and reliable way to detect and identify them.

The rapid growth of IoT (internet of things) and smart environment applications are pushing spectrometric devices towards significantly smaller footprints and decreased energy consumption. Among the most promising technological approaches, one can enumerate the MOEMS- or integrated photonics-based solutions, specifically attractive from the mass market perspective.

The application area of miniaturized spectrometers may cover industrial pollution and production line monitoring, automated sorting, assessment of food quality, biometrics, and health monitoring, to enumerate a few [1-4].

In general, four different types of spectrometers can be distinguished with respect to their operation principle [5]. These are devices based on: (I) dispersive/diffractive optics, (II) narrowband filters, (III) Fourier transform, and (IV) reconstruction techniques.

In this work, we present and discuss the features of a compact mid-IR spectrometer belonging to the II category, operating in the wavelength range of 3-4 µm, that uses a non-discrete, linear-variable, thin-film optical filter (LVF) and an array of InGaAs photodiodes. The device is depicted in Fig. 1.

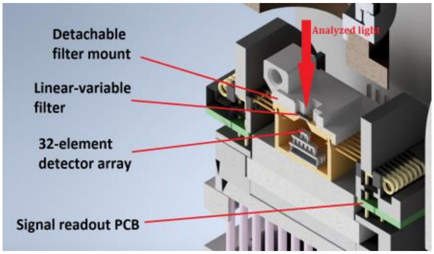

Fig. 1. Overview of the device's structure

The InGaAs array consists of 32 photodiodes, each of which has a 125 µm wide and 1000 µm long photosensitive area. The array is mounted on a three-stage TEC, inside a 40-pin, butterfly-type package, which permits cooling it down to 230 K, increasing the detectivity of photodiodes by up to two orders of magnitude.

The LVF's spectral response in the 3-4 µm region changes linearly along its length. Spectral selectivity is achieved by placing the LVF close to the detector array, effectively limiting the spectral response of each channel to a narrow peak, allowing us to sample 32 discrete spectral points. The device offers a spectral resolution of 60-80 nm and is capable of detecting and identifying various polymer samples, such as polystyrene (PS), low-density polyethylene (LDPE), and polyimide (PI).

A standalone demonstrator was developed to test the concept, comprising an internal thermal light source, a light beam modulator, and an optoelectronic detection setup. System tests have been performed, proving the applicability of the developed device to identifying the various polymer materials through analysis of their spectral response compared to the reference spectra.

As this work is a part of a bigger project focused on developing fully integrated miniature mid-IR spectrometers, the perspectives of further miniaturization will be discussed, with the specific focus on the potential of photonic integrated circuits (PICs) technology.

References:

[1] P. Daponte, et al. "A review on the use of drones for precision agriculture." IOP Conference Series: Earth and Environmental Science. Vol. 275. No. 1. IOP Publishing, 2019.

[2] C. Araujo-Andrade, et al. "Review on the photonic techniques suitable for automatic monitoring of the composition of multi-materials wastes in view of their posterior recycling." Waste Management & Research 39.5 (2021): 631-651.

[3] J. Müller-Maatsch, and S.M. van Ruth. "Handheld devices for food authentication and their applications: A review." Foods 10.12 (2021): 2901.

[4] L. Wang, G. Leedham, and S-Y. Cho. "Infrared imaging of hand vein patterns for biometric purposes." IET computer vision 1.3-4 (2007): 113-122.

[5] Yang, Zongyin, et al. "Miniaturization of optical spectrometers." Science 371.6528 (2021): eabe0722

Single-frequency integrated ring lasers with hybrid intra-cavity wavelength filtering

S. STOPIŃSKI[1,2], R. PIRAMIDOWICZ[1,2]

[1]Warsaw University of Technology, Institute of Microelectronics and Optoelectronics, Koszykowa 75, 00-662 Warsaw, Poland
[2]VIGO Photonics, Poznańska 129/133, 05-850 Ożarów Mazowiecki
e-mail address: stanislaw.stopinski@pw.edu.pl

Cutting-edge photonic integration technologies open entirely new possibilities with respect to designing novel, compact, and energy-efficient sensing systems. The development of a new type of monolithic ring lasers may pave the way to realizing a fully integrated optical gyroscope, as it can combine single-mode operation, narrow laser linewidth, and a relatively large effective sensing area.

In our previous works, we demonstrated ring lasers realized in InP generic integration technology either with an arrayed waveguide grating (AWG) [1] or asymmetric Mach-Zehnder interferometers (AMZI) [2] used as intra-cavity wavelength filters. Here we report a laser system that combines these two methods of wavelength filtering in a single photonic integrated circuit.

The operational scheme of the discussed PIC is presented in Fig. 1. The main amplifier (SOA 1) is used as the gain section of the laser. Wavelength filtering is provided by AMZI 1 and 2, with a free spectral range of FSR_1 = 90 nm and FSR_2 = 0.4 nm, and a 4×8 AWG with the channel spacing of $\Delta\lambda$ = 0.8 nm and FSR_3 = 25.6 nm.

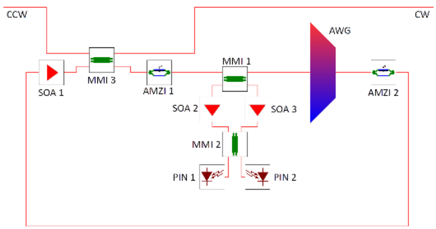

Fig. 1. A functional scheme of the integrated ring laser

The ring laser has been realized as a part of research on the development of a fully integrated gyroscope system. Therefore, the ring laser circuit is complemented by a detection circuit of the beating signal between the clock-wise (CW) and counter clock-wise (CCW) modes. These are coupled to monitoring photodiodes PIN 1 and 2 through multi-mode interference couplers (MMI 1 and 2). Furthermore, the semiconductor optical amplifiers (SOA 1 and 2) are used to equalize the power of the CW/CCW modes.

An additional coupler (MMI 3) is used to couple the CW and CCW signals out of the photonic chip to enable basic optical characterization of the device.

In Fig. 2 there is presented a microscope picture of the fabricated photonic integrated circuit, with the dimensions of 4.0 × 4.6 mm^2. Two variants of the ring laser are visible – in the second one the second Mach-Zehnder filter (denoted AMZI 2 in Fig. 1) is not present.

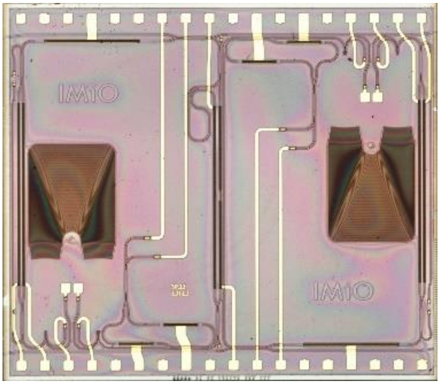

Fig. 2. A microscope picture of the fabricated photonic integrated circuit

Initial characterization results confirm single-mode operation with a side-mode suppression ratio over 30 dB and the fiber-coupled output power up to 200 µW.

Acknowledgments: Studies were funded by FOTECH-1 project granted by Warsaw University of Technology under the program Excellence Initiative: Research University (ID-UB).

References:

[1] S. Stopinski, L. Augustin and R. Piramidowicz, "Single-Frequency Integrated Ring Laser for Application in Optical Gyroscope Systems", IEEE Photonics Technology Letters, vol. 30, no. 9, pp. 781-784 (2018)

[2] S. Stopiński, M. Siennicki, R. Piramidowicz, „Integrated ring lasers for optical gyroscope applications", Integrated Optics – Sensors, Sensing Structures and Methods (IOS 2019), Szczyrk, Poland, 25.02-01.03.201

Non-invasive patient's breath monitoring during MRI diagnosis with the use of integrated photonic interrogator

M. SŁOWIKOWSKI[1,2], A. KAŹMIERCZAK[1], M. BIENIEK[1], S. SZOSTAK[1], S. STOPIŃSKI[1], R. PIRAMIDOWICZ[1]

[1]Warsaw University of Technology, Institute of Microelectronics and Optoelectronics, 00-662 Warsaw, Poland;
[2]Warsaw University of Technology, Centre for Advanced Materials and Technologies CEZAMAT, 02-822 Warsaw, Poland;
e-mail address: mateusz.slowikowski@pw.edu.pl

In modern medicine, one can observe a systematic effort to improve the quality of medical care by implementing various automated monitoring tools and life-support systems, improving the quality and efficiency of diagnosis, therapy, and patient care. A number of solutions based on advanced technologies of electronics and photonics have been implemented so far, like pulse oximeters, cardiac monitors, electroencephalography (EEG) monitors, to enumerate a few.

In this work, we present and discuss a new solution for non-invasive heart and respiratory rate monitoring of patients exposed to magnetic resonance imaging (MRI) scanning procedures. During such an examination, patients may experience significant discomfort due to a claustrophobic environment of the MRI measuring chamber. This might result in anxiety, claustrophobia, and panic attacks, specifically when the scan lasts for several or a few tens of minutes. Therefore, monitoring the patient's condition is highly desirable, as the symptoms of increasing stress can be detected by changes of the respiratory and heart rate, thus giving immediate feedback to the medical staff. The monitoring is even more important in the case of unconscious patients, who are not able to communicate with medical personnel.

The presence of a strong electromagnetic field inside the MRI chamber makes using standard electronic sensors for monitoring the patient's condition impossible. However, a promising solution might be offered by fiber Bragg gratings (FBGs) sensors. It has been confirmed that both heart and respiratory rate signals can be extracted from FBGs reflectance signal, changing with the changes of the pressure imposed on FBGs by a patient's body. This, in turn, can be recorded using an appropriate interrogating device.

In this work, we summarize our research on the interrogating part of the system, the core of which is realized as an application specific photonic integrated circuit (ASPIC), designed and fabricated on the InP generic platform and driven by dedicated electronic circuitry. We will present the details of the PIC design, system assembly and the tests results confirming the proper operation of the developed system.

Acknowledgments: This work was supported by the National Centre for Research and Development (project of the third Applied Research Programme OPTO-SPARE, grant agreement PBS3/B9/41/2015).

Advances in development of SiN-based integrated photonic platform for visible spectral range

M. LELIT[1,2], M. SŁOWIKOWSKI[1,2], M. GOLAS[2], M. FILIPIAK[2], M. JUCHNIEWICZ[2], B. STONIO[1,2], B. MICHALAK[2], K. PAVŁOV[2], M. MYŚLIWIEC[1,2], P. WIŚNIEWSKI[1,2], A. KAŹMIERCZAK[1], K. ANDERS[1,3], S. STOPIŃSKI[1,3], R. B. BECK[1,2] AND R. PIRAMIDOWICZ[1,3]

[1]Warsaw University of Technology, Institute of Microelectronics and Optoelectronics, Koszykowa 75, 00-662 Warsaw, Poland
[2]Warsaw University of Technology, Centre for Advanced Materials and Technologies CEZAMAT, Poleczki 19, 02-822 Warsaw, Poland
[3] VIGO System S.A., Poznańska 129/133, 05-850 Ożarów Mazowiecki, Poland
e-mail address: marcin.lelit@pw.edu.pl

Over the past few years, photonic integrated circuits (PICs) have been gaining an increasingly strong position in the photonics market, particularly in the fields of telecom and datacom, sensing, biomedical applications etc. This is due to their numerous advantages: compact size, high reliability, energy efficiency, reduced manufacturing and packaging costs.

Silicon nitride (Si_xN_y) is a promising material for developing a versatile photonic platform due to its wide transparency window extending from the visible to mid-infrared range, CMOS compatibility, low loss, and relatively small footprints. Silicon nitride becomes the third major material next to indium phosphide and silicon with an obvious potential for developing a specialized technology.

PICs operating in the visible spectral range [1] may significantly expand the applications' portfolio towards e.g. biosensing and digital health monitoring. Exemplary, Si_xN_y-based PICs can be used as building blocks for lab-on-chip devices involving microfluidic systems [2].

The following key steps can be distinguished in a single iteration of the development process of passive photonic integrated circuits:

1. definition of operational parameters required by the end-user,
2. calculations and simulations defining the geometrical properties of the components,
3. fabrication including surface preparation, oxide growth, Si_xN_y deposition, lithography, etching and structure separation,
4. characterization.

Several full production cycles have been performed in the scope of presented research, including iterative design, fabrication, and characterization of a series of photonic integrated structures to verify the potential of the developed technological platform.

The technology enables manufacturing a set of essential passive components such as waveguides, tapers, multimode interferometer power splitters (MMIs), and arrayed waveguide gratings (AWGs).

Results obtained during first production run constitute a backbone for introducing new elements to the library of platform building blocks, like ring resonators (RRs), grating couplers (GC) and Mach-Zehnder interferometers (MZIs). They also provide important feedback for the improvement of already developed elements.

In particular, waveguide losses have been improved from 1.7 dB/cm for multimode WGs fabricated in the 1st run to 1.15 dB/cm for single-mode WGs fabricated in the 2nd run. 1x2 MMI losses have been improved from 0.5 dB in the 1st run to 0.22 dB in the 2nd run. For both elements further improvement is expected as a result of future work that includes advanced coupling interfaces and elements geometry optimization. An example illustration of the chip with grating couplers in the characterization setup is presented in Fig. 1.

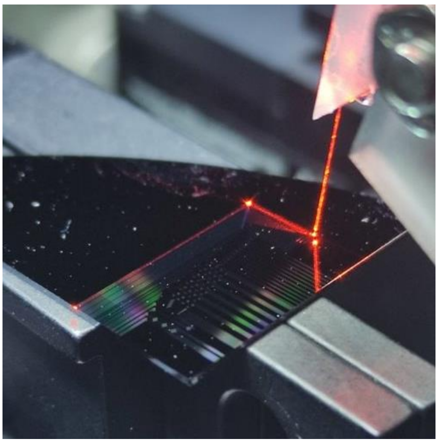

Fig. 1. PICs comprising grating couplers with vertically coupled light in characterization setup.

SEM micrograph of ring resonator gap, which width is one of the crucial parameters of the element, is presented in Fig. 2.

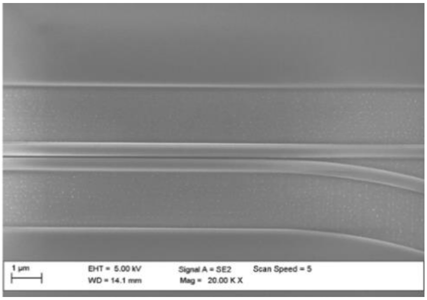

Fig. 2. SEM image of ring resonator detail – gap between bus waveguide and ring

The results obtained so far show the clear potential of developed technology and confirm the initial assumptions on their applicability to manufacturing photonic integrated circuits.

Acknowledgments: This research was partially supported by the project "Development of a silicon nitride-based integrated photonics platform for the visible band for sensing applications" agreement no. 5/2021 1.02.2021 under programme The Innovation Incubator 4.0." operated on Warsaw University of Technology by Applied Research Institute and financed by the Ministry of Science and Higher Education.

References:

[1] P. Muñoz et al., "Silicon Nitride Photonic Integration Platforms for Visible, Near-Infrared and Mid-Infrared Applications," Sensors (Basel), vol. 17, no. 9, Sep. 2017.

[2] A. Leinse, S. Zhang, and R. Heideman, "TriPleX: The versatile silicon nitride waveguide platform," in 2016 Progress in Electromagnetic Research Symposium (PIERS), 2016, pp. 67–67

Grey-tone mask aligner lithography optimization for micro-optics applications

K. PAVŁOV[1], M. FILIPIAK[1], M. JUCHNIEWICZ[1], B. MICHALAK[1], M. MYŚLIWIEC[1], M. SŁOWIKOWSKI[1], B. STONIO[1], P. WIŚNIEWSKI[1], R. BECK[1]

[1]Centre for Advanced Materials and Technologies CEZAMAT,
Warsaw University of Technology, Poleczki 19, 02-822, Warsaw, Poland
e-mail address: krystian.pavlov@pw.edu.pl

Grey-tone lithography has been researched as a rapid manufacturing technology for multi-level structures, mostly microoptics [1,2]. The principle is to encode intensity distribution into a 2D pixelated pattern, either by pulse-width modulation, pulse density modulation or a combination of those [2]. Because of potential high-volume production applications, grey-tone lithography was mostly optimized for wafer steppers, where reduced image of the reticle is projected on resist surface. Much less focus was put on mask aligner systems, where dimension requirements for the photomask are much stricter due to 1:1 mask-pattern ratio. We present complete design and process flow to obtain 2,5D micro-optical structures with standard mask aligner lithography setup.

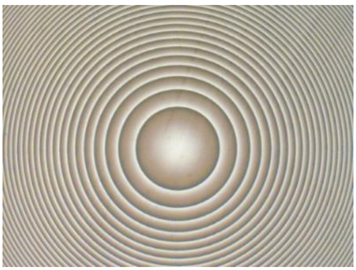

Fig. 1. Amplitude mask (Cr on glass)

Pulse width modulation approach was chosen due to constant grid parameters, optimal for the utilized mask manufacturing process. Different lithography parameters were then tested, including exposure dose, proximity, post-exposure bake and development time.

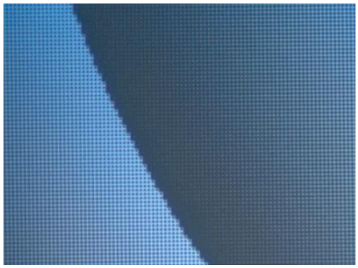

Fig. 2. Chrome mask detail

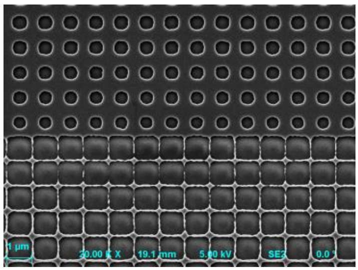

Fig. 3. SEM image of Cr microholes

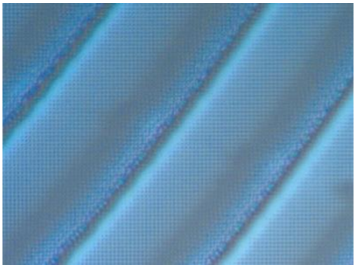

Fig. 4. Pattern pixelation in photoresist

Because of the pixelated photomask pattern structure, each microhole can be treated as point source, with its point spread function (PSF) dependent on propagation distance. High proximity results with better resolution and rougher, more pixelated surface. This mode is suitable for structures with sharp edges, like kinoforms. Larger mask-wafer distance provides smooth surfaces with less details, good for sinusoidal gratings. An experiment was performed to determine this function via cross-section examination. Similar experiments had previously been documented for electron beam lithography [3,4].

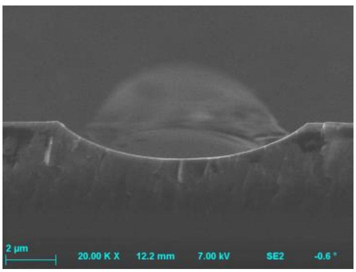

Fig. 5. Cross-section of single line exposure

PSF influence cannot be eliminated, but pattern corrections can be performed to diminish it. PSF was therefore used as gaussian filter kernel for deconvolution operation on the initial pattern data. New photomask was manufactured and tested to verify the correction algorithm.

Developed and optimized process flow can be used in micro-optics applications, without the need for expensive wafer scanner systems. Specific process parameters depend on the structures and their requirements, and pattern is optimized to achieve maximum resolution at these parameters.

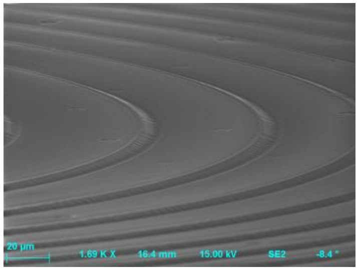

Fig. 6. 2.5D structure exposed with an amplitude mask

References:

[1] B. Wagner et al., Sensors and Actuators A, 46-47 (1995)

[2] K. Reimer et al., Proceedings of SPIE - The International Society for Optical Engineering. 3008, 279-288 (1997)

[3] T. H. P. Chang, Journal of Vacuum Science and Technology 12, 1271-1275 (1975)

[4] B. A. Nilsson et al., Journal of Vacuum Science & Technology B 29, 06F311 (2011)

Mathematical Aspects of Backscattering Cross-Section Estimation of Nanoparticles by Optical Coherence Tomography

J. PLUCIŃSKI, M. R. STRĄKOWSKI

Department of Metrology and Optoelectronics,
Faculty of Electronics, Telecommunications and Informatics, Gdańsk University of Technology,
11/12 Gabriela Narutowicza St., 80-233 Gdańsk, Poland
e-mail address: pluc@eti.pg.edu.pl

The ability to measure backscattering cross-sections of nanoparticles and their changes is crucial for new medical applications of optical coherence tomography (OCT) systems, such as selective detection of chemical or biological molecules using nanoparticles whose surfaces have been activated with appropriate chemical or biological affinity. Due to the affinity, the detected molecules attach to the surface of the nanoparticle and change its scattering properties, including backscattering cross-section, which can be the basis for the selective detection of chemicals, proteins, pathogens, etc. Although the power of backscattered optical radiation measured by the OCT system is proportional to the power of its scanning beam and the backscattering cross-section of the nanoparticle, the power also depends on the position of the nanoparticle with respect to the axis and the waist of the beam. This power is also influenced by the extinction coefficient of the substance in which the nanoparticles are located.

For simplicity, assume that the density of scatterers (nanoparticles) in a sample is so small that the average distance between them is much greater than the longitudinal and transverse resolution of the OCT system and the signal from backscattering can be distinguished for each nanoparticle separately (Fig. 1).

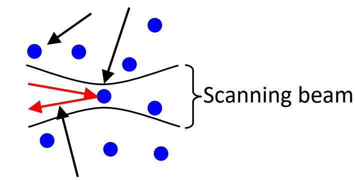

Fig. 1. Scattering of the scanning beam by nanoparticles

The power of radiation P_{n} from a single nanoparticle measured by the OCT system can be determined from the dependence:

$$P_{\mathrm{n}} = I\sigma_{\mathrm{bc}}KAe^{-\mu_{\mathrm{e}}d_{\mathrm{m}}}, \qquad (1)$$

where I is the intensity of optical radiation at the position of nanoparticles, σ_{bc} is the backscattering cross-section of the nanoparticle, K is the power coupling coefficients of the backscattering waves from the nanoparticle to the optical fiber that transmit the optical signal to the detector of the OCT (or from the nanoparticle through a pinhole, if it used, to the detector), A is the constant that describes losses due to attenuation of the optical fiber, Fresnel reflections of the wave on the surfaces of the lenses, faces of the optical fiber, etc. (this constant can be measured during system calibration), d_{m} is the distance that photons propagate from the source to the nanoparticle inside the sample, and μ_{e} is the extinction coefficient that equals the sum of the absorption coefficient μ_{a} and scattering coefficient μ_{s} of the sample:

$$\mu_{\mathrm{e}} = \mu_{\mathrm{a}} + \mu_{\mathrm{s}}. \qquad (2)$$

From Equation (1), we obtain:

$$\sigma_{\mathrm{bc}} = \frac{P_{\mathrm{n}}}{IKAe^{-\mu_{\mathrm{e}} d_{\mathrm{m}}}}. \qquad (3)$$

For a Gaussian beam [1], which is the most used scanning beam in OCT systems, from Equation (3), we obtain:

$$\sigma_{\mathrm{bc}} = \frac{P_{\mathrm{n}} \pi w(z)^2}{2P_0 KA \exp\left(\frac{-2\rho^2}{w(z)^2}\right) e^{-2\mu_{\mathrm{e}} d_{\mathrm{m}}}}, \qquad (4)$$

where P_0 is the power of the scanning beam, $w(z)$ is the beam radius, z is the axial distance from the beam waist, and ρ is the radial distance from the center axis of the beam.

If we use a single-mode fiber to transmit backscattering optical signal from nanoparticle to the detector, the power coupling coefficient K can be calculated based on an overlap integral approach [2, 3]:

$$K = \frac{\left(\iint U_{\mathrm{bs}} U_{\mathrm{f}}^* dxdy\right)^2}{\iint U_{\mathrm{bs}} U_{\mathrm{bs}}^* dxdy \iint U_{\mathrm{f}} U_{\mathrm{f}}^* dxdy}, \qquad (5)$$

where $U_{\mathrm{bs}} = U_{\mathrm{bs}}(x, y)$ is the amplitude of backscattering wave from nanoparticle that reach the face of the optical fiber and $U_{\mathrm{f}} = U_{\mathrm{f}}(x, y)$ is the field distribution of the fundamental mode of the optical fiber.

The problem in determining the coefficient K is that, having a single A-skan or B-scan, we do not know the radial distance of the nanoparticle from the center axis of the beam. Fortunately, having a 3D image, we can choose an A-scan for which the power P_{n} reaches the maximum and assume that in this case the nanoparticle lies on the axis of the scanning beam. Then the coefficient K can be determined numerically or, in some cases, analytically and next implemented in the OCT system in a table form.

The presented mathematical analysis shows that it is possible to measure cross sections for the backscattering of nanoparticles with the OCT system, which, in combination with the activation of their surfaces, will allow the detection of various chemical or biological substances. Moreover, allowance of the power coupling coefficient K in the imaging of nanoparticles by an OCT system allows us to obtain the same intensity in OCT images at equal cross-sections, regardless of the position of the nanoparticles in the measured sample which is not the case with the currently available commercially available OCT systems.

Acknowledgments: This work was supported by the DS program of the Faculty of Electronics, Telecommunications and Informatics, Gdańsk University of Technology.

References:

[1] B.E.A. Saleh, M.C. Teich: Fundamentals of Photonics, Third Edition. John Wiley & Sons, New York, 2019

[2] P.F. Goldsmith: Quasioptical Systems – Gaussian Beam Quasioptical Propagation and Applications. IEEE Press, New York, 1998

[3] J. Pluciński, K. Karpienko, Proc. SPIE, 100340H (2016)

The optical coherence tomography for thin-film profiling enhanced by spectroscopic analysis

M. R. STRĄKOWSKI[1], J. PLUCIŃSKI[1], A. M. KAMIŃSKA[1], P STRĄKOWSKA[2]

[1]Department of Metrology and Optoelectronics, Faculty of Electronics, Telecommunications and Informatics, Gdańsk University of Technology, 11/12 G. Narutowicza, 80-233 Gdańsk, Poland
[2]Institute of Ocean Engineering and Ship Technology, Faculty of Mechanical Engineering and Ship Technology, Gdańsk University of Technology, 11/12 G. Narutowicza, 80-233 Gdańsk, Poland
e-mail address: marcin.strakowski@pg.edu.pl

Optical coherence tomography (OCT) is an imaging technique, which uses low-coherent light to acquire the 2D and 3D tomographic images of scattering and semitransparent objects. The images are captured with micrometer resolution depending on the optical scanning head and the spectral characteristic of the scanning light beam. The metrological abilities and the OCT limitations make this technique applicable for microscopic evaluation, especially in medical diagnosis. However, improving the axial resolution to the sub-micrometer level requires more broadband light sources to be utilized, which increases the cost of the OCT system and its complexity. To overcome this issue, the time-frequency analysis in the OCT, which is known as spectroscopic OCT (Sc-OCT), is proposed. This method is based on retrieving the backscattered signal from particular scanning depths and performing spectral analysis using time-frequency signal processing methods. As a result, spectral information about backscattered light can be gathered from particular points inside the evaluated object. Among others, The Sc-OCT has been used for components recognition [1], oxygen saturation of blood [2], or the contrast agents detection inside tissues [3], and others. The presented research aims at the benefits of spectroscopic (time-frequency) analysis for thin-film evaluation. In general, the back-scattered light from semitransparent thin-film is a product of the Fresnel principles and the interference of multi-scattering beams inside the film. In this case, the spectral characteristic of the back-scattered light may vary referring to the film thickness, which might be detected and analyzed by the OCT enhanced by spectroscopic analysis [4].
A standard OCT system was used during the experiment (Santec IVS-2000). The OCT main features were summarized in Tab 1.

Tab. 1. Main features of the Santec IVS-2000 OCT system.

Features	Values
Light source type	20 kHz swept-source laser
Aver. output power	10 mW
Central wavelength	1290 nm
Wavelength range	140 nm
Axial resolution (in the air)	12 µm
Lateral resolution	15 µm

The two different objects were utilized as the devices under test: a glass wedge-cell and latent fingerprints deposited on the flat polished metal surface. The Sc-OCT measurements of the wedge-cell show the potential and limitations of the method for thin-film evaluation under the sample surface and bring evidence that the subsurface film thickness can be estimated with fine accuracy – better than the two-point resolution of the OCT system, Whereas the latent fingerprints sample exhibits the abilities for imaging contrast enhancement for OCT scans of the complex thin-film patterns. The examples of the fingerprints C-scans, taken with standard OCT and the spectroscopic one, are presented in Fig. 1 and Fig. 2.

Fig. 1. The standard OCT C-scan of latent fingerprints

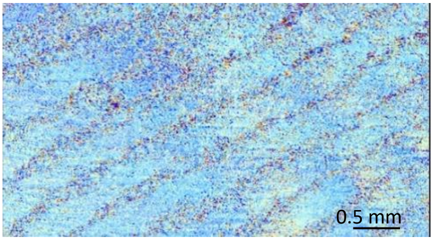

Fig. 2. The Sc-OCT C-scan of latent fingerprints

Comparing both, the standard OCT imaging and the one enhanced by spectroscopic analysis, the Sc-OCT shows more details coded in spectral information (color changes of the pixels in Fig. 2 correspond to spectral characteristics of backscattered light).

Acknowledgments: This work was supported by the DS program of the Faculty of Electronics, Telecommunications and Informatics, Gdańsk University of Technology.

The authors acknowledge the valuable contribution of Mr. Michał Rommel in a form of his master thesis.

References:

[1] T. Ho et. al., Optics Express 22, 5, (2014)

[2] N. Bosschaart et. al., Biomedical Optics Express 4, 11, (2013)

[3] F. Robles et. al., Nature Photonics 5, 12, (2011)

[4] A. M. Kamińska et. al., Sensors 20, 19, (2020)

National Laboratory for Photonics and Quantum Technologies - NLPQT

The National Laboratory for Photonics and Quantum Technologies - NLPQT - is a nationwide investment project carried out by a consortium of 7 scientific units led by the University of Warsaw. The main purpose of the project is to create new research infrastructure in three areas:

1. *Generation and Distribution of Reference Optical Carrier*

   The main goal of the National System for Generation and Distribution of the Reference Optical Carrier is to construct an ultra-stable laser system that can be linked to an optical atomic clock, along with a distribution network using optical fibers. The optical reference signal with low phase noise will be distributed from Toruń to all of the participants of the NLPQT consortium where it will be available to both interested researchers and industry partners.

2. *Photonic Technologies*

   Another aim of the NLPQT project is to build a network of research stations which will either extend the existing or provide completely new research opportunities. The new equipment will be used in a wide variety of applications such as spectroscopic studies of materials (e.g. the analysis of trace air pollutants or characterization of new materials for photovoltaics and medicine), fabrication of specialized optical fibers, development of nano- and microstructures for optoelectronic and medical applications, design, production and characterization of lighting systems, two- and three-dimensional imaging of biological objects and many others.

3. *Quantum Technologies*

   In the area of quantum technologies, the NLPQT project is focused on the development of a country-wide infrastructure enabling practical utilization of properties of individual quantum objects. A particular emphasis is put on the possibility of using single photons in quantum communication, which will enable both research and development work on quantum key distribution (QKD) as well as integration of such solutions with other mechanisms used to secure data transmitted over existing IT and telecommunication systems. Furthermore, test workstations utilizing real-life applications of such quantum objects as single electrons, quantum dots, or atoms will also be established.

The infrastructure built within the framework of the NLPQT project will not only serve the scientists directly involved in the project, but will also be available to other researchers and industry partners. For more information visit the website of the Project at http://nlpqt.fuw.edu.pl.

European Funds Smart Growth
NLPQT
European Union European Regional Development Fund

Ultrastable frequency for metrology network in Poland

M. BOBER[1], K. TURZA[2], A. BINCZEWSKI[2], W. BOGACKI[2], Ł. ŚLIWCZYŃSKI[3], P. KREHLIK[3], M. NAROŻNIK[1] AND M. ZAWADA[1]

[1]Institute of Physics, Faculty of Physics, Astronomy and Informatics, Nicolaus Copernicus University, Grudziadzka 5, PL-87-100 Toruń, Poland
[2]Poznan Supercomputing and Networking Center (PSNC), Poznań, Poland
[3]Faculty of Computer Science, Electronics and Telecommunications AGH University of Science and Technology, Krakow, Poland
e-mail address: bober@fizyka.umk.pl

Ultrastable frequency/phase reference may have many application in precise metrology. It can be used in synchronization, geodesy, remote sensing and optical path stabilization. While it would be expensive and difficult to build state of the art frequency reference in many locations an alternative technology can be used. Here we present a setup for generation of ultrastable frequency reference and dedicated optical fibre network for delivery of the ultrastable frequency signal.
Th first part of the setup is ultrastable laser operating at telecommunication wavelength 1542 nm. The stability of the laser is transferred from the ultrastable cavity with high finesse mirrors. The cavity design with ultra low expansion glass and crystalline mirrors allows for short term instability <1e-16 at 1 s.

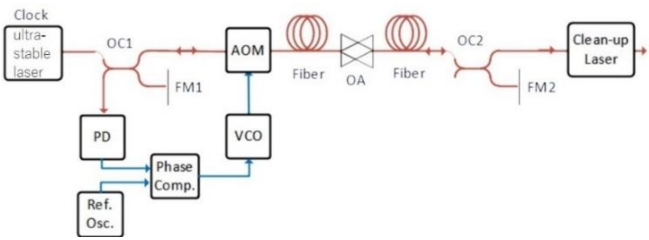

Fig. 1 Simplified scheme of setup.

The ultrastable optical frequency signal may be distribute by telecommunication optical network, however the long-distance transmission of the coherent optical signal suffers not only from attenuation, but also phase/frequency noise, imposed by the fiber, which is vulnerable on environmental conditions. The main reasons of this phase noise are related to acoustic vibrations and stresses, thermal expansion and thermal sensitivity of the refractive index, and also fluctuating birefringence of the fiber. All these factors influence the optical phase at the fiber end in the random manner, and so degrade the signal coherence and frequency stability. In case of the long link (some hundreds of kilometers) the short-term phase noise would be of thousands of optical cycles, and long-term relative frequency instability would be degraded to app. 1e-14. Fortunately, this phase/frequency noise may be dramatically reduced by means of an active noise cancellation scheme, which simplified principle is depicted in Fig. 1.

Finally the end user of such a network may use ultrastable signal on his side either directly at 1542 nm wavelength or transferred with an optical frequency comb to any optical or radio frequency wavelength.

Acknowledgments: The “A next-generation worldwide quantum sensor network with optical atomic clocks” project (TEAM/2017-4/42) is carried out within the TEAM IV Programme of the Foundation for Polish Science co-financed by the European Union under the European Regional Development Fund. This research has received funding from the EMPIR Programme co-financed by the Participating States and from the European Union’s Horizon 2020 Research and Innovation Programme (EMPIR 20FUN08 NEXTLASERS), The research is performed partially at the National Laboratory FAMO (KL FAMO) in Toruń, Poland. and were supported by a subsidy from the Polish Ministry of Science and Higher Education.

Accurate metrology of simple molecules for studying fundamental physics

P. WCISŁO

[1]Institute of Physics, Faculty of Physics, Astronomy and Informatics,
Nicolaus Copernicus University in Toruń, Grudziadzka 5, Torun 87-100, Poland
e-mail address: piotr.wcislo@umk.pl

I will discuss our experimental and theoretical progress aimed at using precision spectroscopy for studying molecular interaction and collisions. I will focus on simple molecular systems for which the molecule structure and collisional perturbation of molecular lines can be calculated from the first principles. We reached an unprecedently well (sub-percent) agreement between theoretical and experimental spectra for the simplest case of atom-molecule collisions, i.e., helium-molecular hydrogen collisions. We observe similarly well agreement for the simplest case of molecule-molecule collisions when distinguishable molecules are considered (in our case deuterium-hydrogen) and clear disagreement in the self-perturbed case (deuterium-deuterium collisions), which indicates that the role of quantum distinguishability should be tested in our calculations of collisional perturbation of molecular spectra. On the experimental side, we use cavity-enhanced spectroscopic techniques referenced to optical frequency comb to measure the shapes of collision-perturbed molecular lines with high signal-to-noise ratio and negligible apparatus effects. I will discuss our progress on implementing the cryogenic optical cavity and the laser system based on the optical parametric oscillator.

Dual-comb generation in a single laser cavity for sensing applications

Ł. A. STERCZEWSKI[1], M. KOWALCZYK[1], J. SOTOR[1]

[1]Laser & Fiber Electronics Group, Faculty of Electronics, Photonics and Microsystems, Wroclaw University of Science and Technology, Wybrzeże Wyspiańskiego 27, 50-370 Wrocław, Poland
e-mail address: lukasz.sterczewski@pwr.edu.pl

Optical frequency combs (OFCs) have transformed the landscape of modern optical metrology by enabling precise measurements at optical frequencies referenced to primary time and frequency standards [1]. A pattern of sharp, equidistant comb lines spanning large optical bandwidths can now be used as a frequency ruler across different parts of the electromagnetic spectrum ranging from the ultraviolet (UV) to terahertz (THz). To resolve individual comb teeth, and access information encoded at optical frequencies, one can employ conventional interferometric or dispersive techniques. However, one of the most elegant ways involves a pair of OFCs that asynchronously probe each on a photodetector. No moving parts are required, as the technique purely relies on optical heterodyne detection. Wideband spectral information about the optical intensity and phase is available within micro to milliseconds from periodic electrical interferograms (IFGs). This emerging technique referred to as dual-comb spectroscopy (DCS) has been widely used in a range of applications like remote sensing, combustion diagnostics or fundamental physics [2].

Despite these advantages, experimental realization of DCS is still challenging. In a typical scenario, a pair of OFCs must be mutually stabilized using high-bandwidth electronic feedback loops exploiting nonlinear spectral broadening (*f*-2*f*) for retrieval of correction signals. The elegance, simplicity, and robustness for out-of-laboratory sensing is often compromised.

A remedy to this issue is dual-comb generation in a shared laser cavity. In DCS the most stringent requirement is the relative stability between the sources, which is natively provided by a pair of combs formed along the same beam path (due to common noise suppression). Among several dual-comb formation mechanisms, of particular attention is polarization multiplexing, which relies on simultaneous generation of optical pulses with orthogonal polarizations. This scheme has been adopted in our work [3].

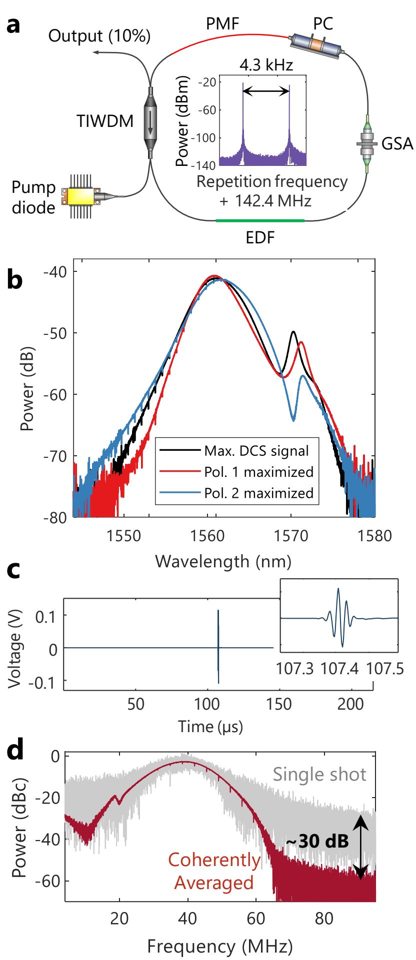

Fig. 1. (**a**) Experimental setup, (**b**) Optical spectra, (**c**) DCS interferogram, (**d**) Dual-comb spectra with HCN in the beam path in 230 μs and averaged (200 ms). See text for details.

Figure 1a shows the experimental setup comprising just a few fiber components (EDF – erbium-doped fiber, PC-polarization controller, TIWDM – hybrid component). The ring-type fiber oscillator that was mode-locked using a graphene saturable absorber (GSA) exhibits weak birefringence due to the presence of a short section of polarization-maintaining fiber (PMF). The laser supports self-starting dual-comb generation on orthogonal polarizations (Pol. 1 / Pol. 2, 5.4 nm 3-dB width, Fig. 1b) with excellent spectral overlap, and tunable repetition rates offset by 4.3 kHz (inset of Fig. 1a). When the oscillator output is guided through a polarization controller followed by a polarizing beam splitter, one can obtain a DCS IFG as shown in Fig. 1c. It is free of any spurious signals that typically plague other free-space DCS lasers. Using a dedicated phase correction algorithm [4], we coherently average thousands of DCS IFGs in post-processing to obtain mode resolved (~142 MHz / 1.16 pm) optical spectra over a 1.7 THz optical span. Fig. 1d already shows sharp absorption features of low-pressure hydrogen cyanide (HCN) detectable in the electrical spectrum even in free-running mode. Accurate and precise measurements of species with Lorentzian half-widths in the ~100 MHz regime are routinely possible.

The concept of polarization multiplexed dual-comb generation has also been recently adopted by the authors in a solid-state dual-comb laser based on a Yb:CNGS medium at a 1 μm wavelength [5]. Future work will focus on real-time correction of spectroscopic signals, and shifting the wavelengths to the mid-infrared or THz range through nonlinear frequency conversion. A mid-

IR chip-based DCS system for molecular sensing is also investigated.

Acknowledgments: This work was partially supported by the National Science Centre (NCN, Poland) under Grant No. UMO-2014/13/D/ST7/02143; Ł. A. Sterczewski acknowledges funding from the European Union's Horizon 2020 research and innovation programme under the Marie Skłodowska-Curie grant agreement No 101027721.

References:

1. T. Udem, *et al.* Nature **416**, 233 (2002).
2. I. Coddington, *et al.* , Optica **3**, 414 (2016).
3. Ł. A. Sterczewski, *et al.*, APL Photonics **4**, 116102 (2019).
4. L. A. Sterczewski, *et al*., Opt. Express **27**, 23875 (2019).
5. M. Kowalczyk, *et al.*, Laser & Photonics Reviews **15**, 2000441 (2021).

Large-area plasmonic nanostructures for SERS applications

M. SUSTER[1], A.SZYMAŃSKA[1], A. KRÓLIKOWSKA[2], P. WRÓBEL[1]

[1]Faculty of Physics, University of Warsaw, Pasteura 5, 02-093 Warsaw, Poland
[2] Faculty of Chemistry, University of Warsaw, Pasteura 1, 02-093 Warsaw, Poland
e-mail address: Piotr.Wrobel@fuw.edu.pl

Metallic nanostructures recently have drawn large research attention due to their unique optical properties connected with the excitation of collective oscillations of free electrons at the structured metal surface - so-called localized surface plasmons (LSP). These resonances exhibit high field enhancement that is limited exclusively to the vicinity of the surface and the high sensitivity to probe the surface events which make them suitable for such applications as (bio)sensors, including those exploiting surface-enhanced Raman scattering (SERS) spectroscopy [1-2]. Over the last decade, several fabrication methods have been developed which are based either on chemical or physical methods like seed-mediated growth, electron-beam, or optical lithography [3]. These common approaches suffer either from a lack of uniformity of the nanoparticle distribution on the solid substrate or a small active area that makes the substrates impractical in use.

In this study, we exploit the modified nanosphere lithography approach for the fabrication of nanostructures exhibiting fine features in the nanoscale and high uniformity over the area of several cm squared. A simplified protocol with the use of randomly distributed silica nanospheres and physical vapor deposition leads to the formation of metallic nanogap structures

showing unique spectral and physical features suitable for sensing and SERS-based applications. Moreover, their plasmonic properties can be easily controlled by the thickness adjustment of the metal layer as well as the size and density of the silica nanospheres. In the experiment, we investigate the influence of geometrical and material properties on the plasmonic response of the structures with the use of reflectometry and spectrophotometry. The performance of the substrates for SERS applications was examined based on the relative standard deviation (RSD) of the plasmon-enhanced Raman signal for the detection of 4-mercaptobenzoic (pMBA) analyte.

References:

[1] B. Špačková, P. Wrobel, M. Bocková, J. Homola, "Optical biosensors based on plasmonic nanostructures: a review" Proc. of the IEEE, 104, 2380-2408 (2016).

[2] J. Langer et al., "Present and Future of Surface-Enhanced Raman Scattering," ACS Nano, 14, 28−117 (2020).

[3] L. Ouyang, et al., "Prosperity to challenges: recent approaches in SERS substrate fabrication," Rev. Anal. Chem 36(1), 20160027 (2017).

Possibilities of using optical fibers sensors in climate change

A. PAŹDZIOR[1], K. KULTYS[2], K. MISZTAL[2], M. DOBEK[3], P. ZAGÓRSKI[3], R. DOBROWOLSKI[3], M. ŁUKOWSKI[4], C. POLAKOWSKI[4], W. BERUS[4], A. BIEGANOWSKI[4], P. MERGO[1,5]

[1]Laboratory of Optical Fibre Technology, Maria Curie-Sklodowska University, Maria Curie-Sklodowska Sq. 3, 20-031 Lublin, Poland
[2]ECOTECH-COMPLEX Analytical and Programme Centre for Advanced Environmentally-Friendly Technologies, Głęboka St. 39, 20-612 Lublin, Poland
[3]Institute of Earth and Environmental Sciences, Maria Curie-Sklodowska University, Kraśnicka Ave. 2cd, 20-718 Lublin, Poland
[4]Institute of Agrophysics, Polish Academy of Sciences, Doświadczalna St. 4, 20-290 Lublin, Poland
[5]CeReClimEn - Centre for Climate Change and Environment Research, Głęboka St. 39, 20-612 Lublin, Poland
e-mail address: adam.pazdzior@mail.umcs.pl

We all feel the climate change – there is less snowfall in the winter than it used to be and the scorching hot summers become increasingly burdensome. The extreme weather phenomena – floods, hailstorms, droughts accompanied by wildfires – are more and more frequent. Climate changes have substantial impact on soils as well. Without sustainable land management humankind won't be able to face the climate crisis, produce enough food, nor to adapt to climate changes.

Constant decrease in soil moisture can contribute to a necessity of heavier irrigation in agriculture and lead to crop yield reduction, even to desertification having potentially dramatic impact on food production. Changes in seasonal temperature distributions can cause shifts in yearly life cycles of plants and animals, which can also result in reduced yield. For example, spring may come early, and the trees may blossom before the insects that are supposed to pollinate them even hatch. With expected persistent world population growth an increase – not a decrease – in food production is a must. Largely this depends on sustainable management of areas subjected to agriculture and keeping the soils healthy.

The profile of vertical distribution of temperature is one of the pivotal soil characteristics linked with sustainable management. Many methods for measurement of such profile are known, but none of them offers adequate resolution.

We present a proof-of-concept for realization of an autonomous distributed fiber-optic system for measurement of temperature profile in soils and discuss the obstacles encountered during its evaluation as well as possible ways of avoiding or overcoming those difficulties. Our system, comprised of LUNA OBR4600 optical backscatter reflectometer as an interrogator and single-mode fiber-optic cable as a sensor, has been installed and tested in real-life environment with minimal supervision or maintenance.

Acknowledgments: This work was partially supported by the project National Laboratory for Photonics and Quantum technologies – NLPQT (POIR.04.02.00-00-B003/18-00).

Photonic sensing of gases and volatiles: needs, technologies and solutions for science and business

K. BARCZAK[1], Z. OPILSKI[1], W. BURLIKOWSKI[2], Z. KOWALIK[2], A. OLSZEWSKA[1], E. MACIAK[1]
[1]Department of Optoelectronics, Silesian University of Technology, 2 Krzywoustego St., 44-100 Gliwice, POLAND
[2]Department of Mechatronics, Silesian University of Technology, 10A Akademicka St., 44-100 Gliwice, POLAND
e-mail address: kamil.barczak@polsl.pl; erwin.maciak@polsl.pl

Dynamic and continuous development of civilization brings side effects in the form of a number of threats, which were not always remembered in the current technical development and perception of the catalog of potential threats. In recent years, the frequency of contamination in the form of Volatile Organic Compounds (VOCs) and unwanted, unpleasant odors is constantly increasing, causing a change in our understanding of urban environment pollution. The growing global awareness of factors affecting our health and quality of life, supported by a series of long-term research, forces us to search for new materials and sensor technologies that are able to meet the current and anticipated challenges that our civilization is currently facing.

The detection of gases is a challenge all market sectors. To address these requirements, many sensor technologies have evolved. Gas detection methods may be split into two groups,

(i) direct methods, which monitor a physical parameter of the specific gas analyte, and

(ii) indirect methods, which use a physico-chemical interaction between gas analyte and receptor material to show the concentration of the gas being sensed. [1-3]. This work will focus on direct gas sensing techniques.

For qualitative and quantitative analysis of the specific gas analyte, based on the phenomenon of radiation absorption in the IR spectra range, we can use dispersive and non-dispersive infrared (NDIR) optoelectronic measurement systems. The NDIR gas sensors are definitely simpler in design. The simplicity of the structure leads to a more compact structure of the measuring system, which, among other things, facilitates the fulfillment of certified safety and reliability standards and reduces the unit cost of the sensor. The basic elements of the measurement configuration of the NDIR sensor are: a broadband IR radiation source, a broadband IR radiation detector equipped with a narrowband filter dedicated to a given gas and a measuring cell in which the IR radiation interacts with the gas. The optical measurement path of an NDIR sensor usually consists of two paths: an active (working) path and a reference path, which is used to monitor changes in the background signal that needs to be compensated. Moreover, the measurement path of the NDIR sensor is often additionally equipped with a conditioning system or optics shaping the radiation beam, the process of which should lead to an increase in the radiation intensity on the active element of the IR detector. As a result, it improves the efficiency of the sensor. Figure 1 shows a schematic structure of a typical NDIR sensor in practical reflection configuration.

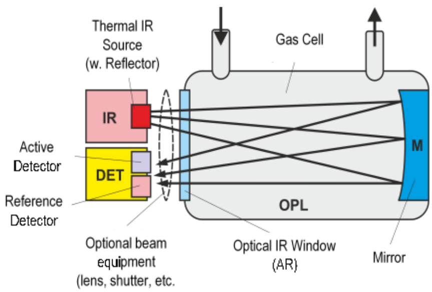

Fig. 1. Schematic, reflection configuration of the NDIR sensor with an example installation of a window protecting the transmitting and the detection block.

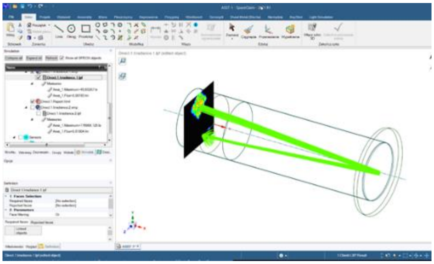

Fig. 2. RayTracing ANSYS-SPEOS showing the image of rays hitting the detector.

The work presents a numerical analysis of the influence of individual components of the optical path on the detector output signal, in particular, it takes into account the spectral characteristics of the components of the modeled NDIR sensor and the absorption spectrum of the tested gas. The analysis leads to the determination of the signal reaching the detector.

The model, using RayTracing ANSYS-SPEOS (Figure 2), returns the spectral transmittance of the system as a function of the optical path and as a function of the tested gas concentration in the conditions of the presence of interfering gases at the assumed gas temperature and pressure. This relationship can then be converted into a function of the useful signal on the optical path length.

The process of modeling the optical path is carried out in such a way as to obtain the optimal usable electrical signal of the detector.

Acknowledgments: This work benefited from facilities and research infrastructure provided by the Department of Optoelectronics Silesian University of Technology, which receives support under project NLPQT – National Laboratory for Photonics and Quantum Technology, POIR.04.02.00-00-B003/18.

References:

[1] J. Janata, Principles of chemical sensors, 2nd edn. (2009) Springer, New York.

[2] T. Seiyama, Chemical sensors – current state and future outlook, in „Chemical Sensors Technology", Vol. 1, Ed. T. Seiyama, (1988) Elsevier, Amsterdam, Kodansha LTD, Tokyo.

[3] J.R. Stetter et al., Journal of The Electrochemical Society, 150 (2) (2003).

Novel ultrafast dynamics of double-frequency breathing-like dissipative solitons

K. KRUPA[1], T. M. KARDAS[2], Y. STEPANENKO[1]

[1]Institute of Physical Chemistry, Polish Academy of Sciences, ul. Kasprzaka 44/52, 01-224 Warsaw, Poland
[2]Fluence sp. z o.o., ul. Kolejowa 5/7, 01-217 Warsaw, Poland
e-mail address: kkrupa@ichf.edu.pl

The fundamental aspects of various nonlinear dissipative soliton interactions within ultrafast fiber lasers have recently been strongly revisited due to the development of a real-time measurement technique called the dispersive Fourier-transform (DFT) [1]. Numerous ultrafast laser dynamics including, for instance, internal motions within soliton molecules [2] or soliton explosions, studied so far only numerically, have become now accessible experimentally. The subject of breathing-like or pulsating dissipative solitons has recently gained significant research attention, as well. Breathing-like structures have been observed experimentally in ultrafast titanium-sapphire lasers, and next in passive optical fiber cavities and optical microresonators [3]. More recently this unique behavior has also been demonstrated in ultrafast fiber lasers [4]. However, all previous experiments showed breathers that have been characterized by a single frequency, that can be superimposed on period-n bifurcations (period doubling, period tripling, etc. [5] of the fundamental frequency of the laser oscillator - laser's repetition rate). In this paper, we observe breathers, the second frequency, in an ultrafast fiber laser without any change of the fundamental frequency. Contrary to previous studies we also observe a third frequency, which manifests as a periodic change of the breathing frequency (f_B) due to the second Hopf bifurcation. Although the presence of double-Hopf bifurcation has been extensively studied theoretically [6], to our knowledge, this is the first experimental observation of such phenomenon in lasers. We propose a more precise methodology that allows us to provide possible explanation to the observed double-Hopf bifurcation-like dynamics.

We consider an all-normal all-polarization maintaining (PM) Ytterbium-doped fiber laser mode-locked by using a nonlinear loop mirror (NOLM) [7]. Our oscillator has a fundamental repetition rate of 17.7 MHz and a total accumulated dispersion of 0.27ps^2 (at 1030nm). To perform a real-time measurement, we implemented a DFT technique with an electronic-based spectral resolution of 0.27 THz (0.98 nm).

All-PM Yb-doped fiber lasers are known to deliver high energy stable ultrashort pulses. Here, we demonstrate that in these class of lasers pulses may also experience breather-like behavior, which manifests by a periodical change of a pulse intensity profile and spectral bandwidth with a return to the original state after multiple cavity roundtrips. We observed that the breathing frequency is not a fixed value, but it is modulated for the pump power (P_p) below the threshold for the stationary dissipative soliton regime.

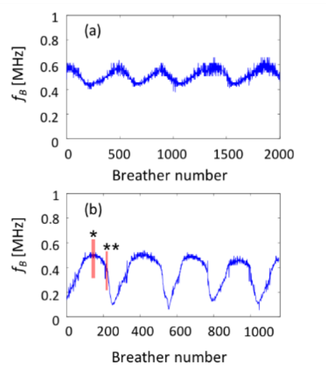

Fig. 1. Breathing frequency evolution obtained at P_p=211mW (**a**) and P_p=213mW (**b**).

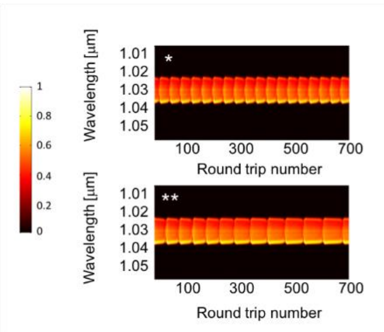

Fig. 2. 2D contour plots of 700 consecutive single-shot spectra corresponding to the two red rectangle of panel (b) of Fig.1 as * (top) and ** (bottom). RT – round trip number.

Such a breathing-like behavior is illustrated in Figs. 1 and 2, presenting the evolution of the numerous consecutive f_B measured at P_p=211mW (Fig.1a) and P_p=213mW (Fig.1b). Examples of evolutions of 2D contour plots of single-shot experimental spectra, as comprised in the two marked-up red rectangles of panel (b) of Fig.1, are displayed Fig.2.

We solved a unidirectional pulse propagation equation (UPPE) for nonlinear pulse propagation, where we apply an exact model of NOLM and a point filter together with the "light hydrodynamic" model of the Ytterbium doped medium for calculation of a gain. This approach enables direct exploration of the dynamics of the electronic level population, as well as saturable absorption and intensity-dependent losses.

References:

[1] K. Goda and B. Jalali, Nat. Phot. 7, 102 (2013).

[2] K. Krupa, K. Nithyanandan, U. Andral, P. Tchofo-Dinda, and P. Grelu, Phys. Rev. Lett. 118, 243901 (2017).

[3] T. M. Kardaś, W. Gadomski, B. Ratajska-Gadomska, and P. Wasylczyk, Opt. Express 18, 26989–26994 (2010).

[4] J. Peng, S. Boscolo, Z. Zhao, H. Zeng, Sci. Adv. 5, eaax110 (2019).

[5] J. M. Soto-Crespo, M. Grapinet, Ph. Grelu, and N. Akhmediev, Phys. Rev. E 70, 066612 (2004).

[6] G. M. Lewis, W. Nagata, SIAM Journal on Applied Mathematics 63:3, 1029 (2003).

[7] J. Szczepanek, T. M. Kardaś, M. Michalska, Cz. Radzewicz, and Y. Stepanenko, Opt. Lett. 40, 3500 (2015).

Ultrafast fiber lasers for ophthalmic imaging applications

J. BOGUSŁAWSKI[1,2,3], D. STACHOWIAK[1], Z. ŁASZCZYCH[1], A. HUDZIKOWSKI[1], A. GŁUSZEK1, M. WOJTKOWSKI[2,3], G. SOBOŃ[1]

[1]Laser & Fiber Electronics Group, Faculty of Electronics, Photonics and Microsystems, Wrocław University of Science and Technology, Wyb. Wyspiańskiego 27, Wrocław, Poland
[2]International Center for Translational Eye Research, Institute of Physical Chemistry, Polish Academy of Sciences, Skierniewicka 10a, Warsaw, Poland
[3]Department of Physical Chemistry of Biological Systems, Institute of Physical Chemistry, Polish Academy of Sciences, Kasprzaka 44/52 Warsaw, Poland
e-mail address: jakub.boguslawski@pwr.edu.pl

Early diagnosis is crucial for the effective treatment of eye diseases. In retinal degenerative diseases, functional changes often precede any structural alterations. Hence, the ability to objectively measure the function of photoreceptors is of utmost importance for the effective treatment of retinal diseases and drug development.

Two-photon excited fluorescence scanning laser ophthalmoscopy [1] is a newly developed method that creates the possibility of functional imaging by tracking the fluorescence of various intermediates of the visual cycle. However, the absorption of most retinal fluorophores lies in the UV spectral range; therefore, direct excitation is not possible due to the absorption in the front part of the eye and high phototoxicity. We utilized a two-photon excitation to bypass this limitation, using femtosecond pulses in the near-infrared. Near-infrared light easily penetrates the back part of the eye, allowing for noninvasive excitation of retinal fluorophores [2].

It has been demonstrated that ultrashort (<100 fs) pulses in near-infrared (700-800 nm) and low pulse repetition rate (<10 MHz) are necessary for efficient excitation of those fluorophores [3]. Those parameters can be obtained using a Ti:sapphire laser connected to a pulse-picker and dispersion pre-compensation unit. However, Ti:sapphire lasers and associated high-upkeep instrumentation pose a significant difficulty in introducing the TPEF-SLO method into the clinical environment.

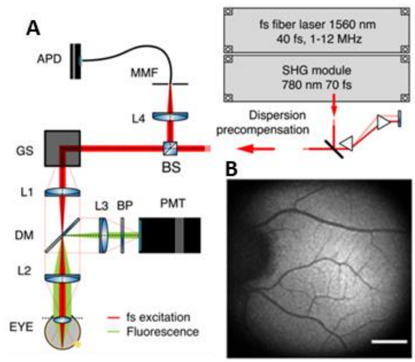

Fig. 1. A: Experimental setup of TPEF-SLO. The laser was connected with dispersion compensation and the SLO unit. L, lens; GS, galvanometer-based x-y scanners; DM, dichroic mirror; BP, bandpass filters; PMT, photomultiplier tube; MMF, multimode fiber; APD, avalanche photodiode. **B:** A selected two-photon excited fluorescence image of the eye fundus.

To this end, we have developed a compact frequency-doubled Er:fiber laser with an adjustable pulse repetition rate within the 1-12 MHz range [1,4]. The laser produces 70 fs at a 780 nm wavelength. The laser has been connected with a prism-pair compressor for dispersion pre-compensation, delivering a short pulse to the retinal plane. The SLO unit is based on a pair of galvanometer scanners and a telescope composed of two lenses (L1, L2). Optics of the human eye is responsible for focusing the beam. The fluorescence is directed towards a photomultiplier tube using a dichroic mirror (DM) and a set of bandpass filters (BP, 400-700 nm). Along with fluorescence-based images, the system also records reflectance images, which are needed for image processing.

As a result, fluorescence-based images of eye fundus are produced. An example of imaging a healthy volunteer's eye is shown in Fig. 1B. The reconstructed image shows a large portion of the optic disk and ends on the macular region. The results show that it is possible to register fluorescence signals originating from retinal fluorophores at safe excitation levels by two-photon excitation in near-infrared. The talk will discuss our recent developments of femtosecond fiber lasers for this application.

Acknowledgments: This work was partially supported by the Foundation for Polish Science within the First TEAM program cofinanced by the European Union under the European Regional Development Fund (First TEAM/2017-4/39) and by the National Centre for Research and Development (NCBR), under the contract no. LIDER/32/0119/L-11/19/NCBR/2020. The International Centre for Translational Eye Research (MAB/2019/12) project is carried out within the International Research Agendas Programme of the Foundation for Polish Science cofinanced by the European Union under the European Regional Development Fund.

References:

[1] J. Bogusławski et al., The Journal of Clinical Investigation 132(2), e154218 (2022).

[2] G. Palczewska et al., Nature Medicine 20, 785 (2014).

[3] G. Palczewska et al., Proceedings of the National Academy of Sciences 117(36), 22532 (2021).

[4] D. Stachowiak et al., Biomedical Optics Express 11(8), 4431 (2021).

Towards two-photon bio-imaging with GRIN lenses and image guides

P. SZCZYPKOWSKI[1], Ł. BIJOCH[2], M. PAWŁOWSKA[1,2], U. WŁODKOWSKA[2], R. CZAJKOWSKI[2], R. KASZTELANIC[3], A. BEROUN[2], R. BUCZYŃSKI[3], L. KACZMAREK[2], R. ŁAPKIEWICZ[1]

[1]Institute of Experimental Physics, Faculty of Physics, University of Warsaw, Pasteura 5, Warsaw 02-093, Poland
[2]Nencki Institute of Experimental Biology PAS, Center of Excellence for Neural Plasticity and Brain Disorders BRAINCITY, Pasteura 3, 02-093, Warsaw, Poland.
[3]Department of Photonic Materials, Łukasiewicz Research Network - Institute of Microelectronics & Photonics, Al. Lotników 32/46, 02-668, Warsaw, Poland
e-mail address: Pawel.Szczypkowski@fuw.edu.pl

Two-photon excitation fluorescence microscopy offers deep tissue penetration, however for some biological applications - like live rodent brain imaging – the maximum depth of 1 mm is not enough. In case one wants to track the live activity in deeper parts of the brain, there are at least two possibilities. One is to use GRIN (GRaded INdex) lenses that optically act as a relay in this case. Another option is to use an image guide – a small diameter coherent fiber bundle, where every fiber core can be treated as a single pixel in the image. Both image guides and GRIN lenses can be implanted into the tissue, and then the free end can be imaged with a regular fluorescence microscope. In such a setting, one can improve the image quality with several illumination strategies. Two-photon excitation with a focused beam is a natural choice because of its excellent optical sectioning capability. In this case, optical sectioning is achieved by selective excitation of the small volume around the beam focus. 3D raster scanning is required to form an image. Interestingly, spatial focusing of the excitation beam is not the only way to achieve selective excitation. Alternatively, the length of a weakly focused excitation pulse can be manipulated such that it illuminates a larger area but only efficiently excites the in-focus plane. This method, termed temporal focusing, enables maintaining the larger area of excitation and widefield detection, therefore dispensing with the need for raster scanning. We will present our preliminary results from live brain imaging via image guides fabricated by us as well as our implementation of two-photon deep-tissue imaging and discuss the pros and cons of various experimental approaches.

Acknowledgments:
This work was supported by the Foundation for Polish Science (FNP) under the FIRST TEAM project 'Spatiotemporal photon correlation measurements for quantum metrology and super-resolution microscopy' co-financed by the European Union under the European Regional Development Fund (POIR.04.04.00-00-3004/17-00; PS,MP, RL) and FNP TEAM (UW, RC, LK), FNP MAB BRAINCITY (LB, AB) and FNP TEAM-TECH (POIR.04.04.00-00-1C74/16; RK, RB). We also thank Benjamin Judkewitz for sharing the microscope design.

Towards on-chip multidimensional quantum key distribution

A. WIDOMSKI[1], S. STOPIŃSKI[2], K. ANDERS[2], R. PIRAMIDOWICZ[2], M. KARPIŃSKI[1],

[1]Faculty of Physics, University of Warsaw, Pasteura 5, 02-093 Warszawa, Poland
[2]Warsaw University of Technology, Institute of Microelectronics and Optoelectronics, Koszykowa 75, 00-662 Warszawa, Poland
e-mail address: mkarp@fuw.edu.pl

We present precise control of temporal and spectral profiles of pulses generated at the telecom wavelength in an indium phosphate (InP) photonic integrated circuit enabling simultaneous temporally and spectrally resolved measurements using single photon counting. We discuss its applications in multidimensional time-frequency quantum key distribution, where security relies on the time-frequency uncertainty [1].

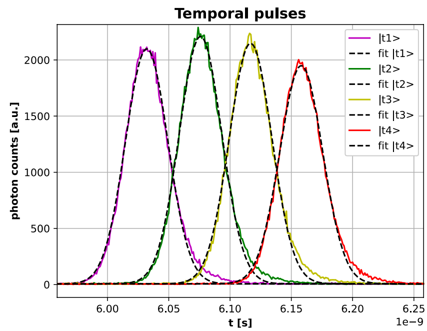

Fig. 1. Temporal pulses: single photon duration and separation measurement measured by time-correlated single-photon counting

The pulses were designed to be gaussian-shaped, and were generated by means of precisely-timed sequential electro-optic amplitude modulation combined with central wavelength shifting followed by attenuation to the single-photon level.

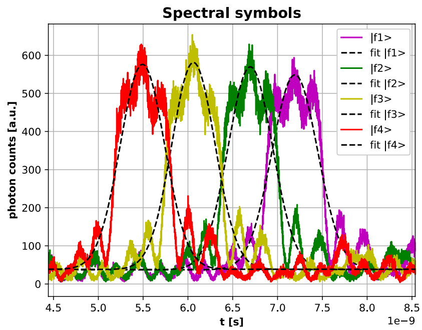

Fig. 2. Spectral pulses (symbols): single photon spectra measured by optical time-stretch technique.

The distributions, measured by high-resolution time- and frequency-resolved single-photon counting present widths and separations which are promising towards the implementation of a 4-dimensional quantum key distribution protocol [2].

Tab. 1. Selected parameters values.

Pulse parameter	**Expected value**	**Measure d value**
Temporal pulse separation	43 ps	41 ps
Temporal pulse width	36 ps	39 ps
Spectral pulse separation	30 pm	29 pm
Spectral pulse width	25 pm	29 pm

The InP photonic integrated circuit is not only compact, energy-efficient, and compatible with fiber optic telecom equipment, but also promising for generating optical pulses of desired properties. Those possibilities can make it meet strict requirements of QKD systems, and therefore become an essential component of secure optical links in future.

Acknowledgments: We acknowledge the NLPQT – National Laboratory for Photonics and Quantum Technologies project, co-financed by the EU under the European Regional Development Fund, as well as funding from the Technical University of Warsaw.

References:

[1] J. Nunn et al., Opt. Express 21, 15959 (2013)

[2] J. Rödiger et. al., Phys. Rev. A 95, 052312 (2017)

[3] S. Pirandola et. al. Adv. Opt. Photon. 12, 1012 (2020)

Quantum Hacking in the Age of Quantum Cryptography – practical issues

M.ŻYCZKOWSKI[1], P. MARKOWSKI[1],

[1]Wojskowa Akademia Techniczna (Kaliski str. 2, 00-908, Warsaw, Poland)
e-mail address: marek.zyczkowski@wat.edu.pl

Cryptography is essential for secure communication in the digital era. Today, public-key cryptography is widely employed, and has provided an efficient method for encrypting content and ensuring both confidentiality and authenticity of electronic communications.
However, the security of these systems is based on assumptions of computational hardness within the constraints of current computing capability. Thus, as quantum computing becomes a reality, public-key algorithms will be genuinely vulnerable to attack. By contrast, quantum cryptography, which is based on quantum physics instead of mathematical assumptions, is able to achieve information-theoretic security.
Advances in practical quantum cryptographic systems have not kept pace with theory, where an eavesdropper can relatively easily exploit loopholes in practical implementations to compromise theory-proved security. Bridging the gap between perfect theory and imperfect practice has become a priority for the growing field of quantum key distribution (QKD) [1], which has strived to strengthen the practical security of QKD systems. Among all the countermeasures against quantum hacking, the measurement-device-independent (MDI) QKD [2] protocol is promising because it is immune to all side-channel attacks on measurement devices. However, the MDI QKD protocol has some limitations that critically restrict its practical usefulness. Technically, the MDI scheme is not compatible with existing QKD systems, and produces a low key rate. In addition, the theory underlying MDI QKD security is based on the use of trusted source stations. Thus, this protocol is not a universal solution. This thesis further investigates the practical security of quantum cryptography in and beyond MDI quantum cryptography.
To overcome the technical limitations of MDI QKD, we first evaluate two other countermeasures against imperfect detections. The first is an industrial patch based on random detection eficiency, recently implemented by ID Quantique in the commercial Clavis2 QKD system. While powerful, experimental testing shows that this countermeasure is not sufficient to defeat the detector blinding attack. The second countermeasure aims to achieve a higher key rate than MDI QKD while maintaining the same security properties. However, our research

shows that detector-device-independent (DDI) QKD security is not equivalent to that of MDI QKD and, further, that DDI QKD is insecure against detector side-channel attacks.

While this initial work points to the superior performance of MDI QKD systems, core challenges remain. The fundamental security assumption adopted for MDI QKD systems, regarding the exclusive use of trustable source stations, cannot always be satisfied in practice.

The work presented here concerns the presentation of practical results of implementing quantum hacking protection methods in QKD circuits [3,4].

The presented work concerns the presentation of practical results of implementation of quantum intrusion protection methods in QKD circuits. Moreover, the results of the research project "Optical technologies of quantum cryptology for data protection in data communication networks" will be presented.

Acknowledgments: This project has received funding from the National Center for Research and Development research and innovation programme under grant agreement DOB-SZAFIR/01/A/013/01/2021

References:

[1] C. H. Bennett and G. Brassard. International Conference on Computers, Systems, and Signal Processing (Bangalore, India), pages 175 -179, 1984.

[2] Y.-L. Tang et. al., Phys. Rev. X, 6:011024, 2016

[3] Y. Zhao et. al., Phys. Rev. A, 78(4) :042333, 2008.

[4] H.-K. Lo et. al., Nat. Photonics, 8:595{604, 2014.

Automatic detection of defects in composite structures by the TDS method

K. KAMIŃSKI[1], N. PAŁKA[1], P. SYNASZKO[2], E. CZERWIŃSKA[1], K. DRAGAN[2]

[1]Institute of Optoelectronics, Military University of Technology, 2 Kaliski Str., 00-908 Warsaw, POLAND
[2]Air Force Institute of Technology, 6 Książe Bolesław Str., 01-494 POLAND
e-mail address: kamil.kaminski@wat.edu.pl

The radiation in the range of about 1 THz (300 μm) is located in poorly "developed" scientifically and technically areas on the border of microwaves and infrared. However, at present, the potential of using this frequency range is more and more noticeable, e.g. to determine the threats and potential defects and damages that may occur, in particular, in composite and hybrid structures used in aviation. These damages can be classified as manufacturing faults and operational damages. The combination of these failures with the load cycles occurring during the operation of aircraft may lead to the formation of critical failures that threaten the safety of further operation. Due to the development of methods for the production of such structures (thermoplastics and out-of-autoclave - OOA) technologies, it is necessary not only to develop new diagnostic methods but also to use data fusion to infer the state of the structure. An important element of the project is the preparation of relevant samples containing damage and manufacturing defects that may occur in such structures (fig. 1) and subjecting them to validation tests.

The paper focuses primarily on the presentation of the aforementioned validation studies obtained with the time domain spectroscopy (TDS) scanner.

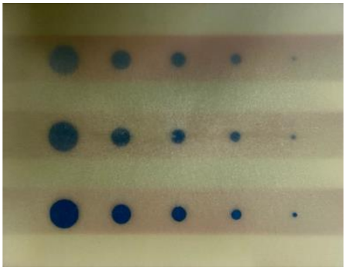

Fig. 1. An example of a sample tested with the use of the TDS scanner

Moreover, an attempt was made to automate the process of analysing the obtained results, using the method of dynamic time wrapping (DTW). This method is used primarily in the situations of comparing two time signals that are out of sync with each other or differ in the speed of the course [1].

For this reason, the authors used the DTW method to automatically compare time signals without defects (reference) and signals potentially containing defects, which then allowed to locate the defects in the tested composite slab and determine the depth of their occurrence, which was illustrated by marking the range of the defect in the tested the sample (fig. 2).

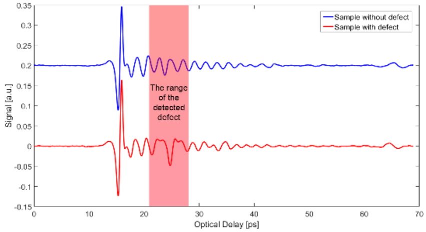

Fig. 2. A-scan of the tested sample with the indication of the defect range detected by the DTW classifier

During the validation studies, the three-dimensional matrices of measurement results were also transformed into two-dimensional matrices, the so-called C-scans, where for each pixel (*x*, *y*) on the surface of the test sample, a single characteristic value (colour) was assigned, revealing the defects (Fig. 3).

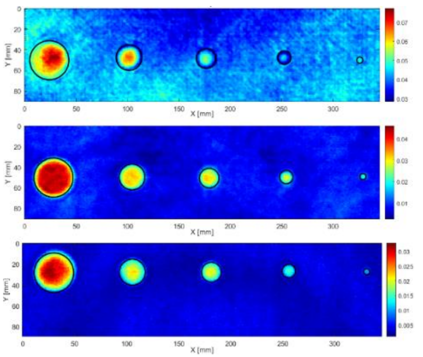

Fig. 3. C-scan of the tested sample

Another way of illustrating the obtained research results was the analysis of the so-called B-scans, which show a cross-section through the tested sample, i.e. a two-dimensional graph, where the ordinate axis shows the time (*t*), which indicates the depth of the defect, and the cut through the sample is selected on the abscissa.

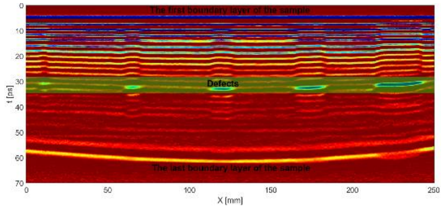

Fig. 4. B-scan of the tested sample

The research results presented in the paper show that the method of time domain spectroscopy is promising for the detection of defects in composite structures, which are commonly used in aviation. In addition, the automation of the results analysis process using the DTW method, undertaken by the authors, effectively accelerated the process of validation studies.

The tests were performed using the Teraview TDS Imaga scanner with the dedicated DataProcess software, as well as the Matlab environment.

Acknowledgments: This work was supported by the National Centre for Research and Development under project DOB-SZAFIR/02/A/001/01/2020.

References:

[1] J. Zhang et. al., Defect identification of layered adhesive structures based on dynamic time warping and simulation analysis, Infrared Physics & Technology, 120, 103943 (2022)

[2] N. Palka et al., Non-destructive evaluation of puncture region in polyethylene composite by terahertz and X-ray radiation, Composites Part B: Engineering, 92 (2016)

The trials of digital data improvement continuously recording by rotational seismometer

B. SAKOWICZ[1], M. KAMIŃSKI[1], M. DUDEK[2], L.R. JAROSZEWICZ[2]

[1]Dep. of Microelectronics and Computer Science, Lodz University of Technology, 221/223 Wółczańska Str., 90-924 Lodz, Poland
[2]Institute of Applied Physics, Military University of Technology, 2 gen. Sylwestra Kaliskiego Str., 00-908 Warsaw, Poland
e-mail address: jarosz@wat.edu.pl

Modern optoelectronics devices use advantage digital systems for data processing directed on deliver reliable information. However, because commonly used DACs have limited accuracy, the same artefacts can be observed in streams of data.

Above situation is general solved by application suitable filtering techniques, which are adequate especially for time independent data, as for example noise investigation of rotational seismographs (see Fig. 1), but for continuum monitoring of same processes can be seriously problem.

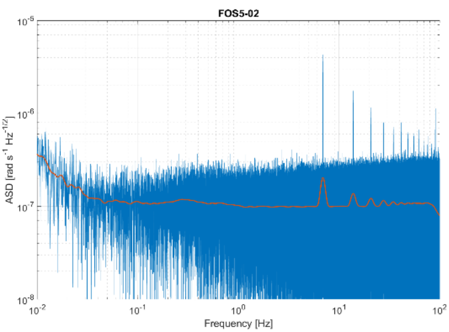

Fig. 1. Amplitude Spectral Density for rotational seismograph FOS5-02: blue line – raw data, red line – data after filtering using a Konno-Ohmachi filter with a smoothing coefficient 40 [1].

Especially for continuum monitoring systems, where existence expected phenomena should be recorded, the automatic start of recording data are critical. For instance such situation exist in seismology during collecting seismic events, where simple procedure for start data collection if signal is higher above same level seems to be reasonable as shown in Fig. 2.

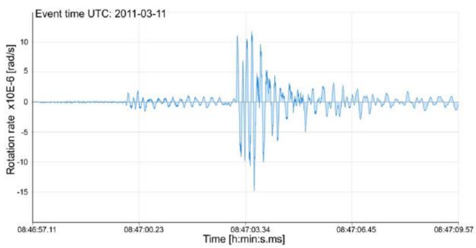

Fig. 2. Proper recorder rotational seismic event by AFORS-1 installed in Książ [2]

However, if ADCs in the electronic part generates artefact (single data with random value over noise level) the above procedure starts recording as is shown in Fig. 3. As one can see it is not proper action, so a

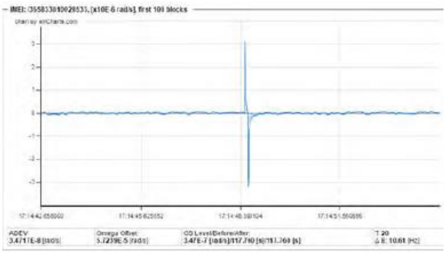

Fig. 3. Seismogram recorded by AFORS-1 for existence artefacts [2].

new more complex algorithm for data collection must be used, for instance such as is shown in Fig. 4, which secures proper elimination given artefacts.

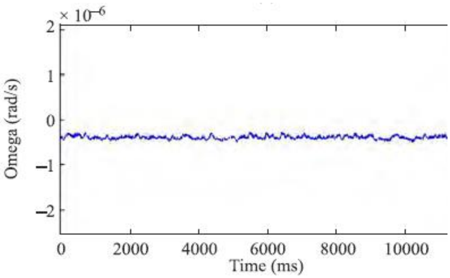

Fig. 4 Seismogram from Fig. 3 after using a new algorithm for artefacts removing [2]

Unfortunately, it is serious problem to proper choice of such algorithms because more complex structure of artifacts or other type imperfections – easy for recognize by eyes can be serious problem. For instance, Fig. 5 presents seismograph re-corded recently in Książ by ours fresh fibre-optic rotational seismograph FOS5-04.

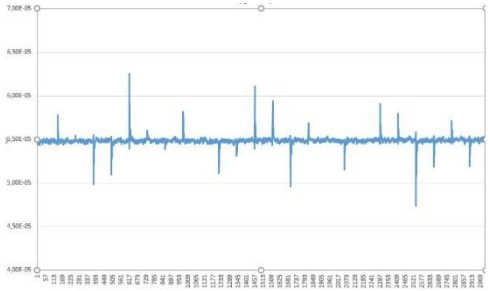

Fig. 5 Seismogram recorded by FOS5-04 with series of unrecognized artefacts.

Ours investigation directed for application the proper algorithm for their removing is still unsatisfactory. The best results shown, so we can with success dumping most of them as is shown in Fig. 6 and Fig. 7 for ASD characteristic,

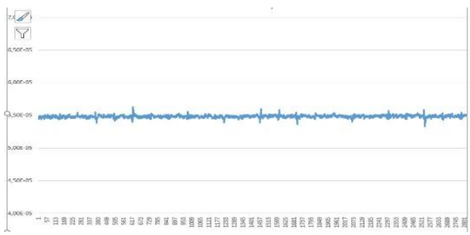

Fig. 6 Seismogram from Fig. 5 after using a recent algorithm for artefacts "dumping"

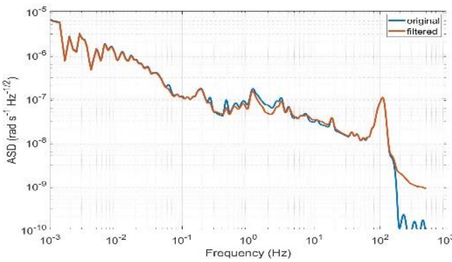

Fig. 7 Compare ASD characteristic for FOS5-04 with and without signal filtering

but for existence seismic event, such approach disturbance their characteristic as is shown for example presented in Fig. 8.

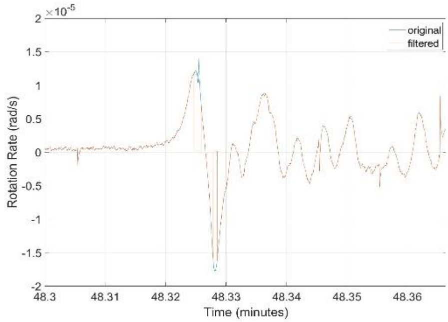

Fig. 8. Seismogram with rotational events and their disturbance by artefacts filtering.

Acknowledgments: This work was supported by GBMON/13-995/2018/WAT.

References:

[1] K. Teisseyre et al., Sensors, 21, (2021)
[2] A, Kurzych et al., Opto-Electron. Rev., 24, 3, (2016)

Nanodiamonds for sensing of magnetic fields, and more…

A.M. WOJCIECHOWSKI, M. MRÓZEK, M. JANI, T. KOŁODZIEJ, A. EBRAHIMI, S. SENGOTTUVEL, P. CZARNECKA, Z. ORZECHOWSKA, AND W. GAWLIK

M. Smoluchowski Institute of Physics, Jagiellonian University in Kraków, Łojasiewicza 11, 30-048 Kraków, Poland
e-mail address: a.wojciechowski@uj.edu.pl

The negatively charged Nitrogen-Vacancy (NV) color center in diamond lattice is a prominent quantum system commonly used as a sensor for the detection and imaging of magnetic and electric fields, temperature, strain, and pressure in micro- and nano-scale. For spatial mapping of the magnetic field, either a bulk diamond with a very thin NV layer is typically used or a small diamond probe is scanned just above the sample. Both methods require a smooth sample surface and the closest achievable proximity of the probing device. The latter is often limiting the sensing capabilities. We propose an alternative approach to sensing and mapping, based on the use of nanodiamond (ND) layers that can be directly deposited on a given material surface [1].

We investigate, so called, optically detected magnetic resonance (ODMR) signals with arbitrarily spatially oriented NDs and aim to use the wide-field microscopy for fast magnetic imaging and sensing. In addition, we study the NDs deposited at the facet of an imaging fiber bundle that may find applications in a high resolution endoscopic magnetic imaging [2]. Our approach can also be extended to the deposition on irregular surfaces, which shows a promising path to nanodiamond-based photonic sensors.

Furthermore, we demonstrate optical fibers with NDs embedded inside glass structures [3]. By recording strong ODMR signals, we show that such sensors can be very effective for sensing applications.

Finally, we discuss applications of NDs for biochemical and biophysical studies. We demonstrate the influence of surface termination and local environment on the spin properties [4,5] of NV centers inside NDs. Combining fluorescence microscopy and ODMR techniques, we also demonstrate local probing within living biological cells.

Acknowledgments: This work was supported by the Foundation for Polish Science under QUNNA project within the TEAM-NET Program (grant agreement POIR.04.04.00-00-1644/18).

References:

[1] A. M. Wojciechowski et al., Materials 12, 2951 (2019)

[2] P. Czarnecka et al., Opt. Mater. Express 12 444-457 (2022)

[3] Z. Orzechowska et al., Adv. Quantum Technol. (accepted), arXiv:2110.0813

[4] M. Mrózek et al., Materials 14, 833 (2021)

[5] M. Mrozek et al., Diam. Relat. Mater. 120, 108689 (2021)

Opto-magnetic fiber probes and magnetic field sensing based on negatively charged nitrogen-vacancy centers in nanodiamonds

A. FILIPKOWSKI[1,2], M. MRÓZEK[3], G. STĘPNIEWSKI[1,2], T. KARPATE[1], M. GŁOWACKI[4], M. FICEK[4], W. GAWLIK[3], R. BUCZYŃSKI[1,2], A. WOJCIECHOWSKI[3], R. BOGDANOWICZ[4], M. KLIMCZAK[1]

[1] University of Warsaw, Faculty of Physics, Pasteura 5, 02-093 Warsaw, Poland
[2] Łukasiewicz Research Network Institute of Electronic Materials Technology, Wólczyńska 133, 01-919 Warsaw, Poland
[3] Institute of Physics, Jagiellonian University in Kraków, Łojasiewicza 11, Kraków, 30-348 Poland
[4] Faculty of Electronics, Telecommunications and Informatics, Gdańsk University of Technology, Narutowicza 11/12, Gdańsk, 80-233 Poland
e-mail address: adam.filipkowski@fuw.edu.pl

Integration of nitrogen-vacancy centers-containing nanodiamonds (ND) with optical fibers is a broad group of powerful techniques for scaling of ND magnetic sensing and single-photon source functionalities. Implementations involving fiber tip or fiber taper functionalization with NDs enable ultra-sensitive and highly localized magnetic sensing [1,2]. Distributed, highly sensitive magnetic field detection can be realized with NDs incorporated directly into the fiber core [3,4]. We demonstrate a new approach for incorporation of NDs with nitrogen vacancy centers into an optical fiber by multiple stacking of hundreds of nanodiamond-coated glass canes in the fiber core. The fabricated fiber has an external diameter of 125 µm and the core diameter is 50 µm. During the drawing, the diameter of the fully fused canes in the core stack was decreased to less than 2 µm. Images of the fiber are shown in Fig. 1. Due to low refractive index contrast, the core area is indistinctive from the cladding under a scanning electron microscope, but it was observable under a standard optical microscope. The mode field of the red fluorescence of NV^- color centers, filtered with a high-pass filter to cut the 532 nm laser pump is also shown.

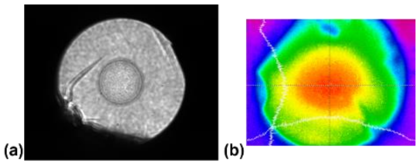

Fig. 1. Nanodiamond-doped fiber: (a) optical microscope image of the fiber, (b) mode field image over a red high-pass filter.

In contrast to previous ND-doped fiber demonstrations and owing to this methodology [3,4], we arrive at the following achievements: (1) careful adjustment of drawing conditions enabled fully fused core without air inclusions neither in the core nor at the core-cladding interface, (2) nanodiamond agglomeration is avoided and uniform longitudinal and transverse plane diamond distribution is obtained, confirmed with confocal microscopy, (3) the multi-step drawing procedure does not impair magnetic sensitivity of the fiber – to the contrary: both ODMR and microwave-free B-field measurement results are demonstrated with 60 cm long fiber samples and the NV^{-} fluorescence is excited and collected over a >20cm long fiber section in every case.

The ND distribution in the fiber core was evaluated using confocal microscopy and by measurements of the distances between the directly adjacent ND pairs along the fiber obtained from 7 samples. Fig. 2 shows histograms obtained for two cases: computed either along the longitudinal or transverse planes of the examined fiber samples. In the longitudinal plane, the major observed share of ND particle pairs are separated by between 12 µm and 29 µm. Diamond-to-diamond separations outside of this range are also observed, but with smaller contribution to the histogram. In the transverse plane, the ND separation of roughly 1.5-2.2 µm dominates, which almost ideally corresponds to the lower than 2 µm diameter of the estimated individual cane diameter in the final fiber core.

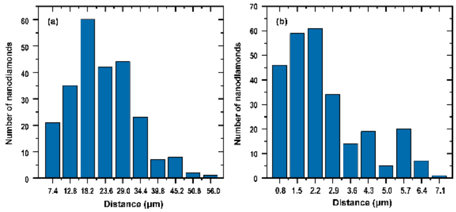

Fig. 2. Histograms of separations between adjacent nanodiamonds: (a) along the optical fiber and: (b) across the fiber core.

The developed fiber was tested in two magnetic sensitivity experiments. In one scenario the fiber was spun on a microwave antenna and optically detected magnetic resonance was measured with readout contrast of up to 1.3%, which was scalable with and limited by the coverage of the fiber by the antenna. In the second test experiment, we measured the NV^{-} fluorescence intensity change in a 35 mT dynamics range of magnetic flux density from an electromagnet. This successful demonstration confirms technological feasibility for manual control of agglomeration-free and air inclusion-free nanodiamond distribution at arbitrarily defined transverse layouts (i.e. single core, multicore or arbitrary core-cladding interface) of a new class of magnetically sensitive fibers.

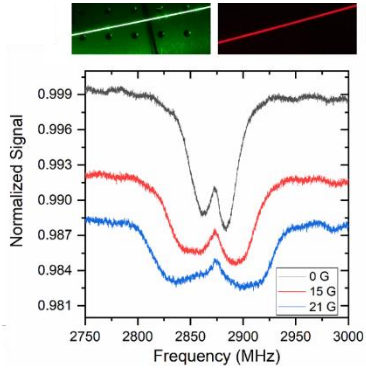

Fig. 3. Typical ODMR spectra collected from the ND-doped fiber, visible fluorescence of the fiber: the 532 nm pump laser, red light: high-pass filtered NV^{-} color center fluorescence.

Acknowledgments: Foundation for Polish Science, TEAM NET POIR.04.04.00-00-1644/18.

References:

[1] I. V. Fedotov et al. Optics Letters 41, 472 (2016).

[2] R. N. Patel et al. Light: Science & Applications 5, e16032 (2016).

[3] D. Bai et al. APL Materials 8, 081102

(2020)

Implementation of nanodiamonds to enhance the sensing properties of fiber optic sensors

M. JANIK[1,2,*], M. FICEK[1], M. SAWCZAK[3], M. ŚMIETANA[2], R. BOGDANOWICZ[1]

1Department of Metrology and Optoelectronics, Faculty of Electronics, Telecommunications and Informatics, Gdańsk University of Technology, 11/12 Gabriela Narutowicza St.,
80-233 Gdańsk, Poland
2Warsaw University of Technology, Institute of Microelectronics and Optoelectronics, Koszykowa 75, 00-662 Warsaw, Poland;
3 The Centre for Plasma and Laser Engineering, The Szewalski Institute of Fluid-Flow Machinery, Polish Academy of Sciences, 14 Fiszera St., 80-231 Gdańsk, Poland
situtution/Company Name,
e-mail address: monika.janik@pg.edu.pl

In the past few years, a variety of new fields for the use of nanoscale diamonds have emerged. Except for diamonds' properties such as high hardness, or thermal conductivity, there is also a strong interest in other properties of diamond: color centers (defects in their crystal lattice) and their surface structure/chemistry [1]. Both opened a broad range of applications in magnetometry, single-photon generation, biological systems, electronics, or sensing technology. To take advantage of all the diamonds' properties, they should be integrated with other photonic structures.

In this work, NV-rich diamond particles have been integrated with the optical fiber sensor – microcavity in-line Mach-Zehnder interferometer (µIMZI) creating a dual-mode interrogation platform. A set of cylindrical microcavities (diameter 54 µm, depth 62.5 µm) were micromachined with a femtosecond laser in a single-mode optical fiber forming µIMZI sensing structure as described in [2]. The suspension of the 40, 140, and 750 nm (avg. particle size) nanodiamonds (ADAMAS nano) in DI water in a concentration of 1 mg/mL (0.1% w/v) have been prepared and deposited within a set of µIMZIs. Each nanodiamonds deposition has been followed by extensive washing in water and methanol to check the stability of the deposited nanodiamonds layer. The changes in sensitivity of the sensor after each deposition has been evaluated tracing the optical transmission spectrum of the µIMZI in water and solutions with different refractive indices. Moreover, the efficiency of nanodiamonds fluorescence coupling was also studied. The fluorescence signal originated from deposited nanodiamonds' NV^- centers excited with a laser beam at the end of the fiber was analyzed in two ways from the top of the microcavity and the end of the fiber. Due to carboxylic groups present at the nanodiamonds surface, the detection of model protein – bovine serum albumin – has been tested as a part of preliminary dual-mode biosensing studies. The nanodiamond-functionalized sensor was incubated with three different concentrations of the protein for 45 min. Each incubation was followed by extensive washing to obtain the reference results. The protein binding process was interrogated by tracing the µIMZI transmission minimum as well as changes of the fluorescence signal of the deposited nanodiamonds.

It was found that the nanodiamond-functionalized µIMZI enabled dual-mode detection of protein. The nanodiamonds layer was stable over the course of the experiments and provide a strong and stable fluorescence signal which could be detected from both the top of the microcavity as well as from the end of the fiber. What is more, nanodiamonds layer greatly enhanced the surface sensitivity of the µIMZI. Thanks to the rich chemistry of the nanodiamond surface it was possible to detect the chosen protein without any additional chemical functionalization of the sensor's surface which greatly simplifies the sensing procedure.

Acknowledgments: This work was supported by the TEAM-NET program of the Foundation for Polish Science co-financed by the European Union under the European Regional Development Fund QUNNA POIR.04.04.00-00-1644/18.

References:

[1] N. Nunn et al., *Curr. Opin. Solid State Mater. Sci.* 21, 1, pp. 1–9, (2017)

[2] M. Janik et al. *IEEE Sens. J.* 17, 11, pp. 3316–3322 (2017)

Silicon nitride as a new mirror in fiber optic sensors

S. PAWŁOWSKA[1],

[1]. Department of Metrology and Optoelectronics, Faculty of Electronics, Telecommunications and Informatics, Gdansk University of Technology, 11/12 Narutowicza Street, 80-233 Gdansk, Poland
e-mail address: sandra.pawlowska@pg.edu.pl

Mirrors are used in optical sensors and measurement setups [1]. This creates a demand for mirrors made of new materials [2, 3] and having various properties tailored to specific applications [4, 5]. In this work, we propose silicon covered with a thin silicon nitride layer as a mirror for near-infrared measurements [6, 7]. SiN layer was deposited on a standard silicon wafer with a Low-Pressure Chemical Vapor Deposition furnace. Then, the created layer was investigated using ellipsometry and scanning electron microscope. Subsequently, the mirror was used as a reflecting surface in a Fabry-Perot fiber-optic interferometer. The mirror performance was investigated for wavelengths used in telecomunication 1310 nm and 1550 nm [8] and then compared with results obtained with the same measurement setup, with a silver mirror [9] instead of silicon covered with SiN, as reference. Results showed that the proposed mirror can replace the silver one with satisfying results for investigated wavelengths.[10,11]

Acknowledgments: This work was supported by the DS programs of Faculty of Electronics, Telecommunications and Informatics of Gdańsk University of Technology for the support. Financial support of these studies from Gdańsk University of Technology by the DEC-11/2020/IDUB/I.3/CC grant under the Curium - Combating Coronavirus, DEC-1/2021/IDUB/II.2/Np grant uder NEPTUNIUM Enhancing Baltic Region Research Cooperation and DEC-8/2020/IDUB/III.4.1/Tc grant under the Technetium Talent Management Grants - 'Excellence Initiative - Research University' program is gratefully acknowledged.

References:

[1] T. Ștefanov et al. Journal of Non-Crystalline Solids: X 7, 100050, (2020).
[2] M. Jędrzejewska-Szczerska et al. Sensors and Actuators A: Physical, 221, (2015).
[3] M. Kosowska et al. Diamods and related materials, (2020).
[4] M. Jędrzejwska-Szczerska, Sensors, 14, 4, (2014).
[5] M. Hirsch et al. Sensors and Actuators A: Physical, 298, (2019).
[6] X.Wang et al. Appl. Opt. 56, 4113, (2017).
[7] J. Steinlechner et al. Precision Metrology and Sensing. Phys. Rev. Lett. 120, 263602, (2018).
[8] R. Phillips, L. Book Rvw: Fiber Optic Communications. By Joseph C. Palais. Opt. Eng. 32, 3338, (1993).
[9] M. Boccas et al. Thin Solid Films 502, 275–280, (2006).
[10] S. Pawłowska et al. Scientific Reports, (2021).
[11] J. Gierowski et al. Photonics Letter of Poland, (2021).

Boron-doped carbon nanowalls for sensing application

M. FICEK[1], K.J. SANKARAN[2], P. NIEDZIAŁKOWSKI[3], M. PIERPAOLI[1], P. JAKÓBCZYK[1], R. BOGDANOWICZ[1]

[1]Department of Metrology and Optoelectronics, Faculty of Electronics, Telecommunications and Informatics, Gdansk University of Technology, 80-233 Gdansk, Poland
[2]CSIR-Institute of Minerals and Materials Technology, Bhubaneswar 751013, India
[3]Department of Analytical Chemistry, Faculty of Chemistry, University of Gdansk, 63 Wita Stwosza St., 80-308 Gdansk, Poland
e-mail address: matficek@pg.edu.pl

Sensing applications are achieved in boron-doped carbon nanowalls (B:CNW) grown in a single-step chemical vapor deposition process co-doped with boron and nitrogen [1]. The structure consists of sharp, highly conductive graphene edges supplied by a solid, diamond-rich bottom. The Raman and transmission electron microscopy studies reveal a hybrid nature of sp^3-diamond and sp^2-graphene in these nanowalls. The B:CNW samples were deposited by the microwave plasma assisted CVD using a gas mixture consisting of H_2, CH_4, B_2H_6 and N_2. Growth results in flat and long carbon nanowalls rich in sp^2 as well as sp^3 hybridized phases. The SEM analysis, Raman spectroscopy, and electrochemical properties were particularly presented [3,4].

B:CNW have attracted much attention for numerous applications in electrical devices because of their peculiar structural characteristics. However, it is possible to set synthesis parameters to vary the electrical and optical properties of such B:CNW. We demonstrate the direct growth of highly transparent boron-doped nanowalls (B-CNWs) on optical grade fused silica glass. The effect of growth temperature and boron doping on the behavior of B:CNW was studied in particular. Temperature and boron inclusion doping level allow for direct tuning of B:CNW morphology [4]. It is possible to operate with both parameters to change the optical and electrical parameters; however, boron doping is a preferred factor to maintain the transparency in the visible region, while a higher growth temperature is more effective to improve conductance. Light transmittance and electrical conductivity are mainly influenced by growth temperature and then by boron doping. Tailoring B:CNW has important implications for potential applications of such electrically conductive transparent electrodes.

Acknowledgments: The authors gratefully acknowledge financial support of the Foundation for Polish Science under the project Team-NET No. POIR.04.04.00-00-1644/18.

References:

[1] M. Ficek et. al., Advanced Materials Interfaces 8, 20, (2021)
[2] K.J. Sankaran et. al., Nanoscale 10, 3, (2018)
[3] K. Siuzdak et. al., ACS applied materials & interfaces 9, 15, (2017)
[4] M. Pierpaoli et. al., Materials 12, 3, (2019)

High-performance optical frequency comb sources

A. M. HEIDT, P. HÄNZI, B. SIERRO, D. SPANGENBERG, AND A. RAMPUR

University of Bern, Institute of Applied Physics, Sidlerstrasse 5, 3012, Bern, Switzerland
e-mail address: alexander.heidt@unibe.ch

The low-noise and phase-coherent nonlinear transformation of a narrowband laser into a broadband supercontinuum in an optical fiber forms the basis for optical frequency comb (OFC) technology. New hybrid fiber designs based on silica and silicon materials enable OFCs with unprecedented amplitude and phase stability that form building blocks of new technology, ranging from advanced medical diagnosis to high-speed coherent communications and photonic computers [1, 2].

Acknowledgments: Swiss National Science Foundation (SNSF), PCEFP2_181222.

References:

[1] B. Sierro et al., "Reducing the noise of fiber supercontinuum sources to its limits by exploiting cascaded soliton and wave-breaking nonlinear dynamics," Optica (in press).
[2] R. Sohanpal et al., "Parametric frequency comb generation using silicon core fiber," 2021 Optical Fiber Communications Conference and Exhibition (OFC), 2021.

Machine learning for resolution increase of refractive index measurements

M. SZCZERSKA[1], P. RUDNICKI[2], M. KOSOWSKA[2], A. DRABIK-KRUCZKOWSKA[3], M. KRUCZKOWSKI[2]

[1] Department of Metrology and Optoelectronics, Faculty of Electronics, Telecommunications and Informatics, Gdańsk University of Technology, 11/12 Narutowicza Street, 80-233 Gdańsk, Poland

[2] Faculty of Telecommunications, Computer Science and Electrical Engineering, Bydgoszcz University of Science and Technology, Al. prof. S. Kaliskiego 7, 85-796 Bydgoszcz, Poland

[3] Department of Obstetrics, Gynaecology and Oncology, Faculty of Medicine, Collegium Medicum in Bydgoszcz, Nicolaus Copernicus University in Toruń, 85-094 Bydgoszcz, Poland

e-mail address: *malszcze@pg.edu.pl* ch

Refractive index is one of the most important parameters describing materials, creating the need for development of methods allowing its precise determination. However, the materials needed for measurements are not always available or the obtainedresults are characterized by low resolution. Hence, we present an approach applying machine learning based on a regression model to increase the resolution of the refractive index measurements carried out by a fiber-optic interferometric sensor. The solution includes data pre-processing (filtering, data enrichment, feature extraction and mapping) leading to obtaining feature vectors. The obtained datasets are used for machine learning. The results of cross-validation show scores of 0.99 for the training and validations sets, the maximum standard deviation reached only 0.01 proving a high accuracy of the model predictions. The model was then used with new data to create data mimicking the experimental signals for samples that were not possible to measure in the laboratory, hence, extending the resolution of acquired results. This could be crucial for increasing efficiency of tissue recognition based on refractive index measurements due to greater accuracy of data. The original, experimental data points are overlapping with the predicted results meaning that the adopted model works correctly.

The node-values are in accordance for the measured samples, we can predict the refractive index values of various liquids within the measurement range, even those that were not measured during the experiment. With the machine learning algorithm we can generate data mimicking the experimental signals and predict their values which leads to a great increase of the results resolution. This method can be used for generation of unlimited learning and testing datasets for other machine learning methods, saving the measurement sets for the final tests of the developed models.

Acknowledgments: This work was supported by the Gdańsk University of Technology by 4/2020/IDUB/III.4.1/Tc grant under the - Technetium EIRU program, by 11/2020/IDUB/I.3/CC grant under the combating coronavirus – EIRU, and the DS funds of Faculty of Electronics, Telecommunications and Informatics of Gdańsk University of Technology. DS funds 16th INTEGRATED OPTICS - SENSORS, SENSING STRUCTURES and METHODS, IOS'2022 2 of Faculty of Telecommunication, Informatics and Electronics of Bydgoszcz University of Science and Technology are also acknowledged.

References: [1] M. Kosowska et al. Materials, 12(13), 2019, 10.3390/ma12132124.
[2] M. Hirsch et al. Sensors and Actuators A: Physical, 298, 111594, 2019, 10.1016/j.sna.2019.111594.
[3] Z. Shahbazi et al. Symmetry, 12(9), 2020, 10.3390/sym12091566.
[4] X. Zhang et al., J Healthc Inform Res, 4, p.383–394, 2020, 10.1007/s41666-020-00077-1

Electrically-driven LC:PDMS microstructures for integrated optics applications

K.A. RUTKOWSKA[1], P. SOBOTKA[1], SZ. BACZYŃSKI[1], M. GROM[1], A. DYBKO[2], K. MARCHLEWICZ[2], M. JUCHNIEWICZ[3]

[1]Faculty of Physics, Warsaw University of Technology, Warsaw, Poland,
[2]Faculty of Chemistry, Warsaw University of Technology, Warsaw, Poland,
[3]Center o Advanced Materials and Technologies (CEZAMAT), Warsaw University of Technology, Warsaw Poland.
e-mail address: Katarzyna.Rutkowska@pw.edu.pl

Polydimethylsiloxane (PDMS) is a high-quality organic material for micro-and optofluidic functional systems [1]. PDMS-based photonic devices are typically fabricated using a cast-molding technique. In this way, complex and advanced microstructures can be successfully obtained at a much lower cost when compared to traditional glass or semiconductor components for integrated systems. Additionally, the air channels in PDMS structures can be easily infiltrated with liquid crystalline materials. The latter are highly anisotropic materials with optical properties straightforwardly tuned by external electric fields [2]. Exploiting such birefringent media may lead to intriguing phenomena with numerous potential applications. However, when implementing LC:PDMS structures in practice, one must remember that their functionality depends strongly on the LC molecular arrangement. Therefore, anchoring conditions on PDMS surfaces should be identified [3].

This communication shows several designs and practical realizations of electrically-driven LC:PDMS microstructures. In addition, different cheap and efficient methods for their fabrication are presented [4]. The results of numerical simulations for electric field steering and the possibility of eutectic liquid electrodes application are analyzed.

Acknowledgments: This work was supported by the FOTECH-1 project "Electrically-driven waveguiding systems in LC:PDMS structures" granted by the Warsaw University of Technology under the program Excellence Initiative: Research University (ID-UB).

References:

[1] A.R. Hawkins, H. Schmidt, Handbook of Optofluidics, CRC Press (2010).
[2] K.A. Rutkowska, T.R. Woliński, R. Asquini, L. Civita, L. Martini, A. d'Alessandro, Phot. Lett. Poland 9(2), 48 (2017).
[3] S. Baczyński, P. Sobotka, K. Marchlewicz, M. Słowikowski, M. Juchniewicz, A. Dybko, K.A. Rutkowska, Appl. Sci. 11, 11593 (2021).
[4] S. Baczyński, P. Sobotka, K. Marchlewicz, A. Dybko, K. Rutkowska, Phot. Lett. Poland 12(1), 22 (2020)

Optimizing up-conversion emission in the fluoroindate glasses for biomedical applications

G. L. JIMÉNEZ[1], B. STARZYK[1], M. LESNIAK[1], M. KOCHANOWICZ[2], AND D. DOROSZ[1]

[1]AGH University of Science and Technology, aleja Adama Mickiewicza 30, 30-059, Kraków, Poland
[2]Bialystok University of Technology, Wiejska 45A, 15-351 Białystok, Poland
e-mail address: glesly@agh.edu.pl

Lanthanide up-conversion nanoparticles (UCNPs) have been attracted a huge interest because of their potential use in a wide variety of applications ranging from biomedical to technological applications, because of their ability to convert low energy light, typically in the near-infrared range (NIR), into higher energy visible emission (UV-vis) [1]. Such ability allows their use as light transducers to activate indirectly opsins, proteins utilized in optogenetics to manipulate the neural activity with high specificity and temporal resolution [2–4].

However, this technology needs to overcome some challenges like its photon-converting efficiency, light stimulation pattern, NIR heating effect, and control the cellular localization.

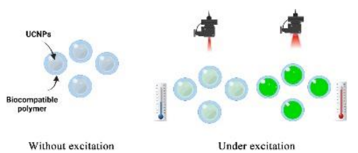

Fig. 1. UCNPs excited using different power.

The present work investigates the UP-converted emission of fluoroindate glasses (FIG) dopped with different lanthanides utilizing melting – quenching technique. The sensitizers used were ytterbium and neodymium in order to be able to stimulate the activators using 980 and 808 nm. The results showed that particles sensitized with YbF_3 have an excellent emission, for that reason, the low power of the source is required avoiding the particles overheating. On the other hand, the particles doped with NdF_3 requires higher power excitation.

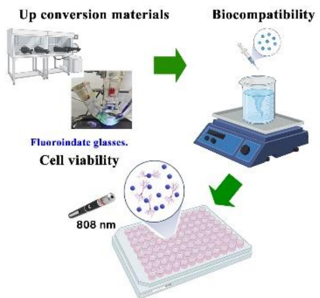

Fig. 2. Synthesis and functionalization of UCNPs with high biocompatibility.

According to these results, it is important to evaluate the heating of the particles suspended in water under different excitation power in order to determine the advantages and disadvantages of each one.

Acknowledgments: This work was supported by the National Science Centre (Poland) granted on the basis of the decision No. 2017/25/B/ST8/02530 and partly by „Excellence initiative – research university" for the AGH University of Science and Technology".

References:

[1] Zhang, Z., Han, Q., Lau, J. W. & Xing, B., *ACS Mater. Lett.* **2**, 1516–1531 (2020).

[2] Lin, X. *et al.* , *Adv. Healthc. Mater.* **6**, 1–11 (2017).

[3] Ao, Y. *et al., ACS Nano* **13**, 3373–3386 (2019).

[4] Wen, S. *et al.*, *Nat. Commun.* **9**, (2018).

Nanocomposite glasses and optical fibers for optical sensing applications

K.CZAJKOWSKI[1], K. SADOWSKA[1], M. LEŚNIAK[2], D. DOROSZ[2], J. DOROSZ[1], M.KOCHANOWICZ[1], P. MILUSKI[1], J. ŻMOJDA[1]

[1]Bialystok University of Technology, Wiejska 45D Street, 15-351 Bialystok, POLAND
[2]AGH University of Science and Technology, 30 Mickiewicza av. Kraków, POLAND
e-mail address: j.zmojda@pb.edu.pl

Nanophotonics is now a rapidly growing interdisciplinary field of science, mainly due to the unique properties of optical waveguide structures with nanoparticles, obtained as a result of their interaction with photons. The most advanced systems are found in the currently used waveguide structures, characterized by sophisticated optical properties and excellent thermal stability parameters required in modern nanostructured optical fiber technology. Therefore, the design of novel nanocomposite materials requires an interdisciplinary approach to combine fields of materials engineering, chemistry, and photonics.

Among possible ways to manage the optical properties of photonic materials, the technology of nanocomposite glasses containing noble metal nanoparticles opens new fields to develop the sensing structures based on LSPR (Localized Surface Plasmon Resonance) [1-4]. According to the local field enhancement phenomenon, we can design an optical sensor for the detection of single molecules of pathogens or chemical pollution [5]. Thus, nanocomposite optical fibers are highly required sensing structures on *lab-on-fiber* or *lab-on-chip* technology for many applications [6].

Another interesting aspect in photonic nanostructures is the technology of glass-ceramic optical fibers. In this case, the rod of fiber is made by modification of matrix by nucleation agents, which leads to partial crystallization of glass, and the transparency remains still relatively high. Moreover, glass-ceramic optical fibers can outperform their traditional glass counterparts in terms of available emission spectral range, quantum efficiency, fabricated sensors sensitivity, and other parameters [7].

In our work, we show the technology of nanocomposite glasses and optical fibers defined as nanostructured glass-fibers doped with metallic nanoparticles, and glass-ceramics optical fibers, manufactured in Bialystok University of Technology. Also, the luminescent properties of fabricated waveguide structures were analyzed in detail. All presented solutions may be used as an active element of the sensing structure.

Acknowledgments: The work was supported by National Center of Science granted on the basis of the decision No. DEC-2019/35/O/ST5/03105.

References:

[1] S. Kuzman, et al., Materials 13, 3071 (2020).
[2] V. P. Prakashan, et al., Plasmonics 14, 673-683 (2019).
[3] J. Zmojda, M. Kochanowicz, P. Miluski et al., Journal of Molecular Structure 1160, 428-433 (2018).
[4] J. Zmojda, P. Miluski, M. Kochanowicz, Applied Sciences 8, 790 (2018).
[5] Y. Tian, W. Wang, N. Wu, X. Zou, X. Wang, Sensors 11, 3780 (2011).
[6] M. Pisco A. Cusano, Sensors 20, 4705 (2020).
[7] A. Veber, et al., Fibers 7, 105 (2019).

Investigation of the luminescent properties of nanophosphors co-doped with lanthanide ions for biological sensing

K. SADOWSKA[1], P. AWRAMIUK[1], K. GRYKO[2], M. KALINOWSKA[2], J. ŻMOJDA[1]

[1]Bialystok University of Technology, Faculty of Electrical Engineering, Wiejska 45D Street, 15-351 Bialystok, POLAND
[2]Bialystok University of Technology, Faculty of Civil Engineering and Environmental Sciences, Wiejska 45E Street, 15-351 Bialystok, POLAND
e-mail address: k.sadowska@doktoranci.pb.edu.pl

Currently, nanophoshors are widely used in many fields, as a new-generation tool for fluorescence imaging and sensing, drug delivery [1-4]. Especially, fluorescent nanoparticles can efficiently act as emission sources in many biological applications, such as *in vivo* imaging, ultra-sensitive bioassays and photodynamic therapy [5].

In this work, the coprecipitation method is presented as a technology to fabricate $LaPO_4$ nanophosphors, which are characterized by emission of radiation in the first (650 nm - 950 nm) and second (950 nm - 1400 nm) therapeutic windows. The possibilities of shaping the emission spectra depending on the type of active dopant, excitation wavelength and possible energy transfer mechanisms are discussed. Lanthanide ions such as europium, neodymium and ytterbium were used in the study.

By obtaining luminescence measurements for three concentrations of active dopants, the most satisfactory results were selected to make co-doped samples. The highest luminescence spectra of $LaPO_4:Eu^{3+}$ and $LaPO_4:Yb^{3+}$ were observed at concentrations of 5 mol% Eu_2O_3 and 5 mol% Yb_2O_3. In the case of $LaPO_4:Nd^{3+}$, the highest luminescence spectra was obtained for 2 mol% Nd_2O_3.

In order to obtain a wide emission band in the 1st biological window, the elements were combined in 2%Nd_2O_3/5%Eu_2O_3 system. Fig. 1 presents the luminescence spectra of fabricated $LaPO_4$ nanophosphor co-doped with europium and neodymium ions. It is worth to noticed that, efficient energy transfer between $Eu^{3+} \rightarrow Nd^{3+}$ leads to the emission at two separate bands at 700 nm (Eu^{3+}: $^5D_0 \rightarrow {}^7F_4$) and at 900nm ($Nd^{3+}$: $^4F_{3/2} \rightarrow {}^4I_{9/2}$) under laser excitation at the wavelength of 395 nm.

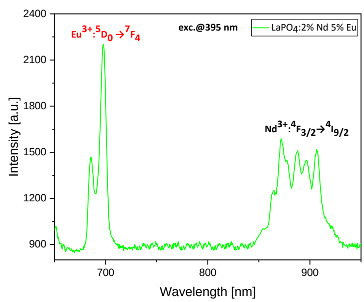

Fig. 1 Luminescence spectra of $LaPO_4$ co-doped with Eu^{3+} and Nd^{3+}.

In order to analyze the possible multi-wavelength emission in 2nd therapeutic window, also we fabricated $LaPO_4$ nanophosphor co-doped with europium, neodymium and ytterbium. Fig. 2 shows the luminescence spectra of co-doped $LaPO_4$ at the range from 950 nm to 1100 nm resulting from the laser excitation at 395 nm.

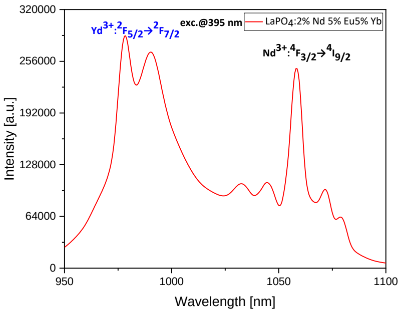

Fig. 2 Luminescence spectra of $LaPO_4$ co-doped with Eu^{3+}, Nd^{3+} and Yb^{3+} ions

As a result of the energy transfer in the transition route Eu→Nd→Yb, we observed wide and strong emission in the main two bands at 980 nm and at 1064 nm originated from $^2F_{5/2}\longrightarrow{}^2F_{7/2}$ for Yb^{3+} ions and $^4F_{3/2}\longrightarrow{}^4I_{11/2}$ for Nd^{3+} ions, respectively.

Acknowledgments: The work was supported by Bialystok University of Technology granted on the basis of the decision No. WI/WE-IA/2/2021.

References:

[1] Y. Kang et al., Scientific Reports 7, 1, (2017).
[2] Q. Shen et al., Journal of Luminescence, 225 (2020).
[3] S.K. Gupta et al., RSC Advances 5, 72, (2015).
[4] Y. Duan et al., Adv. Mater. 30, 47, (2018).
[5] D. Jaque, F. Vetrone, Nanoscale 4 (15), 4301 (2012).

Polarization maintaining nanostructured single-mode optical fiber with artificial anisotropy

A. ANUSZKIEWICZ[1,2], M. BOUET[3], D. MICHALIK[1,4], G. STEPNIEWSKI[1,4], R. KASZTELANIC[1,4], A. FILIPKOWSKI[1,4], D. PYSZ[1], A. CASSEZ[3], M. KLIMCZAK[4], G. BOUWMANS[3], A. MUSSOT[3], R. BUCZYNSKI[1,4]

[1]Łukasiewicz Research Network-Institute of Microelectronics and Photonics, Photonic Materials Group, Al. Lotnikow 32/46, 02-668 Warsaw, Poland
[2]Warsaw University of Technology, Faculty of Electronics and Information Technology, Institute of Electronic Systems, Nowowiejska 15/19, 00-665 Warsaw, Poland
[3]Univ-Lille, CNRS, UMR 8523-PhLAM-Physique des Lasers Atomes et Molécules, F-59000 Lille, France
[4]University of Warsaw, Faculty of Physics, Pasteura 5, 02-093 Warsaw, Poland
e-mail address: alicja.anuszkiewicz@imif.lukasiewicz.gov.pl)

The polarization maintaining (PM) optical fibers are required for many applications, thus numerous fiber designs, i.e. based on stress-applying zones in the cladding, core ellipticity or cladding asymmetry in microstructured fibers have been already proposed. Such a designs ensure isolation between orthogonal components of the fundamental mode, thus random coupling between them is minimized.

The designs presented above have however some drawbacks. The fibers with stress induced birefringence, such as PANDA or bow-tie, have stress zones in the cladding, placed far from the core to preserve circular mode shape. In result, the diameters of these fibers are bigger than 125 µm. Elliptical core fibers suffer from elliptical mode shape, which causes high coupling losses of joints with standard circular core fibers. What is more, their birefringence is very small ($<<10^{-5}$ at 1550 nm). Microstructured fibers are versatile in terms of shaping their optical properties, including obtaining record high birefringence, however due to the microstructure collapse, splicing with all-solid fibers is still an issue and causes low mechanical durability of the interconnection.

The other technique of birefringence forming in the fiber is to use glass with artificial anisotropy (metaglass), first proposed by Wang et al. [1]. The authors used low and high refractive index soft glasses to form multiple layer glass slab and obtained high group birefringence (8.8×10^{-3}). Stepniewski et al. [2] also shown that this approach allow to obtain ultraflat birefringence in wide spectral range. However, the structures made of soft glasses are inconvenient for integration with silica.

Recently we shown numerically that this concept leads to large birefringence even using silica based glasses with significantly lower refractive index contrast [3,4]. We then fabricated the fiber, labelled ZEBRA, composed of subwavelength rods ordered in hexagonal lattice, Fig. 1. Low (pure silica) and high refractive index (8.17 mol.% GeO_2 doped silica) rods are ordered in interleaved layers to create artificially anisotropic glass slab. This approach of core nanostructuring is valid if the size of a single rod is much smaller than λ/2.5 [5]. The cladding of the nanostructured birefringent fiber is made of silica capillary.

We experimentally verified optical properties of the ZEBRA fiber. We measured its attenuation with use of cut-back method and optical time domain reflectometry. The relatively high losses (~0.2 dB/m at 1550 nm) can be reduced using clean room facility and dehydrating cleaning procedures of the stack before drawing.

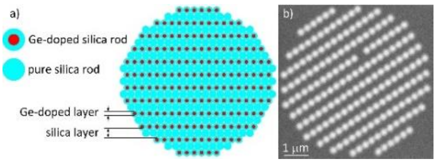

Fig. 1. Internal structure of ZEBRA fiber: a) scheme, b) SEM image.

We analyzed also bending losses, confirming that the ZEBRA fiber is resistant to bending in C-band in the same way as SMF-28. We also carried out measurement of the cut-off wavelength, which equaled to 1113 nm. We applied mode spatial angular distribution analysis in the far field to estimate numerical aperture and effective mode field diameter. Both parameters are similar to these of SMF-28. Next we measured the chromatic dispersion of the ZEBRA fiber. The characteristics is similar to one of SMF-28 with zero dispersion wavelength localized at 1351 nm.

The fiber's polarization properties were also investigated. Polarization extinction ratio (PER) equals 20 dB, whereas phase B and group G birefringence are B=3.35×10^{-5} and G=5.50×10^{-5}, respectively. Although the birefringence is not the record one, the isolation between the orthogonal components of the mode is guaranteed by high PER and moderate B.

We also performed splicing tests of ZEBRA fiber with SMF-28, showing that it can be done with standard splicer and typical program for SM-SM joints. Obtained splice loss equals to 0.11 dB, which is comparable to the splice loses of PANDA and SMF-28 joints.

We experimentally validated a new type of PM silica fiber with metaglass in the core. The ZEBRA fiber is perfectly matched to SMF-28 and maintains polarization. This concept is very promiscuous for further development of space division multiplexing systems based on multicore fibers, where the use of stress zones or asymmetric cores is not straightforward.

Acknowledgments: This work was supported by Foundation for Polish Science (POIR.04.04.00-00-1C74/16); Warsaw University of Technology ISE/2020/GD_AEE_1; Conseil Régional Hauts-de-France (CPER P4S); Agence Nationale de la Recherche (ANR-11-EQPX-0017).

References:

[1] A. Wang et al., Opt. Express 13, 5988 (2005)
[2] G. Stepniewski et al., Opt. Mater. Express 6, 1464 (2016)
[3] D. Michalik et al., J. Opt. Soc. Am. B 37, 1722 (2020)
[4] D. Michalik et al., Opt. Express 29, 22883 (2021)
[5] R. Buczynski et al., Opt. Express 23, 25588 (2015)

Nanostructured few-mode fiber for mode-division-multiplexed systems

R.KASZTELANIC[1,2], D. MICHALIK[1,2], A. ANUSZKIEWICZ[3,2], R. BUCZYNSKI[1,2]

[1]Faculty of Physics, University of Warsaw, ul. Pasteura 5, 02-093 Warsaw, Poland
[2]Photonics Materials Group, Ł – Institute of Microelectronics and Photonics, al. Lotników 32/46, 02-668 Warsaw, Poland
[3]Faculty of Electronics and Information Technology, Warsaw University of Technology, ul. Nowowiejska 15/19, 00-665 Warsaw, Poland
e-mail address: kasztel@igf.fuw.edu.p

A constant increase of byte rate in single-mode network systems has led researchers to develop mode-division multiplexing (MDM). One possibility is to use a weakly-coupled approach which reduces the mode coupling by maximizing the separation of adjacent *LP* modes' propagation constants. The most critical parameters for the weakly-coupled approach are the effective refractive index difference (Δn_{eff}) between adjacent *LP* modes, the effective mode area (A_{eff}), which should have a value above 80 μm^2, and the resistance to unavoidable bending.

In recent years, the most efficient solutions recognized for MDM are few-mode optical fibers (FMF) composed of a step-index core divided into rings with different refractive indices (Fig. 1a). The limitations of circular symmetry are mainly related to the fabrication method, which is the modified chemical vapor deposition (MCVD) [1]. However, a novel methodology with high potential to enhance FMF performance in MDM applications may be the nanostructuring method [2-4]. This fiber design and development technique allow for the tailoring of optical properties by free-form arrangement (not necessarily in circular symmetry) of internal nanostructures made of two glasses differing in the refractive index. An all-solid and arbitrary refractive index distribution is obtained by the stack-and-draw technique, mainly used to fabricate photonic optical fibers. The refractive index pattern in the core and/or cladding prepared in such a way is averaged by incident light according to Maxwell-Garnett mixing theory [5] and can be used to effectively modulate previously specified optical properties.

We study the implementation of the nanostructurization method to improve the performance of weakly coupled 4-LP FMF. We present an optimization method to freely design FMF fibers with selected geometrical parameters – fiber with forced circular symmetry (Fig. 1b). We also present a method allowing optimization of selected optical properties - fibers with the increased difference between effective refractive indices of neighboring mods (Fig. 1c) and fibers with forced equal distance between effective refractive indices of guided mods (Fig. 1d).

The key to obtaining a nanostructured fiber with given optical parameters is determining the optimal refractive index distribution. Since the fiber preform consists of thousands of elements of two types, it is impossible to test all combinations. Thus, an optimization process is needed to determine the distribution of individual rods.

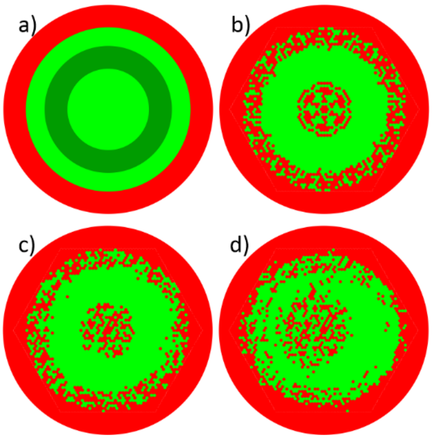

Fig. 1. Few-mode fibers: a) step-index rings, b) nanostructured with forced circular symmetry, c) nanostructured with the increased Δn_{eff}, d) nanostructured with forced equal Δneff.

The basis of the optimization process is to define a fitting function (*FF*) that quantifies how well our requirements are fulfilled. The *FF* can include various parameters that are important to the performance of the target fiber. In the case of FMF, we depend *FF* on only two parameters. On the one hand, *FF* tries to achieve the largest possible separation between neighboring mods, and on the other hand, it attempts to make these distances equal.

Using this simple approach, we find that the optimal fiber consists of 1987 doped by 15 mol.% germanium and 495 undoped rods and achieved a minimum Δn_{eff} of $1.86{\times}10^{-3}$.

Acknowledgments: This work was supported by the project POIR.04.04.00-1C74/16 operated within the FNP Team Programme co-financed by the European Regional Development Fund under Smart Growth Operational Programme (SG OP), Priority Axis IV and project TECHMATSTRATEG-III / 0042 / 2019-00 operated within the NCBiR Techmatstrateg program.

References:

[1] S. R. Nagel, et. al., IEEE Trans. Microw. Theory Tech., 30(4), 305-322 (1982).

[2] R. Buczynski, et. al., Opt. Expr., 23(20), 25588-25596 (2015).

[3] A. Anuszkiewicz, et. al., Sci. Rep. 8, 12329 (2018).

[4] A. Anuszkiewicz, et. al., Optics Letters 47(2), 401-404 (2022).

[5] A. Sihvola, Electromagnetic Mixing Formulas and Applications, The Inst. of Eng. and Techn. (1999).

Light depolarization by dual-frequency nematic liquid crystals

P. MARĆ[1], N. BENNIS[1], A. PAKUŁA[2], E. PAWLIKOWSKA[3], A. SPADŁO[1], K. GARBAT[1], R. WĘGŁOWSKI[1], L. R. JAROSZEWICZ[1]

[1] New Technologies and Chemistry Faculty, Military University of Technology,
[2] gen. S. Kaliskiego St., 00-908 Warsaw, Poland
2 Institute of Micromechanics and Photonics, Warsaw University of Technology,
8 św. A. Boboli St., 02-525 Warsaw, Poland
[3] Institute of Optoelectronics, Military University of Technology,
gen. S. Kaliskiego 2 St., 00-908 Warsaw, Poland
e-mail address: pawel.marc@wat.edu.pl

Dual-frequency nematic liquid crystals are specific self-organized functional materials whose electro-optic properties can be controlled by both voltage and frequency [1]. The right mixture of liquid crystals allows to influence the dielectric anisotropy of the material. In a dual-frequency nematic liquid crystal, the sign of the dielectric anisotropy changes in the frequency domain. It is positive to so-called crossover frequency and then becomes negative. This effect was used to improve response time and reduce energy dissipation in voltage driven liquid crystal cells (LCCs). Moreover, the use of specialty synthetized polymer alignment layers on the glass surface of the LCC allows to induce a vertical orientation of the director in such type of material and we can call it a vertically aligned nematic liquid crystal (VAN). Studies on the electro-optic properties of VAN LCCs with two types of director orientation, i.e., pre-tilted (PT-VAN) and purely vertical (PVAN) have been presented. PT-VAN LCC has a well-defined director orientation when it is frequency driven at the appropriate voltage for frequencies lower than the crossover frequency which is isotropic and/or higher, he cell works as a phase linear shifter similar to planar orientation cells. PVAN LCC has different electro-optic properties. Again, at low frequencies this type of cell remains isotropic character, but above this frequency the cell becomes a pseud-depolarizer [2]. A full polarimetric measurement was done for both types of LCC. Losses, diattenuation, retardance, and depolarization were calculated using the Lu Chipman theoretical model. The analysis shows that the PT-Van cell does not depolarize and is free of diattenuation. The phase shift of a 10 μm thick cell was of around 0.9π, for a driving signal – 4.5 V and 15 kHz. The PVAN cell was characterized by an average degree of polarization and can be called a pseudo-depolarizer.

Acknowledgments: This work was financed by Military University of Technology under research project UGB-844.

References:

[1] X. Xianyu et al., Liquid Crystals, 36:6-7, 717-726 (2009).
[2] N. Bennis et al., Crystals 9, 275 (2019).

The SS-OCT imaging probe based on MOEMS/MEMS Mirau micro-interferometer and 2-axis electrothermal microscanner for endomicroscopic application.

P. STRUK[1], S. BARGIEL[2], B. MIRECKI[5], M. JÓŹWIK[5], Q. TANGUY[2], R. CHUTANI[2], N. PASSILLY[2], P. LUTZ[2], H. XIE[3], F. E. GRACIA-RAMIREZ[2], M. WOJTKOWSKI[4] AND C. GORECKI[4]

[1]Department of Optoelectronics, Faculty of Electrical Engineering, Silesian University of Technology, 2 Krzywoustego Str., 44-100 Gliwice, Poland.
[2]FEMTO-ST Institute (UMR CNRS 6174, Université Bourgogne Franche-Comté), 15B Avenue des Montboucons, 25030 Besançon, France.
[3]University of Florida, P.O. Box 116200, Gainesville, Florida, USA.
[4]Institute of Physical Chemistry, Polish Academy of Sciences, ul. Kasprzaka 44/52, Warsaw.
[5]Faculty of Mechatronics, Warsaw University of Technology, Faculty of Mechatronics of Warsaw University of Technology, ul. Św. Andrzeja Boboli 8, 02-525 Warsaw.
e-mail address: Przemyslaw.Struk@polsl.pl

The Authors would like to present the optical coherence tomography (OCT) system with micromachined endomicroscopic probe fabricated in MOEMS/MEMS technology. The probe is designed for biomedical imaging using OCT method in swept source regime. The presented oct system is composed of illumination part based on tunable laser - swept source with following parameters: central wavelength $\lambda_c=1064nm$, swept range $\Delta\lambda=100nm$, A-scan rate $f_A=200kHz$ and average output power $P=15\ mW$.

The light from swept source is transmitted by a single mode fiber through optical circulator to endomicroscopic probe. The MOEMS / MEMS probe is built based on GRIN lens collimator, Mirau micro-interferometer (where light beams from reference arm and measured arm can interfere together). At the end of the Mirau micro-interferometer is placed 2-axis electrothermal scanner equipped in micro-mirror with diameter d~1mm. The micro-mirror allows scanning of sample by Lissajous trajectory for obtain 3D imaging. Finally interferometric signal is detected by photodiode and measured by data acquisition card connected to PC computer.

The presented experimental results are focused on optimization of the optical and geometrical properties of endomicroscopic probe, design of a new measurement setup for proper operation at λ=1064 nm wavelength range.

Acknowledgments:
This work was supported the INSERM Plan Cancer program (ROBOT project), Labex Action program, ANR-11-LABX-0001-01, the French RENATECH network and its FEMTO-ST

technological facility and by the Collegium SMYLE.

References:
[1] P. Struk et. al., Optics Letters, 43(19) (2018).
[2] P. Struk et. al., IEEE Sensors Journal, Vol. 15, 12, 2015.
[3] Q. A. A. Tanguy et. Al., 2017 19th International Conference on Solid-State Sensors, Actuators and Microsystems (TRANSDUCERS) (2017).

Rib waveguide homogeneous sensitivity with regard to single mode propagation condition

C. TYSZKIEWICZ[1], A. KAŻMIERCZAK[2], A. BUTT[2], P. KARASIŃSKI[1]

[1] Silesian University of Technology, Department of Optoelectronics, B. Krzywoustego 2, 44-100 Gliwice, Poland
[2] Warsaw University of Technology, Institute of Microelectronics and Optoelectronics, Koszykowa 75, 00 662 Warszawa, Poland
e-mail address: cuma.tyszkiewicz@polsl.pl

The relation between morphological parameters of rib waveguides and their homogeneous sensitivity is discussed in papers [1,2]. However, the analysis presented there, concerning SOI, SiON (silicon oxynitride) and Si_3N_4 rib waveguides, did not take into account a single mode operation range and was carried in a limited range of the morphological parameters, where the results obtained using FEM (Finite Element Method) and EIM (Effective Index Method) are compatible. In mentioned papers homogeneous sensitivity was calculated from the mode power flux carried by the waveguiding film, as well as from analytical equations derived on the basis of the EIM method. EIM method allows correct derivation of modal field distributions only if the mode is fully confined to the rib [3]. In this respect it is to be noted that such a mode is weakly sensitive to variations of the cover refractive index.

This work is a continuation of the analysis described in our previous paper [4]. It concerns single-mode, silica-titania rib waveguides on BK7 glass substrates. Two main issues are being considered. The first one concerns the relationship between characteristics of rib waveguide homogeneous sensitivity taken with respect to the rib height and the corresponding characteristics for the parent-slab. The characteristics of the latter are functions of the waveguide film thickness. Second issue concerns the question if homogeneous sensitivity of rib waveguides can exceed the corresponding maximum value for the optimized parent-slab. Regarding similarity of aforementioned sensitivity characteristics, it has been shown that there is the significant difference between HE_{00} and EH_{00} modes. Namely, only sensitivity characteristics of *EH* modes may behave similarly to the characteristics of TE_0 and TM_0 slab waveguide modes. Moreover, considering rib waveguides whose morphological parameters are optimized for maximum homogeneous sensitivity, it was shown that only in the case of EH modes, changes of the light intensity on the interface between the rib and cover, rendered by a small variation of the cover refractive index are the highest on rib sidewalls. Finally, homogeneous sensitivity of HE_{00} and

EH_{00} modes can exceed corresponding values for optimized parent-slab waveguides; however, the magnitude of that increase is very small.

Acknowledgments: The work was funded with the project OPUS 13 from National Science Centre - Poland based on the decision DEC-2017/25/B/ST7/02232

References:

[1] Dell'Olio F., Passaro V.M.N., De Leonardis F.: "Sensitivity analysis of rib waveguides for integrated optical sensors," 2nd International Workshop on Advances in Sensors and Interface (2007), doi:10.1109/iwasi.2007.4420035

[2] Dell'Olio F., Passaro V.M.N.: "Optical sensing by optimized silicon slot waveguides" Optics Express **2007**, 15(8), 4977–4993 (2007)

[3] Robertson M.J.: "Weighted Index Method for Dielectric Waveguide Analysis. In Rib waveguide Theory by the Spectral Index Method" Robson, P.N., Kendall, P.C., Eds.; Research Studies Press LTD.: Taunton, Somerset, England, 1990; Chapter 4.7, pp. 62–65.

[4] Tyszkiewicz C: "Comparison of single mode slab and rib waveguide planar evanescent wave transducers" Proc. SPIE 11045, Optical Fibers and Their Applications 2018, 110450R (15 March 2019); doi: 10.1117/12.2520886

Measurements of the spectral interferogram for single-mode waveguide layers

K. GUT[1],

[1] Silesian University of Technology / Department of Optoelectronics, 2 Krzywoustego St., 44-100 Gliwice, Poland
[2]Isitutution/Company Name, Address (street with number, post code, city, country)
e-mail address: kazimierz.gut@polsl.pl

In recent years, first there have been proposals [1], and then the implementation of broadband planar optical interferometric sensors. The broadband Mach-Zhender [2] and Young [3] interferometers are presented. In sensors of this type, waveguide modes are excited in the visible or near infrared range in the wavelength range of several hundred nanometers. The spectrometer records the interference spectrum at the output of the optical path.

Changing the parameters of the optical path causes a change in the interference spectrum. The papers [4, 5] present the theoretical description of broadband differential interference in planar waveguides. In this interferometric system, fundamental waveguide modes with TE and TM orthogonal polarization in the visible range are excited. The phase change between the TE and TM modes (usually caused by a change in the refractive index of the coverage of the waveguide layer) causes a change in the recorded spectral signal.

A stand was built for introducing light into the waveguide layer and recording the output interference signal. Spectral measurements at the output of the structure allow to determine the derivative of the spectral dependence of the birefringence of the modal waveguide layer.

The work will present the test stand and measurement methodology.

References:

[1] M. Kitsara et al., Optics. Express 18, 8193, (2010).
[2] K. Misiakos et al., Optcs Express 22, 8856, (2014)
[3] E. Makarona, et al., J Opt. Soc. Am. B 34, 1691, (2017)
[4] K. Gut, Optics Express 25, 31111, (2017)
[5] K. Gut, Nanomaterials 9, 729, (2019)

PPB-level NO_2 concentrations sensing by nanostructured ZnO – graft copolymer composites

P. KAŁUŻYNSKI[1], M. PROCEK[1,2],A. STOLARCZYK[3], T. JAROSZ[3], E. MACIAK[1]

[1] Department of Optoelectronics, Silesian University of Technology, Gliwice, Poland;
[2] Department of Electronics Design, Mid Sweden University, Holmgatan 10, SE-85170 Sundsvall, Sweden;
[3]Department of Physical Chemistry and Technology of Polymers, Silesian University of Technology, Gliwice, Poland;
e-mail address: piotr.kaluzynski@polsl.pl

In this work, an organic-inorganic blend of graft comb-copolymer (named PEGSil and DodecSil) mixed with zinc oxide nano-material were studied as a sensitive layer for a sub-ppm nitrogen dioxide (NO_2) resistance gas sensor application. Moreover, the PEGSil graft copolymer has been investigated in two variants, defined by side-chain length of P3HT: shorter hexane fraction (H) and longer chloroform fraction (CH). The elaborated blends were applied to the interdigitated transducers by the drop-casting method, and the obtained sensor structures were subjected to gas measurements. Sensor response characteristics were measured for different concentrations of NO_2. Responses at low concentrations of NO_2 (1–10 ppm) and in ultra-low concentrations (25-1000 ppb) in synthetic air carrier gas were measured and compared (Fig. 1). Measurements were done at room temperature with UV light charge carriers activation. The obtained results show that all material blends were able to sense 200 ppb NO_2 concentration, moreover PEGSil CH was able to detect NO_2 concentration as low as 25 ppb of NO_2. These results show that the composites of these materials has wide potential as a sensing layer for NO_x ultra-low concentration sensing.

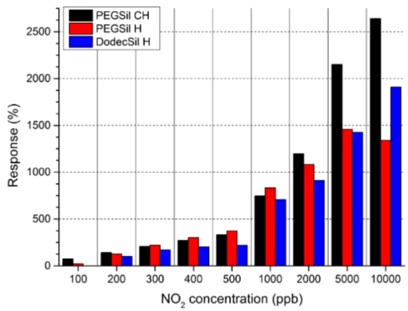

Fig. 1. Response of the sensors utilising different copolymers as a function of utilised NO_2 concentration

Acknowledgments: This research was partially sponsored by the Faculty of Electrical Engineering of Silesian University of Technology within the grant BKM/757/RE4/2021. This work benefited from facilities and research infrastructure provided by the Department of Optoelectronics Silesian University of Technology, which receives support under project NLPQT – National Laboratory for Photonics and Quantum, POIR.04.02.00-00-B003/18.

POSTERS

Nonlinearity enhancement in thermally poled glasses with high alkali content

A. ANUSZKIEWICZ[1,2], A. FILIPKOWSKI[1,3], R. KASZTELANIC[1,3], D. PYSZ[1], R. STĘPIEŃ[1], R. BUCZYNSKI[1,3]

[1]Łukasiewicz Research Network-Institute of Microelectronics and Photonics, Photonic Materials Group, Al. Lotnikow 32/46, 02-668 Warsaw, Poland
[2]Warsaw University of Technology, Faculty of Electronics and Information Technology, Institute of Electronic Systems, Nowowiejska 15/19, 00-665 Warsaw, Poland
[3]niversity of Warsaw, Faculty of Physics, Pasteura 5, 02-093 Warsaw, Poland
e-mail address: alicja.anuszkiewicz@imif.lukasiewicz.gov.pl

Linear electrooptic effect (Pockels effect) is related with the change in the refractive index proportionally to applied voltage in the not centrosymmetric medias. It is then used for modulation of the birefringence in crystals and in anisotropic medias, as well for second harmonic generation [1]. In centrosymmetric and isotropic medias there is no second-order nonlinearity $\chi^{(2)}=0$, therefore second harmonic generation is not straightforward. It can be done with thermal poling method [X], which introduces break of the symmetry of centrosymmetric medium (glass). This can be done in e.g. glasses with alkali ions. The medium have to be heated to high temperatures (200 – 300 ^{o}C) to thermally activate the alkali ions, that are present in the glass, such as K+, Li+ and especially Na+. In elevated temperature the ions are free to move with use of external high voltage. After tens of minutes ions group in the close area (a few micrometres) of anode. While high voltage is applied, the ambient temperature is gradually diminished to the room temperature. In such a conditions the alkali ions mobility is very poor and because of presence of high voltage during the cooling process, the ions position is fixed and so-called frozen-in electrical field $E_{frozen\text{-}in}$ is built in the glass. The area next to the anode experiences high second-order nonlinearity, which equals to $\chi^{(2)}=3\chi^{(3)}E_{frozen\text{-}in}$. Generation of second order harmonic in the medias with stimulated second-order nonlinearity by thermal poling is then possible [2].

We present specially designed in-house glasses labelled ZR3 and SK222 with enhanced alkali ions content for application to nonlinear optics. The third-order nonlinearity estimated for these glasses is much higher than for silica (Tab. 1). Thus second-order nonlinearity obtained through thermal poling can be of one order higher, resulting in efficient second order generation.

Tab. 1. Comparison of second order nonlinearity enhancement in silica and in-house glasses

Nonlinearity	**SiO_2**	**SK 222**	**ZR3**
$\chi^{(3)}$ [$\times 10^{-22}$ m^2V^{-2}]	2	4.13	8.92
$\chi^{(2)}$ [pm/V]	0.48	0.99	2.14

We experimentally confirmed high third-order nonlinearity for ZR3 glass 200 µm thick sample, showing efficient generation of third-harmonic of 1560 nm beam before thermal poling.

Obtained results are very promiscuous for designing centrosymmetric materials for development of optical fiber [3], in which second-order nonlinearity through thermal poling can be induced.

Acknowledgments: This work was supported by National Science Centre within project no. 2017/26/D/ST7/01140, SONATA13 program.

References:

[1] O. Deparis et al., J. Non-Crystalline Solids 351, 2166 (2005).
[2] H. An et al., Opt. Express 20, 7436 (2012).
[3] G. Chesini et al., Opt. Express 17, 1660 (2009).

Optoelectronic system for detecting short-circuits in low voltage networks

K. BARCZAK[1], J. JURASZEK

[1]Department of Optoelectronics, Silesian University of Technology, Gliwice, Poland;
email address: kamil.barczak@polsl.pl

The methodology of measuring electrical quantities in all electric power areas is very important. The measurement methods used in the system by means of direct and indirect methods of electrical quantities, e.g. current, have their limitations. A particular imperfection of the measurement concerns the use of traditional instrument current transformers in the measurement, and the sensitivity of measurement and the transmission speed of measurement data, which are important in some areas.

The proposed new solutions for measuring electrical quantities use the magneto-optical phenomenon. Current sensors constructed on this basis can have enormous use in transmission, distribution and industry. These sensors are characterized by high insulation, insensitivity to electromagnetic interference, high response speed and small size. In addition, they are resistant to exceeding the range, current surges, and in the event of damage caused by e.g. physical influence of current (e.g. high temperature) they minimize the risk of people and property.

The paper presents the concept of using a fiber-optic current sensor with external conversion (OFCS-EC) in a power system. The sensor was developed in the Department of Optoelectronics and was tested in a laboratory. The focus was on the use of OFCS-EC in a real low voltage network. The main purpose of the presented measurement system will be to record network disturbance states with high accuracy. The experiment is to answer the question whether the recorded current waveforms in fault states and the measurement transmission speed will be useful enough to be able to predict, identify and, consequently, prevent losses and damage to devices caused by disturbances in low voltage networks.

Compact Optical Gyroscope for Aerospace Applications

S.BILICKI[1], D. BRAUDA[2], A.LEDZIŃSKI[1],W. LEWOCZKO-ADAMCZYK[3], S. LENZKY[3], S. MARX[3], J. NAWROCKI[4], P. NOGAŚ[4], R. URBANIAK[4] AND H. SCHRÖDER[3]

[1]Institute of Physics, Faculty of Physics, Astronomy and Informatics, Nicolaus Copernicus University, Grudziadzka 5, 87-100 Torun, Poland,
[2]eagleyard Photonics GmbH Rudower Chaussee 29, 12489 Berlin, Germany
[3]Fraunhofer-Institut für Zuverlässigkeit und Mikrointegration, Gustav-Meyer-Allee 25, 13355 Berlin, Germany
[4]Piktime Systems sp. z o.o. ul. Mazowiecka 59, 60-623 Poznan, Poland
e-mail address: slawko@fizyka.umk.pl

We present an advanced project of a resonant hollow- core-fibre (HCF) gyroscope for in-flight applications. The setup will allow for operating into a flight-qualified carrier platform and to test it under real use scenarios in a series of test flights on drones and airplanes. In this project we design and construct a highly sensitive, compact integrated, field-deployable, and based on HCF resonator gyroscope. Within the project we contribute to development of a novel benchmark in the technological roadmap of inertial sensors.

Optical gyroscopes are based on Sagnac effect where a rotation induces phase shift between the two counter-propagating light waves in a ring interferometer [1]. This effect can be enhanced by a fibre resonator and therefore whole gyroscope can be smaller [2,3]. Additionally in the gyroscope based on HCF the absence of solid in the fibre core

makes it free of nonlinear optical effects and much less sensitive to magnetic fields and temperature variations [4].

We manufacture a compact laser source at 780 nm with the linewidth less than 100 kHz and mode- hope free tuning range above 100 MHz. The laser consists out of a laser diode that is stabilized with a volume holographic Bragg grating. This setup is assembled in a hermetically sealed butterfly package.

Fig. 1. DFB laser at 780 nm in the butterfly package with a PM fibre output.

Project of a PID electronic unit to stabilize the laser will be integrated on a PCB board. The detection setup will be based on tight lock by using Pound Drever Hall technique with active auto relock system. The setup will be composed on fibre-coupled electro-optic modulators in order to reduce power consumption of whole system.

The total power consumption is estimated to be 15W. Additionally the setup will include a residual amplitude modulation system in order to minimize bias field of the gyro-resonator.

We characterize the properies of the fibre resonator. From the first scans of the resonances a finesse of the cavity is equal to 16 and free spectral range FSR = 6.6 MHz is obtained for 45 m lenght HCF-fibre.

In conclusions, we have shown key components that are used to build the photonic gyroscope based on hollow-core-fibre. In the next step we integrate the gyroscope in one compact platform. The temperature drift, vibration sensitivity will be tested and rotation factor calibrated. On the end we plan to perform real-live measurements on an aircraft.

Acknowledgments: This project is co-financed by National Centre for Research and Development within 4th call for Poland - Berlin/Brandenburg collaboration programme. This project is co-financed by the European Regional Development Fund (ERDF).

References:

[1] Ezekiel, S. and Balsamo, S., “Passive ring resonator laser gyroscope,” Appl. Phys. Lett. 30(9), 478-480 (1977)

[2] Bohm, K., et.al, “Low Noise Fiber Optic Rotation Sensing,” Optics let, Vol. 6, 1981, pp 64-66.

[3] G. A. Sanders, L. K. Strandjord, J. Wu, W. Williams, M. Smiciklas, M. Salit, C. Narayanan, and T. Qiu, “Development of compact resonator fiber optic gyroscopes,” in 2017 IEEE International Symposium on Inertial Sensors and Systems (INERTIAL), (2017), pp. 168–170.

[4] G. A. Sanders, L. K. Strandjord, and T. Qiu, “Hollow core fiber optic ring resonator for rotation sensing,” in Optical Fiber Sensors, (Optical Society of America, 2006), p. ME6.

Numerical analysis of the broadband interferometric sensor in the planar gradient-step index configuration

M. BŁAHUT

Department of Optoelectronics, Silesian University of Technology, Akademicka 2A, 44-100 Gliwice,
e-mail : Marek.Blahut@polsl.pl

A novel two-mode interferometric optical sensor in planar configuration proposed in this work uses the silver-sodium ion exchange in glass. The sensor is designed to operate with a broadband light source. Its optical configuration is adjusted to examine biological solutions.

Configuration of the planar interference sensor is shown in Fig.1. The structure consists of a gradient-index waveguide made by Ag+-Na+ ion exchange, which forms the single-mode input and output. In the central part the gradient-index waveguide is covered by the step index layer. This step and gradient index structure creates a two-mode waveguide where the interference effects can be observed. It is assumed that the structure is excited by the broadband light source from the range of 0.55-0.85μm. Material parameters of step-index layer refers to the polymer SU-8 waveguide. It is assumed that the optical system will be used to the analysis of biological substances. Hence the suggested refractive index changes of the cover for examined characteristics refers to the water solutions and can be expressed as $n_{H_2O} + \Delta n_c$ It is assumed that Δn_c=(0÷0.005).

The refractive index variation of measured external surrounding affects the modal properties of multimode waveguide. The image variations and spectral distribution are registered at the output of single-mode gradient-index waveguide.

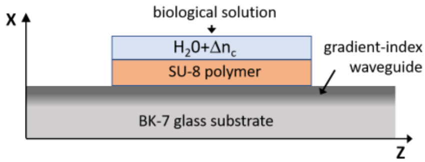

Fig. 1. Configuration of the sensor structure

Gradient index profile is the solution of non-linear diffusion equation in BK-7 glass with diffusion coefficient D and diffusion time t_D. [1]. The assumed diffusion depth $d_D = 4 \cdot \sqrt{D \cdot t_D}$, which changes from 0.96μm to 1.31μm, ensures the single mode propagation in gradient index waveguide. It is assumed that thickness of the step index layer *w* changes from 0.7μm to 0.9μm and its length amounts to 5000μm. The gradient-step index section is single mode for this geometry in whole limits of examined wavelength.

The operation principle of examined optical structure is determined by the modal field analysis. Taking into account results of the paper [2], the power P at the output of the structure can be expressed by the equation:

$$P(\lambda)=\left|\int_{-\infty}^{+\infty}\phi_{grd}(x)\cdot\sum_{l=0}^{1}\phi_l(x)\cdot e^{-j\beta_l\cdot L}dx\right|^2$$

where ϕ_{grd} is the wave function of single-mode waveguide and ϕ_l are the wave functions of multimode section of an order l with propagation constants β_l.

Fig. 2 shows the optical structure response to the refractive index variations of the surrounding for the two different step-index layer thickness the cover for the diffusion depth d_D=1.1μm and the step-index layer thickness w equal 0.8μm.

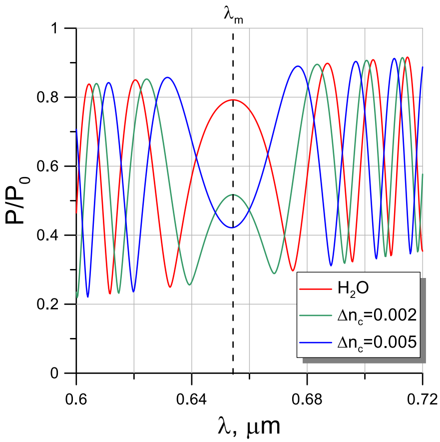

Fig. 2. Spectral characteristics of relative output power for the different values of refractive index of the cover for the diffusion depth d_D=1.1μm and the step-index layer thickness w equal 0.8μm

Spectral characteristics shift is observed with refractive index changes, which is the strongest in the vicinity of λ_m. For the waves of shorter wavelengths, on the left sight from the λ_m, the signal extremes shift towards longer waves with the increase of the refractive index of the cover. On the other hand for the waves of longer wavelengths, on the right sight from the λ_m, the signal extremes shift towards shorter waves with the increase of the refractive index of the cover. Taking into account this feature it is possible to construct the one of the possible operating characteristics of the sensor, by measuring the difference of mutual shifts of extremes, closest to the range λ_m for the different values of the refractive index of the cover.

Similar effects have been observed in the case of broadband differential interferometers [3] and step-index two-mode interferometers [4].

The configuration proposed makes possible to determine refractive index variations from the shifts of the output signal spectral distribution instead of measurements of output power changes. From that reason the method is independent to the excitation level at the input.

References:

[1] M. Błahut, Opt. Appl. , vol.27, pp. 5-16, (1998)

[2] M. Błahut, Opt. Appl. vol. 50, pp. 377-39 (2020)

[3] K.Gut, Optic Express, 25, 31111,(2017)

[3] M.Błahut, Phot. Lett. Pol. vol. 12 pp. 28-30, (2020)

Highly birefringent large mode area fibers with artificially anisotropic silica glass core

R. BUCZYNSKI[1,2], D. MICHALIK[1,2], A. ANUSZKIEWICZ[1,3], A. FILIPKOWSKI[1], G. STĘPNIEWSKI[1], D. PYSZ[2], K. HARAŚNY[1], I. KUJAWA[1], R. KASZTELANIC[1,2]

[1]1Łukasiewicz Research Network - Institute of Microelectronics and Photonics, Department of Photonic Materials, Al. Lotników 32/46 02-668 Warsaw Poland
[2]University of Warsaw, Faculty of Physics, Pasteura 5, 02-093 Warsaw, Poland
[3]Warsaw University of Technology, Faculty of Electronics and Information Technology, Nowowiejska 15/19, 00-665 Warsaw, Poland
e-mail address: ryszard.buczynski@imif.lukasiewicz.gov.pl

We study a new concept of highly birefringent (HB) ZEBRA fibers toward development of large mode area (LMA) silica glass fibers. The fiber core is composed of interleaved subwavelength layers of high and low refractive index silica doped glasses, that form a core composed of an uniform artificially anisotropic glass (Fig. 1).

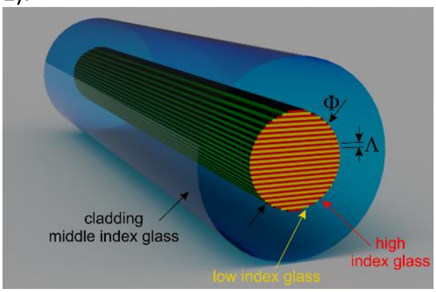

Fig. 1. Highly birefringent silica all-solid fiber with anisotropic core composed of interleaved subwavelength layers of high and low refractive indices. As a high refractive index glass we consider a silica glass doped with GeO_2, while as a low refractive index glass we consider silica glass doped with fluorine.

This is alternative mechanism of introducing birefringence, different than that previously reported in PM fibers where geometrically or stress induced birefringence is applied. Birefringence in the ZEBRA fibers is formed based on the second order Maxwell-Garnett effective medium theory, where volume glass anisotropy is obtained through interleaved subwavelength layers of low and high refractive index glasses in the fiber core [1,2].

Recently we have reported experimental verification of birefringence in the ZEBRA fibers with the diameter of effective mode area of 10.5 µm at the wavelength of 1550 nm. Phase birefringence of 0.3×10^{-4} and polarization extinction ratio of 20 dB is reported [3] .

In this work we show that the above concept can be extended toward LMA fibers if refractive index of low refractive index layers in the core are further decreased by doping silica with fluorine. Adjustment of silica doping levels and geometrical parameters of the core allow to optimize a high birefringence and maintain single mode performance of the fiber. We limited numerical analysis to technological constrains of CVD doping levels considered today for silica glass, and thermal matching conditions of pure and doped silica-based glasses. Therefore we assumed a maximum doping level with germanium of 15 mol.% and fluorine of 6.1 mol.% [4].

The optimized single mode ZEBRA fiber with low bending losses offers phase birefringence of 1.92×10^{-4} for the single mode fiber with the core diameter of 30 μm and the effective mode area equal to 573 μm^2 and 804 μm^2, for both polarization, respectively. In this case, the core is composed of interleaved layers of 2 mol.% F-doped glass and 15 mol.% Ge-doped silica glass with the thickness of 300 nm each.

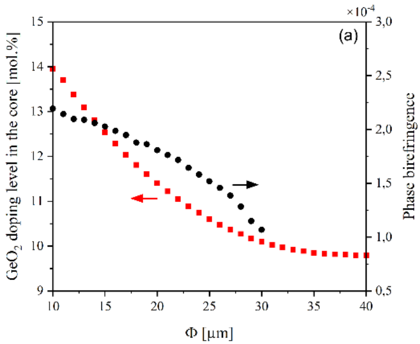

Fig. 2. Phase birefringence for single mode ZEBRA fiber for various core diameters and Ge-doping levels.

Acknowledgments: This work was supported by The Łukasiewicz Research Network grant NWL 1/Ł-IMIF/CŁ/2021 and TEAM TECH/2016-1/1 (POIR.04.04.00-00-1C74/16) operated within the Foundation for Polish Science Team Programme co-financed by the European Regional Development Fund under Smart Growth Operational Programme (SG OP).

References:

[1] A. Sihvola, Electromagnetic Mixing Formulas and Applications (IEE, 1999).

[2] A. J. Waddie, at al., Opt. Mater. Express 1, 1251–1261 (2011).

[3] A. Anuszkiewicz, et al., Opt. Lett. 47(2), 401-404 (2022).

[4] D. Michalik, at al., Opt. Express, 29, 22883-22899 (2021).

Spectral properties of photonic crystal fibers infiltrated with ferroelectric liquid crystals doped with nanoparticles

D. BUDASZEWSKI[1], D.P. SINGH[2], T.R. WOLIŃSKI[1]

[1]Faculty of Physics, Warsaw University of Technology, Koszykowa 75, 00-662 Warsaw, Poland
[2]Universite du Littoral Cote d'Opale, UDSMM, 62228 Calais, France
e-mail address: daniel.budaszewski@pw.edu.pl

Photonic liquid crystal fibers (PLCFs) have attracted significant attention of many research groups since the beginning of the XXI century due to their electro-optical properties. The PLCFs can find many practical applications, including tunable long-period fiber gratings [1], attenuators [2], or polarization controllers [3]. The innovative in-fiber optical devices require liquid crystals (LCs) with improved properties. Chiral smectic C (SmC*) LCs, also called ferroelectric liquid crystals (FLCs), are especially attractive for this purpose mainly due to their fast electro-optical response at low electric fields.
It has been observed that the application of aligning materials to FLCs [4] and doping of nanoparticles in FLCs [5] can further enhance their electro-optical parameters like faster switching times, lower operating voltages, and luminescent properties.

In the present study, we have focused on investigations of spectral properties of isotropic PCFs infiltrated with FLC mixtures doped with titanium dioxide (TiO_2) NPs in different concentrations. As a host material, we have used an LMA-10 isotropic PCF in which we have generated an aligning surface to improve the orientation of the NP-FLC nanocomposite molecules along the PCF's air holes. Two types of FLC mixtures were considered in our studies, a W212 FLC and W206 FLC (both with different values of the spontaneous polarization) in which TiO_2 NPs were dispersed. We have analyzed the influence of NPs concentrations on response times of the investigated PLCFs under the influence of the external electric field.
Based on our observations, a slight improvement in switching times was registered for PLCF samples under the influence of an external electric field. This behavior can be attributed to inhomogeneous alignment of FLC-NPs nanocomposites and aggregation of the NP molecules inside the PCF micro-channels resulting in increased attenuation of the PLCF sample.

Acknowledgments: The research was funded by CB POB FOTECH of Warsaw University of Technology within the Excellence Initiative: Research University (IDUB) program and partially by the National Science Centre under Grant No. 2011/03/B/ST7/02547.

References:

[1] J. Liou, T. Chang, T. Lin, and C. Yu, Opt. Express, 19(7), 6756 (2011).

[2] T.T. Alkeskjold et al., Opt. Quantum Electron., 39(12), 1009 (2007).

[3] A.K. Pitilakis, D.C. Zografopoulos, E.E. Kriezis, J. Light. Technol., 29(17), 2560 (2011).

[4] D. Budaszewski, A.K. Srivastava, A.M.W. Tam, T.R. Wolinski, V.G. Chigrinov, H.-S. Kwok, Opt. Lett., 39(16) (2014).

[5] S.K. Gupta, D.P. Singh, and R. Manohar, Adv. Mater. Lett., 6(1), 68 (2015).

Photopolymerization of AuNP-doped liquid crystals

M.S. CHYCHŁOWSKI[1], M. KAJKOWSKA[1], P. LESIAK[1], T.R. WOLIŃSKI[1]

[1]Faculty of Physics, Warsaw University of Technology, Koszykowa 75, 00-662, Warsaw, Poland
e-mail address milosz.chychlowski@pw.edu.pl

Liquid crystals (LCs) are used as electro-optical modulators in many photonic devices. Their parameters greatly depend on the properties of LC and to enhance or change its base properties one can design a new LC, use its in another state (e.g. change from nematic to smectic) or dope with nanoparticles (NPs). Any modification of a LC changes more than one property, e.g. if smectic phase of LC is used it needs to be kept in a specific range of temperatures, doping LC with Au NP changes TNI, so some means to enforce LC orientation is needed. Here we demonstrate results of stabilization by photopolymerization AuNP-doped LC. Widening of TNI is typical for AuNP-doped LC which increases temperature range for phase separation. Photopolymerization enables stabilization of this effect at room temperature(fig.1).

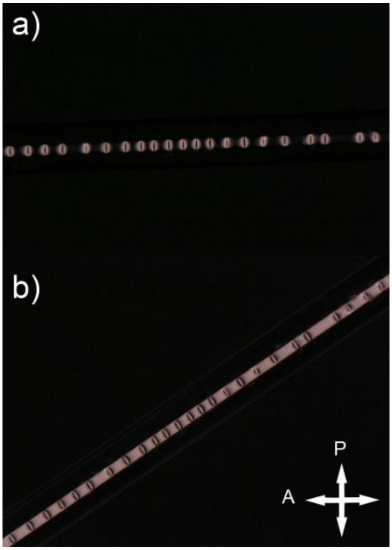

Fig. 1. Photopolymerized phase separation of LC doped with 2nm Au NPs at a) 0 and b) 45 degrees to the analyzer

Acknowledgments:
Studies were funded by FOTECH-1 project granted by Warsaw University of Technology under the program Excellence Initiative: Research University (ID-UB).

References:

P. Lesiak et al.," Self-Organized, One-Dimensional Periodic Structures in a Gold Nanoparticle-Doped Nematic Liquid Crystal Composite", ACS Nano 2019 13 (9), 10154-10160 DOI: 10.1021/acsnano.9b03302

Statistical analysis of raman spectra of reduced graphene oxide obtained using various graphite precursor and various oxidation method

Ł. DREWNIAK[1], S. DREWNIAK[1], M. SAJDAK[2], R. MUZYKA[3]

[1] Department of Optoelectronics, Silesian University of Technology, 2 Krzywoustego St., 44-100 Gliwice, Poland
[2] Department of Air Protection, Faculty of Energy and Environmental Engineering, Silesian University of Technology in Gliwice, 44-100 Gliwice, Poland
[3] Department of Chemistry, Faculty of Medical Sciences in Zabrze, Medical University of Silesia in Katowice, ul. Jordana 19, 41-808 Zabrze, Poland
email address: lukasz.drewniak@polsl.pl

NO_2 is highly reactive and toxic gas. It is generated through combustion of fossil fuels and it is responsible for acid rain and hazardous to human respiratory tract. At concentrations of 10-20 ppm, it causes irritation of the respiratory system, while at 150 ppm could even cause death. [1-5] For NO_2 detection, various materials were proposed as sensor layers, e.g.: ZnO, WO_3, SnO_2, Fe_2O_3, etc. They have excellent performance in NO_2 detection, but at very high temperature. High working temperature causes an increase the energy consumption of the sensor, detoriation of device stability and reduction of operating life. Therefore, there are attempts to replace them by others materials enabling NO_2 detection at lower temperature. In recent years, a special attention has been paid to graphene. Graphene is a zerogap semiconductor which exhibits excellent mechanical, electrical, optical and thermal properties. Due to the huge surface area (2630 m^2g^{-1}), high electron mobility (~20 000 cm^2/V×s at 300 K), carrier density (1012/cm^2 at 300 K) and small resistivity (10-6 W×cm at 300 K), is widely employed as promising sensing material. Similar to graphene, reduced graphene oxide (rGO) is also widely tested as sensing material. Compared to graphene, rGO has dangling bonds, defects and additional functional groups which vitally improve gas adsorption [6]. The various graphite precursor and oxidation's method have a significant influence on the composition and the structure of reduced graphene oxide what have a direct impact on gas sensitivity. We use hierarchical clustering analysis (HCA) and analysis of variance method (ANOVA) to trace the directions of changes of the selected parameters relative to a preparation method of such oxides.

References:

1. Geeta Rani, B.; Sai Bhargava Reddy, M.; Kailasa, S.; Maseed, H.; Bikshalu, K.; Venkateswara Rao, K. Comparative gas sensing analysis of green and chemically reduced graphene oxide. Mater. Res. Express 2019, 6.

2. Park, J.; Kim, Y.; Park, S.Y.; Sung, S.J.; Jang, H.W.; Park, C.R. Band gap engineering of graphene oxide for ultrasensitive NO2 gas sensing. Carbon N. Y. 2020, 159, 175–184.
3. Marcos-Viquez, A.L.; Miranda, Á.; Cruz-Irisson, M.; Pérez, L.A. Tin carbide monolayers as potential gas sensors. Mater. Lett. 2021, 294, 129751.
4. Gomaa, M.M.; Sayed, M.H.; Patil, V.L.; Boshta, M.; Patil, P.S. Gas sensing performance of sprayed NiO thin films toward NO2 gas. J. Alloys Compd. 2021, 885, 160908.
5. Yi, N.; Cheng, Z.; Li, H.; Yang, L.; Zhu, J.; Zheng, X.; Chen, Y.; Liu, Z.; Zhu, H.; Cheng, H. Stretchable, ultrasensitive, and low-temperature NO2 sensors based on MoS2@rGO nanocomposites. Mater. Today Phys. 2020, 15, 100265.
6. Majhi, S.M.; Mirzaei, A.; Kim, H.W.; Kim, S.S. Reduced Graphene Oxide (rGO)-Loaded Metal-Oxide Nanofiber Gas Sensors: An Overview. 2021.

The influence of the graphite precursor and the oxidation method on the number of graphene layers in reduced graphene oxide-statistical approach

S. DREWNIAK[1], Ł. DREWNIAK[1], M. SAJDAK[2], R. MUZYKA[3]

[1] Department of Optoelectronics, Silesian University of Technology, 2 Krzywoustego St., 44-100 Gliwice, Poland
[2] Department of Air Protection, Faculty of Energy and Environmental Engineering, Silesian University of Technology in Gliwice, 44-100 Gliwice, Poland
[3] Department of Chemistry, Faculty of Medical Sciences in Zabrze, Medical University of Silesia in Katowice, ul. Jordana 19, 41-808 Zabrze, Poland
email address: sabina.drewniak@polsl.pl

Graphene and graphene based materials have numerous unique features. High specific surface area, exceptional electrical and thermal conductivity, nanoscalability, mechanical strength, flexibility, ease of chemical functionalization make graphene and graphene-based materials promising candidates for various application [1]. For these reason, extensive research is carried out on the possibility of their use in various areas of electronics and opto-electronics. In gas sensing applications, reduced graphene oxide (rGO) exhibit better properties than pure graphene. The fabrication of rGO is a multistage process which can be realized in various ways. The fabrication method, as well as the parameters of the technological process, have a significant influence on the properties of the obtained rGO and in turns have a great influence on the sensing properties of rGO based sensor. For this reason, it is important to understand how different fabrication methods and process parameters affect the quality and usability of the fabricated rGO. Therefore, we show how such parameters determine the number and sizes of graphene layers. For this purpose, we used the multivariate analysis of variance method (ANOVA). This method focuses on a finding association between independent (qualitative) variables and the quantitative type of dependent variable. In our case, the type of precursor and the oxidation method were an independent variables, while the number of graphene layers (calculated from the AFM measurements) was the dependent variable.

References:

1. Majhi, S.M.; Mirzaei, A.; Kim, H.W.; Kim, S.S. Reduced Graphene Oxide (rGO)-Loaded Metal-Oxide Nanofiber Gas Sensors: An Overview. 2021.

Simulations of micromachined side-hole optical fiber for refractive index sensing based on optical losses

M. DUDEK, K. KÖLLŐ, P. MARĆ, L. R. JAROSZEWICZ

Institute of Applied Physics, Military University of Technology, gen. Sylwestra Kaliskiego 2, 00-908 Warsaw, Poland

e-mail address: michal.dudek@wat.edu.pl

With the increasing interest in the optical fibers, along with the telecommunication properties, the development of fiber optic sensors (FOSs) is also present. To cope with the constantly widening fields of their possible applications, the design of FOSs, as well as the technology to obtain them, had to improve [1]. In the midst of many possibilities of FOSs, the inline sensors with microcavities inside the fibers can be highlighted [2]. This kind of sensor allows to measure the desired physical parameter using for instance the change in the refractive index of the medium the sensor is placed in. The inline cavity sensing is an unusual method, since it requires change in the geometry of optical fiber's core, which in normal conditions is inaccessible. This method however is associated with the need of micromachining of the optical fiber using for example a laser beam or chemical etching [3]. The geometry of the cavity itself can determine optical losses, i.e. insertion loss (IL) and return loss (RL), which are one of the most important parameters in this kind of sensors, as they can be directly measured and translated into specific changes in the cavity's environment.

The presented study was conducted using the finite-difference time-domain (FDTD) method, which is a widely used full-wave technique for approximate description of propagation of electromagnetic waves, especially in systems in which the dimensions of studied structures are comparable to wavelengths used in the simulations [4]. In this work for numerical simulations we used the FDTD solver by ANSYS/Lumerical.

The analyzed S-H OF was based on an actual fiber produced by the Optical Fiber Technology Laboratory, Maria Curie-Sklodowska University. The RI of the S-H OF (its model is presented in Fig. 1) cladding was set to 1.4425, while the RI of the core was set to 1.457. The radii of the elliptic core were 1 µm and 2.3 µm, the cladding radius was 62.5 µm, the holes were ellipses with radii set to 16 µm and 12 µm. The simulation region was 130x130x50 µm^3 with uniform mesh and source wavelength of 1.55 µm.

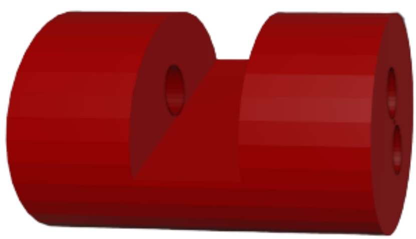

Fig. 1. Example of rectangular cut-out in S-H OF

The simulations of rectangular cut-outs were performed for a cavity with the height of 10 µm and ending 3 µm from the center of the fiber. This allowed for the external liquid to get inside of one of the holes, while the core and the other one were intact. An example cross-sections for liquid's RI set to 1.3 are presented in Fig. 2, where dashed lines denote the positions of the other cross-section.

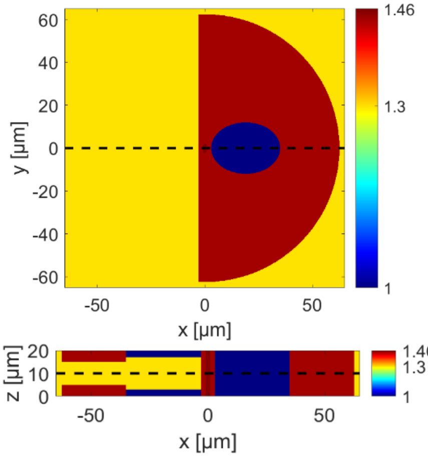

Fig. 2. RI cross-section through the S-H OF perpendicular (top) and parallel (bottom) to its axis with RI of external liquid equal to 1.3

For changing RI of the external liquid it was possible to obtain the IL values. A set of simulations for HE_{11}^{x} and HE_{11}^{y} modes (denoted respectively as fundamental TE and fundamental TM by the117hanginge) were performed in order to analyze the possibility of measuring the117hangingg external RI (Fig. 3) based on the power transmitted through the fiber with cut-out.

The fundamental TM mode of the analyzed S-H OF with rectangular cut-out does not change in a meaningful way with the changes of external RI – in a range of 0.3 dB. It may be due to the fact that this mode propagates along the major axis of the fiber's core and influence from the external RI is lower than on the propagation of TE mode (along minor axis of the core). The IL values for TE mode are apparently oscillating in a range of 1.8 dB and therefore are easily detectable.

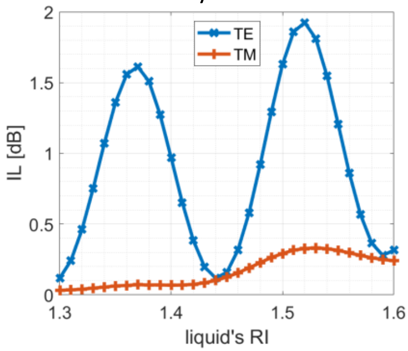

Fig. 3. IL for changing RI of the external liquid

The changes of IL of TE mode presented in Fig. 3 offer to use this kind of S-H OF modification e.g. in its linear part around RI = 1.33, which can be very useful to design a RI sensor for water-based solutions

Acknowledgments: This research was financially supported by the Ministry of the National Defense of the Republic of Poland, project GBMON/13-995/2018/WAT.

References:

[1] K. Grattan et al., Sensors and Actuators 82, (2000)

[2] X. Zhou et al., Optics Express 24, 16, (2016)

[3] Y.-J. Rao et al., Optical Fiber Technology 19, 6, (2013)

[4] A. Taflove, et al., Computational Electrodynamics – The Finite-Difference Time-Domain Method – Third Edition, Artech House, (2005)

Laser stabilization using acousto-optic modulator for ion cooling purpose in ion trap based quantum computer – basic setup examination

SZ. FIDERKIEWICZ[1], M. ŻYCZKOWSKI[1]

[1]Wojskowa Akademia Techniczna (Kaliski str. 2, 00-908, Warsaw, Poland)
e-mail address: szymon.fiderkiewicz@wat.edu.pl

Quantum computer technology is progressing rapidly with different types of architecture available and hance different types of qubits; ion trap qubits, photonic qubits, superconducting qubits and topological qubits. Each of them having their advantages and disadvantages.

In our research group within the project, we have decided to built a quantum computer based on ion trap. That is due to the very high operation accuracies obtained in experiments [1], the relatively low requirements of the physical conditions in which they are used and their scalability. The optical and microwave technology required to operate them is well developed and readily available today [2].

Ions are trapped due to electric potential applied within the trap and their micro-motion is reduced by cooling them using lasers. Qubit states are realized by exciting ions to desired energy level. Transition between energy levels is possible when a valence electron emits or absorbs a photon with a frequency consistent with the energy difference between the levels. For both laser cooling and qubit state preparation the lasers needs to operate at very specific frequency and energy, hence both of those parameters have to remain as stable as possible. For this purpose different stabilization techniques are applied.

Before building the true ion trap setup, we have decided first to learn and master the different laser stabilization techniques. One of them is based on using the acousto-optic modulator (AOM) in the feedback loop. In this work such feedback loop was realized. This work concerns both the optical part of the experimental setup and the electronics hardware from SINARA infrastructure which will also be applied in the future setup for the control of the optoelectronic part of the ion trap.

Acknowledgments:

This project has received funding from the National Center for Research and Development research and innovation programme under grant agreement DOB-SZAFIR/01/A/023/01/2020.

I would also like to acknowledge the help of the Creotech company in understanding the SINARA platform.

References:

[1] C. J. Ballance, T. P. Harty, N. M. Linke, M. A. Sepiol, and D. M. Lucas, "High-fidelity quantum logic gates using trapped-ion hyperfine qubits."

[2] T. P. Harty, MA Sepiol, D. T. Allcock, C. J. Ballance, J. Tarlton, D. Lucas, High-fidelity trapped-ion quantum logic using near-field microwaves, Phys Rev Lett American Physical Society 117:14 (2016) 140501

Variability of fluorescence of nitrogen-vacancy centers in nanodiamonds

M. J. GŁOWACKI[1], M. FICEK[1], M. SAWCZAK[2], R. BOGDANOWICZ[1]

[1]Gdańsk University of Technology, 11/12 Narutowicza Str., 80-233 Gdańsk, Poland
[2]Institute of Fluid-Flow Machinery, 14 Fiszera Str., 80-231 Gdańsk, Poland
e-mail address: maciej.glowacki@pg.edu.pl

Nitrogen-vacancy (NV) color centers are fluorescent defects found in nanodiamonds. They are extensively researched due to their intensive and time-stable fluorescence, and an electron spin which is very sensitive to external stimuli. The fluorescence of NV centers may be affected by various factors, including temperature, size of the nanodiamonds [1], and properties of a surrounding environment [2]. In the present study an impact of these factors on the signal emitted by NV centers is presented.

To examine the effect of temperature on the fluorescence of NV centers, a thin layer of the nanodiamonds was integrated with temperature control microscopy stage. With decreasing temperature the relative intensity of the zero-phonon lines of NV centers to their phonon sidebands has been found to rise.

To investigate the impact of the nanodiamonds' size on the fluorescence of NV centers, a series of suspensions of the nanodiamonds was prepared and subjected to an ultrasonic treatment with various durations (5, 10, 15, 20 or 60 minutes). The fluorescence of the resulting suspensions was analyzed. Moreover, droplets of every suspension were dried on silicon substrates and later imaged using scanning electron microscopy (SEM). Particle size distributions in the samples were calculated from SEM images.

Finally, to assess the influence of the dispersion medium on the performance of NV centers, a series of solvents with pH levels in the range of 2-12 were prepared. In these solvents the nanodiamonds were suspended, and their fluorescence later examined. The ratio of photon counts at the zero-phonon line of the negatively-charged NV centers (NV^-; 637 nm) to the photon counts at the zero-phonon line of the neutral NV centers (NV^0; 575 nm) was calculated and plotted versus resulting pH of the suspensions. Moreover, the zeta potential of the samples was investigated.

Acknowledgments: This research has been carried out within the TEAM-NET program of the Foundation for Polish Science co-financed by the European Union under the European Regional Development Fund (project POIR.04.04.00-00-1644/18).

References:

[1] M. Ficek et. al., Coatings 11, 11, 1332 (2021)
[2] W. Białobrzeska et. al., Journal of Molecular Liquids 342, 117338 (2021)

Numerical analysis of silicon nitride planar Bragg gratings

M. GOLAS[1,2], M. LELIT[1,3], M. SŁOWIKOWSKI[1,3], K. PAVŁOV[1], B. STONIO[1,3], M. FILIPIAK[1], M. JUCHNIEWICZ[1], P. WIŚNIEWSKI[1], R.B. BECK[1,3],

[1]Warsaw University of Technology, Centre for Advanced Materials and Technologies CEZAMAT, Poleczki 19, 02-882 Warsaw, Poland
[2]Warsaw University of Technology, The Faculty of Electronics and Information Technology, Nowowiejska 15/19, 00-665 Warsaw, Poland
[3]Warsaw University of Technology, Institute of Microelectronics and Optoelectronics, 00-662 Warsaw, Poland;
e-mail address: michal.golas.stud@pw.edu.pl

For several decades, Bragg gratings have been studied and used as photonic sensors, filters, demultiplexers, and attenuators. Deploying these as the elements of photonic integrated circuits allows controlling their parameters with far higher precision than in fiber Bragg gratings.
Due to its low material absorption and light scattering, silicon nitride is considered one of the attractive materials for developing integrated photonic circuits [1]. Compared to the other material stacks, for example, SOI, near-zero dispersion can be easily achieved in silicon nitride [2].
In this work, the authors present the results of simulations of integrated Bragg gratings designed for operation in the third communication window and visible band. The geometrical parameters of the structure shown in Fig. 1. were carefully modified to provide single-mode propagation of the signal of a specific wavelength [2].

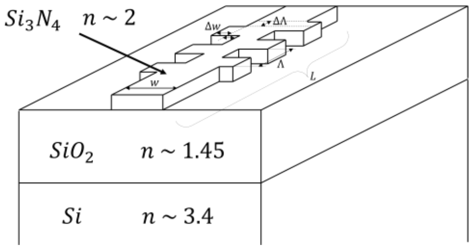

Fig. 1. Integrated Bragg grating scheme and its geometrical parameters.

An example of the simulated transmission characteristic of integrated Bragg grating is presented in Fig. 2. It depends on material refractive index, the waveguide width and height, Δw, period, and phase shift [3].

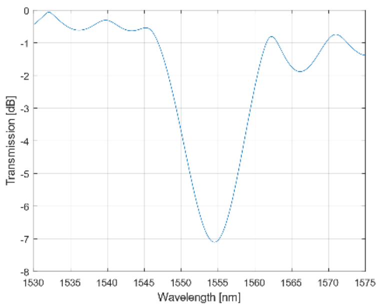

Fig. 2. Transmission spectrum of integrated Bragg Grating.

The transmission characteristic shown in Fig. 2 was obtained for the Bragg grating centered at 1555 nm with FWHM of 5 nm. This element is currently prepared for fabrication in silicon nitride platform, developed in CEZAMAT WUT.

Acknowledgments: This work was supported by the Institute of Applied Research Warsaw University of Technology Sp. z o.o., Poland, the research project Innovation Incubator 4.0 „Development of an integrated photonics platform based on silicon nitride for the visible spectrum for sensing applications" (No. 5/2021).

References:

[1] Hu Y., et al. IEEE Journal of Selected Topics in Quantum Electronics, 2018
[2] Yaping H. et al. Photonics, 2021: 161
[3] Zubkova E. et al. Journal of Physics: Conf. Series 917, 2017, Saint Petersburg

Fabrication of nonlinear chirped fibre Bragg gratings

A. GOLESTANI[1,2], R. H.S. BANNERMAN[2], J. C. GATES[2],
P. G. R. SMITH[2], M. KARPIŃSKI[1]

[1]Faculty of Physics, University of Warsaw, Pasteura 5, 02-093 Warszawa, Poland
[2]Optoelectronics Research Centre, University of Southampton, Southampton, SO17 1BJ, UK
e-mail address: Ali.Golestani@fuw.edu.pl

The spectral-temporal degree of freedom of the light is considered as promising candidate for realization of high dimensional optical networks. This requires development of optical devices that can shape the optical pulses in time and frequency domains. In this context, chirped fibre Bragg gratings (CFBG) have become popular in optical signal processing applications due to their efficiency in dispersion engineering. The linear CFBGs have been fabricated to engineer dispersion in optical systems. However a grating structure that can eliminate nonlinear aberration in optical devices is still missing. Here we aim to fabricate a nonlinear CFBG that compensates a nonlinear dispersion profile. This nonlinear CFBG particularly designed to eliminate aberration in an electro-optic time lens system driven by a nonlinear temporal phase profile.

In this research a direct UV writing technique based on phase-controlled interferometry as a fabrication process for inscription of grating structures inside an optical fibre is presented. In this process, a non-uniform modulation of refractive index along the core of the optical fiber length is applied to make chirped grating structure.

To implement this, the core of the optical fibre is placed under exposure of the interfering UV laser beams in which an electro-optic phase modulation is applied into one arm of the interferometer to manipulate the fringe pattern and control the applied energy [1]. By controlling the UV induced refractive index change and the Bragg period along the core of optical fiber, we managed to write designed pattern of linear CFBG and get desired spectral reflection at 1560 nm. Preliminary results shows the capability of this technique for fabricating the nonlinear CFBG structures.

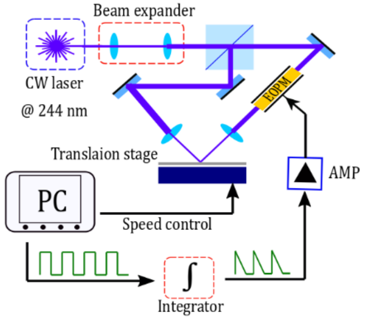

Fig. 1. Optical setup for direct UV writing of Bragg gratings based on phase modulated interferometry.

Acknowledgments: This work was supported by Foundation of Polish Science in the framework of First TEAM programme.

References:

[1] C. Sima et. al., Optics Express 21, 13 (2013)

Luminescent temperature sensor based on glass and glass-ceramic optical fiber.

P. GOLONKO[1], J. ŻMOJDA[1],

[1]Bialystok University of Technology, Faculty of Electrical Engineering,
45D Wiejska St.15-351 Bialystok, Poland
e-mail address: p.golonko@doktoranci.pb.edu.pl

Glass and glass-ceramic (GC) fibers doped with lanthanides ions can be used as a temperature sensor [1][4]. These kinds of sensors are based on the temperature-dependent variation of spectroscopic properties of rare-earth ions embedded in glass or GC matrix. In this case, several mechanisms can be used to measure the temperature optically. These measurements can be based on the following: fluorescence intensity ratio (FIR)[5] asymmetry ratio (AR)[6] between electric-dipole transition (EDT) and magnetic-dipole transition (MDT), spectral shift [7], lifetime [8], or absolute intensity (AI) [9].

To measure temperature with AI mechanism where luminescence changes with the temperature a Bloltzamn distribution [10] can be used to explain this mechanism. This technique describes the occupation of the different levels and changes line position with temperature.

Equation (Fig.1) describes the estimated temperature dependant property of luminescence.

$$I(T) = \frac{I_0}{1+Aexp^{\frac{-E_b}{k_B T}}}$$

Fig. 1. Boltzmann's distribution estimate equation.

Where T is the sample- temperature, I(T) is the photoluminescence, I_0 is the photoluminescence intensities at temperature 0 K, A is a pre-exponential constant, k_B is the Boltzmann constant, and E_b is exciton binding energy.

In this paper, europium and erbium ions were used in $35SiO_2$, $5Al_2O_3$. $30GeO_2$, $20Sb_2O_3$, $10Na_2O$, (SGS) matrix. The matrix was doped with a small concentration of Eu_2O_3 or Er_2O_3 and P_2O_5 as a nucleation agent. Those materials were a core material for fibers with F2 glass cladding. The fiber was obtained in a modified rod in tube technique.

Fibers were examined in temperatures ranging from room temperature to 500 °C. During temperature changes, luminescence was measured with spectroscopy and a 395nm laser source. AR was also determined dor Eu3+ materials, where the $^5D_0 \rightarrow {}^7F_1$ and $^5D_0 \rightarrow {}^7F_2$ were measured.

Based on the results of the study, it should be concluded that the SGS material has a great potential for the construction of temperature sensors.

Acknowledgments: This work was supported by the National Science Centre (Poland) granted on the basis of the decision No. DEC-2019/35/O/ST5/03105

References:

[1] R. Yatskiv, P. Kostka, J. Grym, and J. Zavadil, "Temperature sensing down to 4 K with erbium-doped tellurite glasses," *J. Non. Cryst. Solids*, vol. 575, p. 121183, Jan. 2022, doi: 10.1016/J.JNONCRYSOL.2021.121183.

[2] Z. Y. Zhang, T. Sun, K. T. V. Grattan, and A. W. Palmer, "Erbium-doped intrinsic fiber sensor for cryogenic temperature measurement," *Sensors Actuators A Phys.*, vol. 71, no. 3, pp. 183–186, Dec. 1998, doi: 10.1016/S0924-4247(98)00191-5.

[3] S. F. León-Luis, U. R. Rodríguez-Mendoza, E. Lalla, and V. Lavín, "Temperature sensor based on the Er3+ green upconverted emission in a fluorotellurite glass," *Sensors Actuators B Chem.*, vol. 158, no. 1, pp. 208–213, Nov. 2011, doi: 10.1016/J.SNB.2011.06.005.

[4] Y. Dwivedi and S. B. Rai, "Temperature-sensing behavior of Eu:BaB4O7 nanocrystals," *Sensors Actuators A Phys.*, vol. 163, no. 1, pp. 37–41, Sep. 2010, doi: 10.1016/J.SNA.2010.06.021.

[5] D. Chen, M. Xu, S. Liu, and X. Li, "Eu2+/Eu3+ dual-emitting glass ceramic for self-calibrated optical thermometry," *Sensors Actuators B Chem.*, vol. 246, pp. 756–760, Jul. 2017, doi: 10.1016/J.SNB.2017.02.159.

[6] S. K. Sharma, T. Köhler, J. Beyer, M. Fuchs, R. Gloaguen, and J. Heitmann, "Extending the temperature sensing range using Eu3+ luminescence up to 865 K in a single crystal of EuPO4," *Phys. Chem. Chem. Phys.*, vol. 21, no. 29, pp. 16329–16336, 2019, doi: 10.1039/c9cp03501j.

[7] X. Li *et al.*, "Optical temperature sensing of Eu3+-doped oxyhalide glasses containing CsPbBr3 perovskite quantum dots," *J. Lumin.*, vol. 219, p. 116897, Mar. 2020, doi: 10.1016/J.JLUMIN.2019.116897.

[8] P. Lopez-Iscoa *et al.*, "Spectroscopic Properties of Er3+-Doped Particles-Containing Phosphate Glasses Fabricated Using the Direct Doping Method," *Materials (Basel).*, vol. 12, no. 1, p. 129, Jan. 2019, doi: 10.3390/ma12010129.

[9] B. Klimesz, R. Lisiecki, and W. Ryba-Romanowski, "Thermosensitive Tm3+/Yb3+ co-doped oxyfluorotellurite glasses – spectroscopic and temperature sensor properties," *J. Alloys Compd.*, vol. 823, p. 153753, May 2020, doi: 10.1016/J.JALLCOM.2020.153753.

[10] K. Binnemans, "Interpretation of europium(III) spectra," *Coord. Chem. Rev.*, vol. 295, pp. 1–45, Jan. 2015, doi: 10.1016/j.ccr.2015.02.015.

[11] P. Golonko, J. Bednarek, and J. M. Żmojda, "Effect of temperature on luminescent properties of Eu3+ ions doped antimony-gemanate glass and glass-ceramic," *https://doi.org/10.1117/12.2607075*, vol. 12040, pp. 11–18, Nov. 2021, doi: 10.1117/12.2607075.

High-efficiency transmission gratings obtained using azobenzene poly(etherimide) and holographic method

A. HERNIK[1], D. SZMIGIEL[2], J. KONIECZKOWSKA[3], E. SCHAB-BALCERZAK, A. KOZANECKA-SZMIGIEL[1*]

[1]Faculty of Physics, Warsaw University of Technology, 75 Koszykowa Str., 00-662 Warszawa, Poland
[2]Łukasiewicz Research Network - Institute of Microelectronics and Photonics, al. Lotnikow 32/46, 02-668 Warszawa, Poland
[3]Centre of Polymer and Carbon Materials Polish Academy of Sciences, 34 M. Curie-Sklodowska Str., 41-819 Zabrze, Poland
e-mail address: anna.szmigiel@pw.edu.pl

Diffraction gratings are essential optical components used in spectrometers, telecommunications and laser systems. High diffraction efficiency is desirable in many specific applications, but maximizing this parameter for a selected diffraction order may be challenging for certain grating types. Azobenzene polymers are important optical materials showing sensitivity to light polarization. They are known for unique photoinduced processes such as optical birefringence generation and surface relief grating formation. The latter phenomenon involves polymer mass transport under spatially inhomogeneous irradiation, which leads to the appearance of sinusoidal deformations of initially flat polymer surfaces. The efficiency of the relief grating formation strongly depends on azopolymer chemical structure and applied irradiation geometry; however, only general relationships between the structural features or illumination conditions and the obtained optical response have not been established yet. Recently, we have reported large-amplitude surface deformation in a synthesized azopoly(etherimide) (azoPEI), which had not been observed before for other azopolymers belonging to polyimide family [1].

In this work, we present the results of systematic studies of the relief formation in azoPEI under irradiation with blue-light polarization pattern formed by two coherent beams with left- and right - circular polarization. We show that for a specific experimental geometry, the diffraction efficiency may reach as high values as ca. 30 % or 20 % for the first or the second spectral order, respectively.

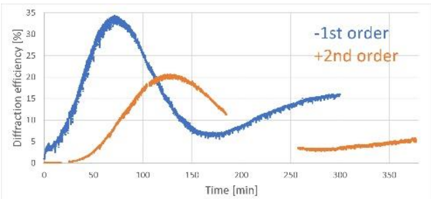

Fig. 1. Time evolution of the 1st and 2nd order diffraction efficiency of the fabricated grating

Acknowledgments: This work was partially supported by the FOTECH-1 project granted by the Warsaw University of Technology, under the program Excellence Initiative: Research University (ID-UB).

References:

[1] J. Konieczkowska et al., Materials Science and Engineering B 273 115387 (2021)

Magnetically-sensitive nanodiamond thin-films on glass fibers

M. JANI[1], P. CZARNECKA[1], S. SENGOTTUVEL[1], M. MRÓZEK[1], P. DĄBCZYŃSKI[1], A. FILIPKOWSKI[2,3], I. KUJAWA[3], D. PYSZ[3], W. GAWLIK[1] AND A. M. WOJCIECHOWSKI[1]

[1]Institute of Physics, Jagiellonian University, Łojasiewicza 11, 30-348 Kraków, Poland
[2]Faculty of Physics, University of Warsaw, Pasteura 5, Warsaw, 02-093, Poland
[3]Łukasiewicz Research Network - Institute of Microelectronics and Photonics, Al. Lotników 32/46, Warsaw, 02-668, Poland
e-mail address: mona.jani@uj.edu.pl; a.wojciechowski@uj.edu.pl

By assembling 140 nm-sized fluorescent nanodiamonds in a thin-film on (3-aminopropyl) triethoxysilane functionalized glass surface, we prepare magnetically-sensitive FND-fiber probes for endoscopy [1]. The obtained FND layers show good uniformity over large surfaces and are characterized using confocal, fluorescence, and atomic force microscopes. Further, FNDs are assembled on single large-core multimode optical fibers and imaging fiber bundles end face to detect optically detectable magnetic resonance signals. The optically detectable magnetic resonance signals are recorded through the fiber's far end in magnetic fields between 0 to 2.5 mT. A multi-channel sensor is demonstrated with the capability of parallel-in-time mapping and instantaneous readout from individual pixel and enabling magnetic mapping at high spatial resolution. Results of this study are promising for early stage detection in bio-diagnostic applications.

Acknowledgments: This work was supported by the Foundation for Polish Science in scope of the TEAM NET POIR.04.04.00-00-1644/18.

Reference:

[1] P. Czarnecka, M. Jani et. al., Opt. Mater. Express. 12, 444–457, (2022).

A novel non-pathogenic method for testing virus filtration ability of protective masks using the fluorescence phenomenon

D. KOGUT[1,2], P. KAŁUŻYNSKI[3*], M. KONIECZNA[1,2], I. ŚLĘZAK-PROCHAZKA[2], A. KAZEK-KĘSIK[4,2]

[1]Department of Systems Biology and Engineering, Silesian University of Technology, Gliwice, Akademicka 16, 44-100 Gliwice, Poland
[2]Biotechnology Center, Silesian University of Technology, Krzywoustego 8, 44-100 Gliwice, Poland
[3]Department of Optoelectronics, Silesian University of Technology, Krzywoustego 2, 44-100 Gliwice, Poland
[4]Department of Inorganic, Analytical Chemistry and Electrochemistry, Faculty of Chemistry, Silesian University of Technology, B. Krzywoustego 6, 44-100 Gliwice, Poland partment of Optoelectronics, Silesian University of Technology, Gliwice, Poland;
e-mail address: piotr.kaluzynski@polsl.pl

During the Covid-19 pandemic, wearing personal face masks has become an integral part of our lives. The role of such masks should be to protect healthy people from potential infections and to limit the spread of viruses and bacteria from sick people. For this reason, the filtering capacity of commonly used face masks was tested experimentally using the methodology developed by our team. In this method, we use polystyrene nanospheres with a size of about 100 nm coupled with a luminescent dye FITC, which was to be a phantom of a real virus. In order to carry out the research, a system for testing the filtration efficiency of masks was built, consisting of an aerosol generator in which nanospheres were suspended. The aerosol was then passed through the test mask and then through the Andersen cascade impactor, where fluorescent nanoparticles were collected for qualitative results (Fig. 1). As the analyzed materials, the hand-made masks made of cotton fabrics and different types of protective masks commonly available in retail and medical trade (eg. surgical, FFP2, FFP3) were chosen (Fig. 2).

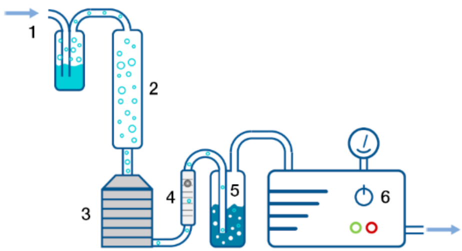

Fig. 1. Schematic diagram of the laboratory stand, 1) nebulizer with air inlet, 2) aerosol chamber, 3) Andersen cascade impactor, 4) flow meter, 5) water filtering chamber, 6) vacuum pump with air outlet.

Additionally, specially prepared materials with the use of nanofibers with metal admixtures were tested. These materials were used for casually weared masks as an additional protective layer increasing the filtering capacity of the mask. This method allows researchers to be conducted in a safe manner without the use of potentially pathogenic organisms.

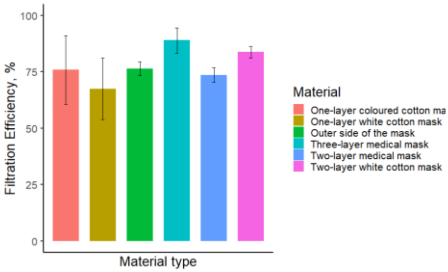

Fig. 2. Filtration efficiency for selected materials as a percentage of particles retained by the mask

Acknowledgments: This work was financially supported by Pro-quality grant 32/007/RGC20/0027.

Thermal properties of polymers containing QD CdSe produced in high and low boiling organic solvents

A.KICZOR[1], P.MERGO[1]
[1]Maria Curie-Sklodowska University in Lublin/ Laboratory of Optical Fiber Technology, Sq Marii Curie-Sklodowskiej 3, 20-031 Lublin
anna.kiczor@umcs.lublin.pl

Optical fibers can be covered with various coatings to improve their properties and enable their specific application. Quantum dots are characterized by a long lifetime of fluorescence, very high stability and resistance to whitening. By manipulating the shape and size, you can influence their properties in a specific way, needed for a given application. They are characterized by high quantum efficiency, extremely narrow bands of photoluminescence emission.

Compared to standard organic dyes, they have a long fluorescence lifetime, very high stability and resistance to photobleaching. The synthesis of CdSe quantum dots in an organic solvent with high boiling point - octadecane (boiling point 317°C) was optimized. The obtained compounds were doped with methyl methacrylate during prepolymerization, mixed and annealed in order to complete the polymerization process [Fig. 1].

The structures obtained were characterized by very high luminescence.

Fig. 1. Preforms with pure PMMA and PMMA doped with CdSe quantum dots in octadecane (orange preform)

Similarly, quantum dots were made using a light solvent - hexane with a boiling point of 69°C. During the polymerization process, the solvent inside the polymer boiled strongly, as a result of which the resulting structure had many air bubbles and an uneven surface. This was due to insufficient solvent evaporation due to the omission of the prepolymerization process. A similar synthesis was performed, however, CdSe quantum dots in hexane were added immediately to the polymerization mixture [Fig. 2].


a)
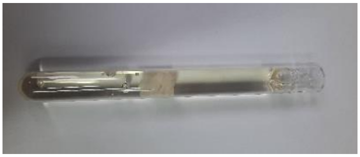
b)

Fig. 2. PMMA preforms doped with CdSe quantum dots in hexane a) preform with added QD after the prepolymerization process, b) preform with QD added to the polymerization mixture

Emission spectra of structures made with the use of both solvents were compared, as well as TG thermogravimetry and DSC differential scanning calorimetry graphs. Relevant conclusions were made, which show that the obtained materials may be promising in application as coatings for optical fibers.

Acknowledgments: This work was supported by National Science Center (Maestro 8, DEC-2016/22/A/ST7/0008. The purchase of the scientific apparatus used for the syntheses was financed by the project National Laboratory for Photonics and Quantum technologies – NLPQT (POIR.04.02.00-00-B003/18-00).

References:

[1] Jacak L., Hawrylak P., Wójs A., Quantum Dots, Springer, eBOOK ISBN 978-3-642-72002-4, Heidelberg 1998

[2] Murray C.B., Norris D.J., Bawendi M.G., Synthesis and characterization of nearly monodisperse CdE (E=S, Se, Te) semiconductor nanocrystallites, Journal of the American Chemical Society 115, 8706-8715, 1993

[3] Rogach A. L., Semiconductor Nanocrystal Quantum Dots- Synthesis, Assembly, Spectroscopy and Applications, SpringerWienNewYork, Wien 2008

[4] Asokan S., Krueger K. M., Alkhawaldeh A., Carreon A.R., Mu Z., Colvin V. L., Mantzaris N. V., Wong M.S., The use of heat transfer fluids in the synthesis of high-quality CdSe quantum dots, core/shell quantum dots, and quantum rods, Nanotechnology 16, 2000-2011, 2005

[5] Anolini F., Orazi L., Quantum Dots Synthesis Through Direct Laser Patterning: A Review, Frontiers in Chemistry, Volume 7, Article 252, 2019

[6] Brichkin S.B., Razumov V. F., Colloidal quantum dots: synthesis, properties and applications, Russian Chemical Reviews, 85(12) 1297-1312, 2016

Analysis of planar waveguides with a high index overlayer and nonlinear cladding

J.M.KUBICA

Central Institute for Labour Protection – National Research Institute
Czerniakowska 16, 00-701 Warsaw, Poland
e-mail address: kubica@ieee.org

Optical waveguide sensors based on the evanescent waves in the cladding have been proposed for many applications, such as chemical and biochemical sensing [1] or detection of ultraviolet (UV) radiation [2]. In that case, optical properties of the guided modes are modified by a change in the refractive index of the cladding due to the presence of the analyte or a change in its concentration. Among the many material and geometry configurations, one can find proposals of optical structures that utilize Kerr-type nonlinear cladding for sensing applications [3].

The aim of this paper is to analyze a planar optical waveguide with Kerr-type nonlinear cladding and additional high index overlayer separating the cladding and the guiding core (Fig. 1). Such overlayers have been suggested to improve sensitivity of waveguide sensors in linear cases.

The structure has been analyzed by the standard transfer matrix method applied in the self-consistent iteration procedure [4]. This procedure involves a sequence of numerical solutions of the dispersion equation expressing the modal condition for linear waveguides. The starting point corresponds to the linear waveguide structure with negligible power flow. The electric field profile $E_y(x)$ corresponding to the resulting propagation constant $\beta^{(0)}$ is used in the next iteration loop to modify the intensity dependent refractive index in the

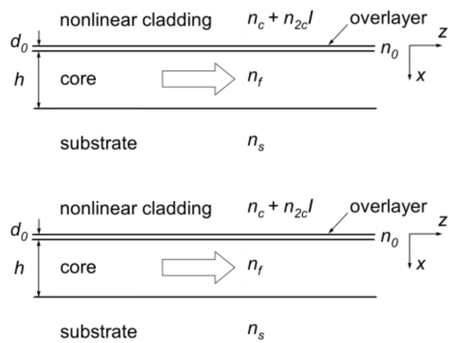

Fig. 1. (a) Geometry of the waveguide; (b) multilayer configuration for the transfer matrix approach.

nonlinear cladding. For this purpose, the cladding is divided into a sufficient number of thin homogeneous sublayers along the effective depth d_c, as shown in Fig. 1(b). It is assumed that the power flow is negligible for $x < -d_c$, and the sublayers are thin enough to ignore local changes in refractive index and electric field amplitude. In practice, when $n_c \gg n_{2c} I$, for the j-th layer, we use

$$n_j^2\left(E_y(x_j)\right) = n_c^2 + \alpha_j \left|E_y(x_j)\right|^2, \quad (1)$$

where $E_y(x_j)$ is the electric field amplitude in the middle of the j-th layer, $\alpha_j = n_{2c} n_c^2 (\varepsilon_0/\mu_0)^{1/2}$, ε_0 is the free space permittivity, and μ_0 is the free space permeability. The new refractive index profile is then used to calculate the corresponding propagation constant $\beta^{(1)}$ and relevant electric field distribution. The iteration process is repeated until the successive difference of propagation constants $\beta^{(n)} - \beta^{(n-1)}$ is sufficiently small. In each iteration loop, the zero-power refractive index n_c is used on the right side of (1), rather than that resulting from the previous loop. In addition, each time the resulting field profile $E_y(x)$ is normalized to the input power per unit width P_0. For TE modes, this is done by selecting the field profile $E_y(x)$ to obtain

$$P_0 = \frac{\beta}{2}\left(\frac{\varepsilon_0}{\mu_0}\right)^{1/2} \int_{-\infty}^{+\infty} E_y^2(x)dx. \quad (2)$$

The number of iterations needed for convergence of the method depends on the starting parameters and accuracy required. In general, the method provides stable solutions for a given power flow. Each linear multilayer problem in the iteration scheme has been solved by using the standard transfer matrix method that provides an algebraic equation expressing the modal condition [5]. The numerical solution of the equation gives values of the propagation constants of the guided modes.

For numerical analysis, the following waveguide parameters have been used: λ = 0.515 μm, h = 1.0 μm, n_f = 1.57, n_o = 1.70, n_c = n_s = 1.55, and n_{2c} = 10^{-9} m^2/W. Power dependence of β for several values of the overlayer thickness d_o is presented in Fig. 2. As can be seen, the presence of the overlayer eliminates the unstable solutions characteristic for single layer waveguides with the same core thickness, along with the relevant bistability effect. This can be of interest for sensing applications where single value functions are preferred.

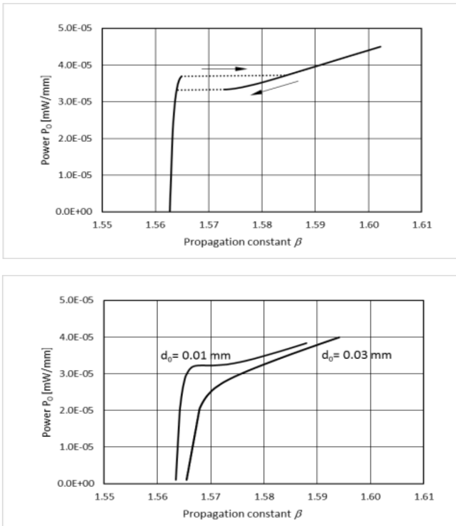

Fig. 2. Power P_0 vs propagation constant β: (a) without an overlayer; (b) with an overlayer of thickness d_0 = 0.01 mm and 0.03 mm.

Acknowledgments: This work has been based on the results of a research task no 3.SP.13 carried out within the scope of 5th National Program "Improvement of safety and working conditions" supported by the National Centre for Research and Development.

References:
[1] W. Lukosz, Sens. Actuators B, 29, 37, (1995).
[2] T. Shen et al., Sens. Actuators A, 307, 111989, (2020).
[3] S. A. Taya et al., Optik, 121, 860, (2010),
[4] F. Dios et al., Optics Commun., 72, 54, (1989).
[5] J. Chilwell et al., J. Opt. Soc. Am. A, 1, 742, (1984).

Growth of B/N co-doped CVD grown homoepitaxial diamond films: optical and electrical properties

S. KUNUKU[1], M. FICEK[1], A. WIELOSZYNSKA[1], M. TAMULEWICZ-SZWAJKOWSKA[2], K. GAJEWSKI[2], M. SAWCZAK[3], A. LEWKOWICZ[4], J. RYL[5], T. GOTSZALK[2] AND R. BOGDANOWICZ[1]

[1]Department of Metrology and Optoelectronics, Faculty of Electronics, Telecommunications and Informatics, Gdańsk University of Technology, 11/12 Narutowicza St., 80-233, Gdańsk, Poland
[2]Department of Nanometrology, Wrocław University of Science and Technology, Janiszewskiego 11/17 St., 50-372, Wrocław, Poland
[3]The Szewalski Institute of Fluid-Flow Machinery, Polish Academy of Sciences, 80-231, Gdansk, Poland
[4]Institute of Experimental Physics, Faculty of Mathematics, Physics and Informatics, University of Gdansk, Wita Stwosza 57, 80-952 Gdansk, Poland
[5]Department of Electrochemistry, Corrosion and Material Engineering, Gdansk University of Technology, 11/12 Narutowicza Str., 80-233 Gdansk, Poland
e-mail address: srinivasu.kunuku@pg.edu.pl

B doping into diamond (BDD) converts the insulating nature to p-type diamond due to acceptor characteristics of B in the diamond lattice. (BDD) is a prominent material for electro- chemistry due to its low carrier activation energy ~ 0.37 eV, wide potential window, and low-background current[1]. Hence, BDD electrodes were employed in several promising applications like electrochemical sensing [2–4], electron field emission devices [5], wastewater treatment [6], and electrodes for the construction of supercapacitors [7,8].

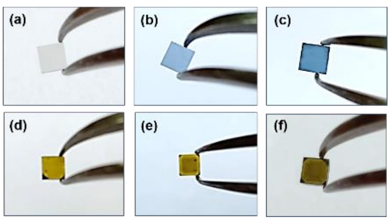

Fig. 1. Photographs of B/N co-doped CVD diamond layer (N/C = 0.02) on SCD IIa; (a) B/C ~ 2500 ppm (b) B/C ~ 5000 ppm (c) B/C ~ 7500 ppm, and photographs of B/N co-doped CVD diamond layer (N/C = 0.02) on SCD Ib; (d) B/C ~ 2500 ppm (e) B/C ~ 5000 ppm (f) B/C ~ 7500 ppm.

The growth parameters, substrates, and synthesis method play a prominent role in the growth of semiconducting BDD to metallic BDD. Doping of boron (B) with other elements into diamond illustrated the enhanced efficacy in doping of B and unique properties. In the present study, B and nitrogen (N) co-doped diamond films have been synthesized on single crystalline diamond (SCD) IIa and SCD Ib substrates in a microwave plasma-assisted chemical vapor deposition process. The B/N co-doping into CVD diamond has been conducted at constant N flow of N/C ~ 0.02 with three different B/C doping concentrations of B/C ~ 2500 ppm, 5000 ppm, 7500 ppm. AFM topography portrayed the flat and smooth surface with low surface roughness for low B doping, whereas surface features like hillock structures and un-epitaxial diamond crystals with high surface roughness were observed for high B doping concentrations. KPFM measurements revealed that the work function (4.74 eV to 4.94 eV) has not varied significantly for CVD diamond synthesized with different B/C concentrations. Raman spectroscopy measurements described the growth of high-quality diamond and photoluminescence studies revealed the formation of high-density nitrogen-vacancy centers in CVD diamond layers. X-ray photoelectron spectroscopy results confirmed the successful B doping and the increase in N doping with B doping concentration. The room temperature electrical resistance measurements of CVD diamond layers (B/C ~ 7500 ppm) have shown the low resistance value ~ 9.29 Ω for CVD diamond/SCD IIa, and the resistance value ~ 16.55 Ω for CVD diamond/SCD Ib samples. The boron doping introduces impurities band revealed surficial conductivity in the range of a few Ohms, which is enhanced additionally by nitrogen co-doping particularly benefiting at low boron-doping. The tailoring of B/N co-doping CVD diamond at SCD substrates allowed to achieve high quality and low resistivity layers attractive in the frame of joint quantum/electronic or electrochemical applications. Moreover, the inhomogeneous hillock defects distribution could be utilized for specific coherence effects of NV centers for quantum sensing applications.

Acknowledgments:
The authors would like to thank the Polish Science grant TEAM NET POIR.04.04.00-00-1644/18 for funding.

References:
1. A. Kraft, I.nt. J. Electrochem. Sci. 2, 31 (2007).
2. N. Yang, H. Uetsuka, E. Osawa, and C. E. Nebel, Angew. Chem. 120, 5261 (2008).
3. J. Ryl, L. Burczyk, A. Zielinski, M. Ficek, A. Franczak, R. Bogdanowicz, and K. Darowicki, Electrochimica Acta 297, 1018 (2019).
4. M. Sobaszek, K. Siuzdak, J. Ryl, R. Bogdanowicz, and G. M. Swain, Sensors and Actuators B: Chemical 306, 127592 (2020).
5. K. J. Sankaran, M. Ficek, S. Kunuku, K. Panda, C.-J. Yeh, J. Y. Park, M. Sawczak, P. P. Michałowski, K.-C. Leou, R. Bogdanowicz, I.-N. Lin, and K. Haenen, Nanoscale 10, 1345 (2018).
6. P. V. Nidheesh, G. Divyapriya, N. Oturan, C. Trellu, and M. A. Oturan, ChemElectroChem 6, 2124 (2019).
7. D. Banerjee, K. J. Sankaran, S. Deshmukh, M. Ficek, C.-J. Yeh, J. Ryl, I.-N. Lin, R. Bogdanowicz, A. Kanjilal, K. Haenen, and S. Sinha Roy, Nanoscale 12, 10117 (2020).
8. J. Wang, Z. He, X. Tan, T. Wang, X. He, L. Zhang, J. Huang, G. Chen, and K. Du, Surface and Coatings Technology 398, 126103 (2020).

A historical perspective of the fibre-optic seismographs and their field application: the past, present and exciting future

A.T. KURZYCH[1,2], L.R. JAROSZEWICZ[1,2], M. DUDEK[1,2], P. MARĆ[1,2], J.K. KOWALSKI[2]

[1]Institute of Applied Physics, Military University of Technology, 2 S. Kaliskiego Str., 00-908 Warsaw, Poland
[2]Elproma Elektronika Ltd., 2D Duńska Str., 05-152 Czosnów, Poland
e-mail address: anna.kurzych@wat.edu.pl

It is now over 50 years since the era of optical fibre sensors started with the non-contact vibration monitoring sensor based on bifurcated fibre bundles (U.S.03327584; 1967) [1]. The first single-mode optical fibres have appeared a decade later which raised possibility to design interferometers which promised immense engineering benefits compares to their free space preursors bolted on optical tables. Optical fibre sensors offer many advantages (i.a. immunity to electromagnetic interference, minimal invasiveness and lightweight) making them a leading technology in many areas. The fibre-optic gyroscope (FOG) based on the Sagnac interferometer is today arguably the most successful fibre sensor technologies. The Sagnac effect makes it possible to obtain directly information about the component of the angular movement perpendicular to the sensor plane. Its principle has been determined in 1913 [2] and its first fibre implementation appeared in 1976 by Vali and Shorthill as an operational FOG [3].

The exciting adventure with a system for angular velocity recording in the Institute of Applied Physics at Military University of Technology has been originated with the FOG named GS-13P in the nineties [3]. The system was characterized by the sensitivity equals $9.7\cdot10^{-7}$ rad/s. The system included: optical head constructed according to the minimum FOG configuration using Hi-Bi fibre optic elements, signal proceeding system based on EG&G lock-in 7260 type, and IBM PC with special software. The next device, constructed in 2001 was named FORS-I (Fibre-Optic Rotational Seismometer) [4,5] with sensitivity equals $2.2\cdot10^{-6}$ rad/s. It used 400 m of Panda fibre, and following FORS-II (2003) [6-8] with sensitivity equals $4.2\cdot10^{-8}$ rad/s used 11 000 m of single-mode optical fibre. FORS-I and -II have been successfully applied to record seismic rotational events in seismological observatory in Ojców and Książ, Poland [9-11]. The next generation of FORS was more advanced device with remote control - AFORS (Autonomous Fibre - Optic Rotational Seismograph) (2010) [12] which was constructed with sensor loop of 15 000 m single-mode optical fibre and sensitivity at level $5.0\cdot10^{-9}$ rad/s. AFORS has been effectively recording rotational effect in period 2010-2017 in seismological observatory in Książ, Poland [13-16]. In order to perform mobile, remote device with wider measuring range the FOSREM (Fibre-Optic System for Rotational Events and Phenomena Monitoring) has been proposed in 2015 [17]. This rotational seismograph uses optimized 5 000 m of single-mode optical fibre and has sensitivity at level $2 \cdot 10^{-8}$ rad/s. It meets almost all technical requirements of rotation seismology, both in seismological and engineering application [18]. Finally, basing on FOSREM parameters optimization and its remote control the sensors named FOS (Fibre-Optic Seismograph) have been constructed and applied for rotational seismology investigation. They were applied for rotational movements monitoring in building [19], in an international experiment comparative sensor test [20, 21], for seismic events recording [22, 23]. The area of applications of FOS is enormous (Fig. 1), from seismic rotational waves observation in seismological observatory to wind farm or glories monitoring. Having such instrumentation it is extremely important to gather data and their analysis in order to better understand the origin of earthquakes and in particular to relate them to the geological context as well as to analyze engineering aspects of high and complex construction.

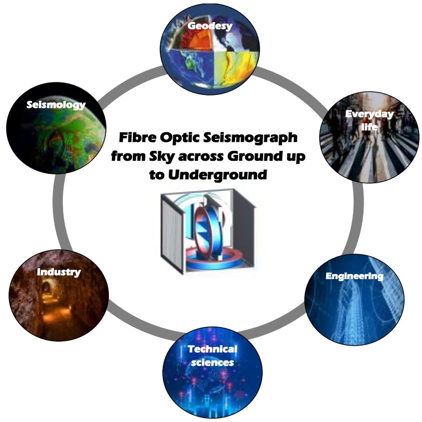

Fig. 1. Visualization of three-axial Fibre-Optic Seismograph with its applications.

But the authors do not plan to limit their work only to gather records. The incessant requirements imposed by the science and industry stimulated the emergence of more and more modern devices, therefore presently authors work on an innovative three-axial system (Fig. 1) for study rotational movements in seismology as well as in engineering and technical sciences.

Acknowledgments: This work was supported by GBMON/13-995/2018/WAT

References:

[1] B. Culshaw, A. Kersey, J. Lightwave Technol., 26, 1064–1078 (2008)

[2] G. Sagnac, C. l'Acad. Sci., 95, 708-710, (1913)

[3] L. R. Jaroszewicz, A. Szelmanowski, Proc. SPIE 3479, (1998)

[4] L. Jaroszewicz, et al., Molecular and Quantum Acoustics, 22, 133-144, (2001).

[5] L. R. Jaroszewicz, Z. Krajewski, Proc. SPIE, 4900, (2002)

[6] Z. Krajewski, et al., Proc. SPIE, 5484, (2004)

[7] L. R. Jaroszewicz, et al., Proc. SPIE, 5776, (2005)
[8] Z. Krajewski, et al., Proc. SPIE, 5952, 240-248, (2005)
[9] L. R. Jaroszewicz, et al., Proc. Intern. Micro-Opt. Conf. IMOC, 661-666, (2003)
[10] L .R. Jaroszewicz, et al., Opto-Electron. Rev., 16, 3, (2008)
[11] L .R. Jaroszewicz, et al., Springer, (2008)
[12] L. R. Jaroszewicz, et al., Acta Geophys., 59, 3, (2011)
[13] A. Kurzych, et al., Sensors, 14, 5459-5469, (2014)
[14] L. R. Jaroszewicz, et al., Acta Geophys, 59, 578-596, (2011)
[15] L. R. Jaroszewicz, et al., J Seismol, 16, 573-586, (2012)
[16] L. R. Jaroszewicz, et al., InTech, 335-354, (2012).
[17] L. R. Jaroszewicz, et al., Springer, 49-64 (2015)
[18] L. R. Jaroszewicz, et al., Sensors, 16(12), (2016)
[19] A. T. Kurzych, et al., Opto-Electron. Rev., 28(2), (2020)
[20] A. T. Kurzych, et al., Sensors, 6107, (2020)
[21] F. Bernauer, et, al., 21, 264, (2021).
[22] K. P. Teisseyre, et al., Sensors, 21, 4120, (2021)
[23] L. R. Jaroszewicz, et al., Opto-Electronics Review, 29, 213-219. (2021)

3D-printed mechanical transmission element with a Fiber Bragg Grating sensor in a replaceable measuring head

P. LESIAK[1], K. POGORZELEC[1], A. BOCHENEK[1], PIOTR SOBOTKA[1], K. BEDNARSKA[1],A. ANUSZKIEWICZ[2], T. OSUCH[2,3], M. SIENKIEWICZ[4], P. MAREK[4] AND T. WOLIŃSKI[1]

[1] Faculty of Physics, Warsaw University of Technology, Nowowiejska 15/19, 00-665 Warsaw, Poland;
[2] Faculty of Electronics and Information Technology, Institute of Electronic Systems, Warsaw University of Technology, Nowowiejska 15/19, 00-665 Warsaw, Poland;
[3] National Institute of Telecommunications, Szachowa 1, 04-894 Warsaw, Poland,
[4] Faculty of Power and Aeronautical Engineering, Warsaw University of Technology, 00-665 Warsaw, Poland;
e-mail address: piotr.lesiak@pw.edu.pl

Compliant mechanisms have gained an increasing interest in recent years [1], especially in relation to the possibility of using 3D printers for their production. These mechanisms typically find application in precise positioning systems of building robotic devices or in sensors where they can be used to characterize displacement. 3D printing with PLA materials allows a fiber optic sensor to be incorporated into the structure of a properly designed compliant mechanism [2]. Therefore, in this work, technology of a Fiber Bragg Grating (FBG) sensor printing in a measuring head which was then inserted into a specially designed mechanical transmission element was presented. The shape of this element allows to freely modify amplification of the displacement amplitude so that the FBG sensor always works in the most optimal regime without the need to modify its external dimensions.

References:

[1] J. Hricko, Š. Havlík, Advances in Service and Industrial Robotics. RAAD 2019. Advances in Intelligent Systems and Computing, vol 980. Springer, Cham. (2020)

[2] M. Liu et. al., Sensors, 19, 1931 (2019)

Microsphere-based fiber-optic temperature sensor for galvanic electric cells

P.LISTEWNIK[1]

[1]Department of Metrology and Optoelectronics, Faculty of Electronics, Telecommunications and Informatics, Gdańsk University of Technology, 11/12 Narutowicza Street, 80-233 Gdańsk, Poland

e-mail address: pauliste@pg.edu.pl

The need for gaining knowledge about innerworkings of the electric cells, especially their internal temperature, is constantly increasing due to growing demand for portable electronic devices. Thanks to such knowledge it is possible to improve the technology of the cells, therefore extending their lifetime and performance.

Internal temperature of an electric cell can be measured and monitored using microsphere-based fiber-optic sensors with thin ALD ZnO coating. Their compact size will allow to integrate them easily and effectively within the electric cells. Utilization of presented sensors allows to detect, in real time, damages to the structure of the sensor head that may occur during measurement execution, which is especially important in when the sensor accessibility is impeded [1,2]. Moreover, deposition of metal-based coatings on the surface of the optical microsphere allows to broaden range and sensitivity of refractive index and temperature measurements [3,4]. Optimization of the metrological properties of microsphere-based fiber-optic sensors can be achieved by varied modification of optical microspheres and thin ALD metal-based coating deposited on their surface. The investigation of the electric cells was performed in an interferometer setup, operating in reflection mode. The study indicates, microsphere-based fiber-optic temperature sensor can be successfully utilized for internal measurements and monitoring of electric cells.

Acknowledgments: This research was funded in part by National Science Centre [2021/41/N/ST7/03801]. For the purpose of Open Access, the author has applied a CC-BY public copyright licence to any Author Accepted Manuscript (AAM) version arising from this submission. The author acknowledges the financial support of the DS Programs of the Faculty of Electronics, Telecommunications and Informatics of the Gdańsk University of Technology.

References:

[1] Listewnik P, Hirsch M, Struk P, Weber M, Bechelany M and Jędrzejewska-Szczerska M 2019 Preparation and Characterization of Microsphere ZnO ALD Coating Dedicated for the Fiber-Optic Refractive Index Sensor *Nanomaterials* **9** 306

[2] Listewnik P, Bechelany M, Jasinski J B and Szczerska M 2020 ZnO ALD-Coated Microsphere-Based Sensors for Temperature Measurements *Sensors* **20** 4689

[3] Hirsch M, Listewnik P, Struk P, Weber M, Bechelany M and Szczerska M 2019 ZnO coated fiber optic microsphere sensor for the enhanced refractive index sensing *Sensors and Actuators A: Physical* **298** 111594

[4] Listewnik P, Bechelany M, Wierzba P and Szczerska M 2021 Optical-Fiber Microsphere-Based Temperature Sensors with ZnO ALD Coating—Comparative Study *Sensors* **21** 4982

Type – II superlattice interband quantum cascade detectors - future higher operating temperature sensors

P. MARTYNIUK

Institute of Applied Physics, Military University of Technology, 2 Kaliskiego Str., 00-908 Warsaw, Poland
e-mail address: piotr.martyniuk@wat.edu.pl)

In the last years a several new approaches have been proposed to increase the higher operating temperature (HOT) parameters of photon detectors to include numerous kinds of materials like type-II $A^{III}B^{V}$ superlattices: InAs/GaSb and InAs/InAsSb (T2SLs). Among them the most promising is an interband quantum cascade photodetector (IB QCP) based on T2SLs $A^{III}B^{V}$ "Ga-free" InAs/InAsSb.

Why IB QCPs? In the photodiode the detector's responsivity and diffusion length are closely related and an increase in the absorber's thickness (single active layer) beyond the diffusion length does not improve signal to noise ratio. This effect is mainly observed at HOT conditions, where diffusion lengths are reduced, and limited part of the generated carriers contributes to the quantum efficiency.

In order to circumvent the conditions imposed by reduced diffusion length and increase the absorption efficiency (extra decrease of the shot noise) the IB QCPs were implemented.

This paper answers the question why T2SLs IB QCPs should be considered as a future IR HOT sensors to include comparison to the "Law 19" benchmark.

Acknowledgments: This work was supported by Polish National Science Centre within Project No. 2018/30/M/ST7/00174.

References:

[1] R.Q. Yang et al., J. Appl. Phys. 107, 054514-1–6 (2010).
[2] R.T. Hinkley et al., J. Appl. Phys. 114, 104506-1-18 (2013).
[3] K. Hackiewicz et al., IEEE J. Quantum Electron. 55(4), 4000306 (2019).
[4] P. Martyniuk et al., Phys. Rev. Applied (2022) - accepted.

Thermo-optical properties of hybrid structure based on tapered optical fiber and mixture of alkanes with nanoparticles of ZnS:Mn

J. E. MOŚ, K. A. STASIEWICZ, L. R. JAROSZEWICZ

WAT, Instytut Fizyki Technicznej, ul. Gen. Kaliskiego 2, 00-908 Warszawa

Thermo-optical properties of tapered optical fiber and mixture of higher alkanes with nanoparticles of ZnS:Mn were investigated and demonstrated. Switching functionality is realizing by step changes of refractive index of alkanes, which is result of the temperature dependence and solid-liquid phase modification. Step thermally-induced changes of refractive index cause changes in the intensity of the light propagated in tapered optical fiber. The application of pure alkanes as a taper cladding causes rise of hysteresis of optical power between heating and cooling process . This is a result of high value of latent heat and low thermal conductivity of alkanes. Alkanes were doped by ZnS:Mn nano particle to reduce this effect. The nanoparticles of ZnS:Mn are characterized by better thermal conductivity and influence of thermal histeresis. Transmission results are presented in the optical range of 550–1200 nm. In this research, hexadecane and heptadecane alkanes were used. The higher alkanes were doped with nanoparticles of ZnS: Mn, which concentration varying between 1 and 5% (wt%). Our experimental results demonstrated that the thermo-optical change for applied hybrid structure could be a used like thermo-optical switcher or a tunable temperature sensor for wide range of applied laser sources.

Monocrystalline free-standing blue phase crystals for photonic applications

E. OTÓN-MARTINEZ[1], W.PIECEK1, P. MORAWIAK[1], M. MUSZYŃSKI[2], J. SZCZYTKO[2]

[1]Institute of Applied Physics, Faculty of Advanced Materials and Technologies, Military University of Technology, gen. S. Kaliskiego 2 St, 00-908 Warszawa, Poland
[2]Institute of Experimental Physics, Faculty of Physics, University of Warsaw, Ludwika Pasteura 5, 02-093 Warszawa, Poland
e-mail address: wiktor.piecek@wat.edu.pl

Photonic crystals (PCs) are micro- or nanostructures able to modulate the light due to their specific structure which can be altered by external physical fields.

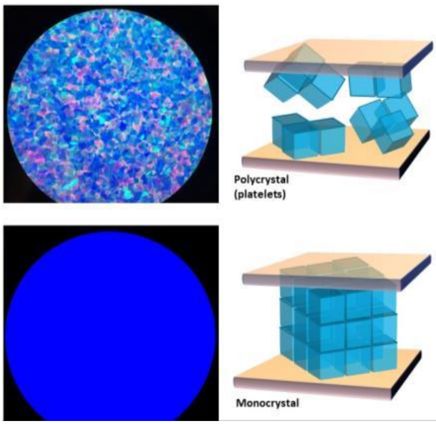

Fig. 1. Polycrystal and monocrystal structures of the liquid crystal at the blue phase.

Our proposal for the creation of photonic structures is based on the use of a self-assembling materials (SAM). A special type of SAM is the liquid crystalline blue phase (BP), where the cubic structure on a nanometer scale is created due to self-organization of molecules. Since the size of the basic elements of the BP structure is on the order of nanometers, they can be considered as a nanophotonic crystals. 3D BP structures exhibit optical phenomena analogous to those generated by other photonic materials, including those found in nature. The creation of macroscopic BP single crystals of controlled spatial orientation of structure remains a challenge nowadays. BP structures produced currently are most often polycrystalline, where the size of a single crystallite is usually very limited (of the order of micrometers, see Fig. 1).

The spatial orientation of the structure and its parameters, determining the photonic properties, are controlled by properties of boundary orienting layers.

The obtained photonic single crystals have a specific properties designed for the implementation of a microlaser with topologically protected spatial distribution of radiation (when doped with emitters), a light-controlled optical switch (when doped with a photoactive material), a holographic transducer (as part of a holographic system), optical sensors dedicated to stress, pressure or/and temperature sensing.

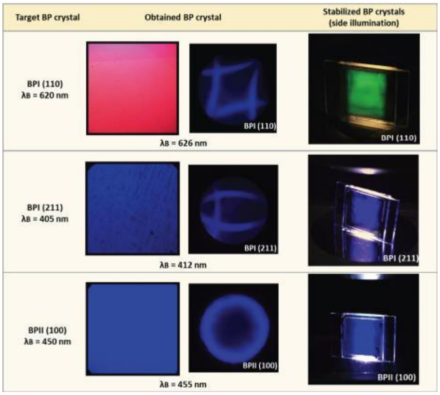

Fig. 2. Blue phase (mono)crystals. Left column displays the selective light reflection observed at the direction normal to the cel surface. The column in the middle shows a diffraction patterns specific for single crystal structure orientation. The right column depicts the selective reflection at the oblique angle.

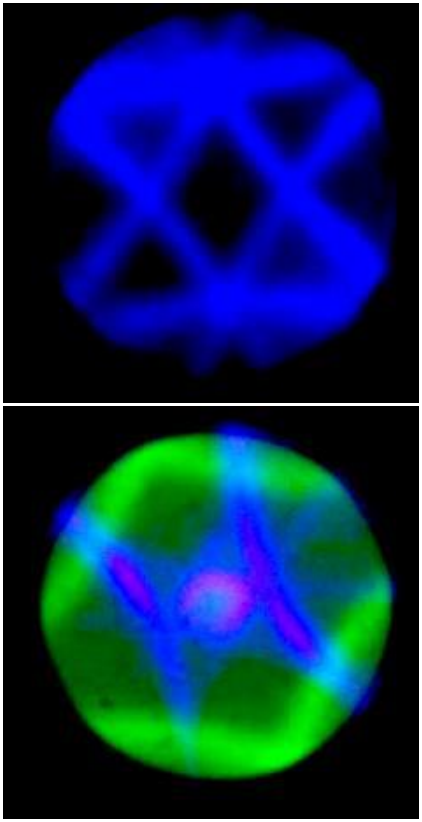

Fig. 3. A Kossel figure from a thin layer of a blue phase obtained at illumination with a blue light emitting diode (top picture) and Kossel figure from of a blue phase doped with green light emitting dye obtained at illumination with a blue light emitting diode (bottom picture).

Acknowledgments: This work was supported by NCN project 2019/35/B/ST3/04147 (NCN/07-079/2020/WAT)

References:

[1] A. Anderson et. al., Optic Letters 29, 8, (2014)

Long-range swept-source optical coherence system for in-vivo assessment of intraocular scattering

S. PANEZAI[1], A. GUPTA[1], A. JIMENEZ-VILLAR[1], E. MĄCZYŃSKA-WALKOWIAK[1], G. GONDEK[1], D. RUMIŃSKI[1], I. GRULKOWSKI[1]

[1]Institute of Physics, Faculty of Physics, Astronomy and Informatics, Nicolaus Copernicus University in Toruń, ul. Grudziądzka 5, 87-100 Toruń, Poland
e-mail address: igrulkowski@fizyka.umk.pl

The human eye is a complex and dynamic optical structure enabling visual perception [1, 2]. Although generally the ocular components are transparent, the microstructural changes associated with ageing or external factors lead to deterioration of the optical properties of the eye. Hence, it directly affects intraocular light scattering – a factor responsible for vision quality. The presence of opacifications is an indicator of vision-affecting diseases such as corneal dystrophies, crystalline lens cataracts, vitreous floaters etc.

Optical coherence tomography (OCT) is an imaging modality that has revolutionized ophthalmic diagnostics. OCT enables non-invasive probing / mapping the light back-scattered from the optical inhomogeneities of the object. The method allows for generation of cross-sectional and volumetric images of the object with micrometer resolution by scanning the object with the infrared light beam [3].

We demonstrate a reconfigurable optical platform for three-dimensional (3-D) visualization of the structures of the human eyes in vivo that enables assessment of intraocular scattering. The prototype instrument is based on a long-depth-range swept source OCT (SS-OCT). the schematic of the system is shown in Fig. 1.

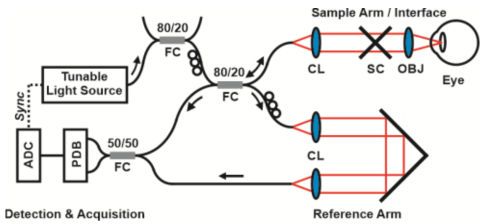

Fig. 1. Scheme of the developed instrument. FC – fiber coupler, CL – collimator lens, SC – galvanometric scanners, OBJ – objective lens, PDB – balanced photodetector, ADC – analog/digital converter.

The light source used in the device is a wavelength-tunable laser (vertical cavity surface emitting laser) [4] operating at different sweep rates ranging from 10 kHz to 400 kHz and with the central wavelength of 1 µm (wavelength tuning range 1.04 µm-1.07 µm) (HSL-1, Santec). The exceptional feature of the laser is a long instantaneous coherence length exceeding 100 mm, which was measured using a test fiber-optic Michelson interferometer. The fiber-optic Michelson interferometric configuration provides the power level incident on the cornea (1.9 mW) that does not exceed American National Standard Institute standards. The long focal length of the objective lens (f = 150 mm) allows to achieve the depth of focus sufficient to cover the entire axial imaging range and to optimize the photon collection efficiency for the entire axial range of the OCT images.

The detection and acquisition is performed by a wide-band balanced photodetector (PDB-480-C, Thorlabs) and a high-speed digitizer of 1 GS/s bandwidth (Alazar). The depth range of the system depend on the selected sweeping rate of the laser. This allows to perform high-resolution imaging of different ocular structures (e.g. the anterior segment or through the entire eye length).

Volumetric data sets of cataractous eyes are acquired and processed by a custom-made software to obtain contrast-enhanced high-resolution images of ocular structures and opacifications. The scan protocol included 300x300 A-scans in 8x8 mm^2 area [5, 6].

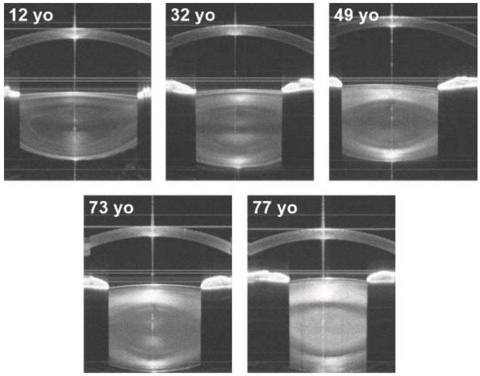

Fig. 2. In vivo imaging of the anterior segment of the eye using SS-OCT. Subjects at different age were measured. Logarithmic scale of the OCT was used to demonstrate light scattering.

Figure 2 presents selected central cross-sections of the eyes of subjects at different ages. The imaging mode covering the anterior segment of the eye was selected. The SS-OCT images show the cornea, the anterior chamber with the aqueous (completely transparent), highly scattering iris and the crystalline lens of ageing eyes. OCT signal from the crystalline lens increases considerably with the age, which is attributed to the ageing processes in the lens that impact lens transparency.

To summarize, the results demonstrate the potential of SS-OCT imaging to characterize and quantitate intraocular scattering.

Acknowledgments: This work was supported by European Regional Development Fund within National Laboratory for Photonics and Quantum Technologies – NLPQT Project.

References:

[1] R. Michael and A. J. Bron, Philos. Trans. R. Soc. Lond. B Biol. Sci. 366, 1278 (2011)
[2] P. Artal, Adv. Opt. Photon. 6, 340 (2014)
[3] I. Grulkowski, Anterior segment OCT, in: Handbook of Visual Optics, Volume Two: Instrumentation and Vision, P. Artal, ed. (CRC Press, 2016).
[4] I. Grulkowski, et al., Biomed. Opt. Express 3, 2733 (2012)
[5] I. Grulkowski, et al., Optica 5, 52 (2018)
[6] A. de Castro, et al., Invest. Ophthalmol. Vis. Sci. 59, 897 (2018)

Monitoring the polarization state in a phase-modulated QKD system to protect against eavesdropping.

E. PAWLIKOWSKA[1], M. ŻYCZKOWSKI[1]

[1] Wojskowa Akademia Techniczna (Kaliski st. 2, 00-908, Warsaw, Poland)
e-mail address: estera.pawlikowska@wat.edu.pl

Optical fibers are used in QKD systems as quantum channels to transmit quantum states. Practically, fiber optic systems use phase modulation for state coding [1], which, unlike polarization coding, is not susceptible to birefringence in optical fibers.

The main objective of this work is to investigate the developed optical quantum cryptography technology in polarimetric terms. This is realized by polarimetric characterization of individual components of the system and determination of their interaction in terms of radiation propagation in the system.

The investigated system operates on the principle of a self-compensating interferometer [2]. In part, it is built on optical fibers that maintain a polarization state, and the communication channel uses a standard single-mode fiber, the properties of which are sensitive to changes in external conditions. Stress in the standard single-mode fiber causes local birefringence within the fiber, which changes the polarization state of the pulses propagating in it along the length of the system [3].

According to the authors' assumptions, determination of the polarization characteristics for the proposed system and continuous measurement of the polarization state will be one possible practical way to secure QKD systems against optical hacking attacks. We would like to investigate the possibility of extracting some characteristic polarization features for a given system, which detectable change would signal the presence of eavesdropping. Than the system itself would take on the characteristics of a fiber optic sensor. Such features would be derived primarily from the polarization properties of the individual system elements. It is also necessary to consider the nature of the changing properties of the system, which are associated with the varying birefringence of a single-mode optical fiber in the communication channel.

In presented work, we determine how individual elements and modifications introduced to the system change the polarization state of the propagating radiation. The individual elements selected to build the proposed QKD system are characterized. The interaction of these elements at the laboratory level was also determined based on intensity measurements.

Acknowledgments: This project has received funding from the National Center for Research and Development research and innovation programme under grant agreement DOB-SZAFIR/01/A/023/01/2020.

References:

[1] C. Gobby, Z. L. Yuan and A. J. Shields, Appl. Phys. Lett., 84, 19:3762–3764, (2004)

[2] S. Pirandola et. Al., Adv. Opt. Photonics 12, 4, (2020)

[3] P. Wai and C. Menyak. Lightwave Technol., 14:148– 157, (1996)

Sensor probes for distributed measurement of temperature profile in soils

A. PAŹDZIOR[1], J. KOPEĆ[1], P. MERGO[1]

[1]Laboratory of Optical Fibre Technology, Maria Curie-Sklodowska University, Maria Curie-Sklodowska Sq. 3, 20-031 Lublin, Poland
e-mail address: adam.pazdzior@mail.umcs.pl

Rayleigh-scattering-based methods of fiber-optic distributed temperature measurement used with standard telecommunication single-mode optical fiber (SSMF) as a sensor are capable of measuring only a change in temperature, not its absolute value, and they suffer from cross-sensitivity to both temperature and strain.

We report our progress in development of cheap sensor probes for distributed measurement with optical frequency-domain reflectometry (OFDR) of vertical temperature profile in soils. A series of sensors having different construction, but all based on standard telecommunication single-mode optical fiber was prepared and tested in real-life environmental conditions. We compare their performances and discuss the possibility of obtaining a SSMF-based and insensitive to strain absolute temperature readout with them.

Acknowledgments: The purchase of the measurement equipment used in the experiments was financed by the project National Laboratory for Photonics and Quantum technologies – NLPQT (POIR.04.02.00-00-B003/18-00).

Ultrafast all-polarization-maintaining Yb-doped fiber laser oscillator working at negative net cavity dispersion

M. PIELACH[1], A. JAMROZIK[1], J. SZCZEPANEK[2], K. KRUPA[1], Y. STEPANENKO

[1]Institute of Physical Chemistry Polish Academy of Sciences, Kasprzaka 44/52, 01-224 Warsaw, Poland
[2]Fluence sp. z o. o., Kolejowa 5/7, 01-217 Warsaw, Poland
e-mail address: mgpielach@ichf.edu.pl

All-fiber lasers generating ultrashort pulses are crucial for numerous novel technologies. In particular, there is a growing interest in configurations built exclusively out of polarization-maintaining (PM) fibers, which allow such systems to work in harsh environments, for instance, in the presence of mechanical vibrations and temperature changes. Currently, novel all-PM oscillators are being investigated towards tuning their parameters such as repetition rate [1], pulse energy [2], and temporal duration [3, 4].

Among others, dispersion managing is one of the ways to modify the oscillators' characteristics. Typically, net cavity dispersion (NCD) can be tuned by using two types of fibers with positive and negative group velocity dispersion (GVD) and changing their lengths. However, standard fused silica optical fibers with negative GVD at the wavelength of 1 μm are not available. Therefore, in that case, the promising method to implement negative group delay dispersion into all-PM cavities is to use a chirped fiber Bragg grating (CFBG).

This report presents an ultrafast all-PM Yb-doped oscillator operating at the negative cavity dispersion of -0.098 ps^2, which incorporates a nonlinear optical loop mirror (NOLM) as a saturable absorber. The system operates in a dispersion-managed dissipative soliton Raman-free regime.

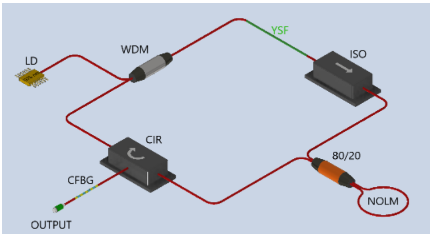

Fig. 1. Scheme of the oscillator. LD - laser diode operating at 976 nm; WDM - wavelength division multiplexer; YSF - Ytterbium-doped fiber PM-YSF-HI; ISO - optical isolator; NOLM - nonlinear optical loop mirror; CIR - optical circulator; CFBG - chirped fiber Bragg grating.

Fig. 1 presents the scheme of the ultrafast all-fiber oscillator. The system was spliced out of single-clad, single-mode, PM PANDA optical fibers characterized by the group velocity dispersion of 0.023 ps^2 at 1030 nm. Our setup utilizes a core-pumping scheme. A semiconductor laser diode (3SP-1999CHP) pumps a piece of active Yb-doped fiber (YSF) via a wavelength division multiplexer (WDM). An optical isolator (ISO) prevents pulse propagation in the anti-clockwise direction. Pulsed operation is provided by a NOLM based on a 20/80 2x2 fiber coupler. An optical circulator (CIR) enables the introduction of the CFBG into the cavity. The CFBG is used as a dispersion-managing component, which introduces a group delay dispersion of -0.237 ps^2 (at 1030 nm). Due to the limited reflectivity of the used grating (maximum reflectivity of 32% at 1033 nm), only a part of the light is reflected and goes back to the circulator for the next roundtrip, while the transmitted part of the beam is used as an output. Moreover, the CFBG acts as a super-Gaussian bandpass filter with full width at half-maximum intensity (FWHMI) of 10.4 nm.

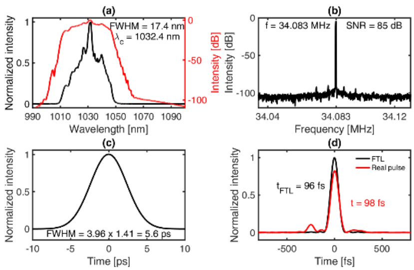

Fig. 2. Spectral and temporal characteristics of the dispersion-managed oscillator. (a) Optical output spectrum. (b) Radio frequency spectrum of the output pulse train. (d) Autocorrelation function trace of the chirped pulse directly from the oscillator. (e) Reconstructed temporal electrical field intensity of the pulse (red curve) compared to transform-limited pulse (black curve).

Fig. 2(a) presents an optical output spectrum, in linear (black) and logarithmic (red) scales, that is centered at 1030 nm and has a 3 dB width of about 17.4 nm. Note that the spectrum is wider than the filter characteristics of the CFBG, as it is broadening due to the self-phase modulation effect. The single-pulse regime was verified by measuring the radio frequency (RF) spectrum at the laser output (Fig. 2(b)). A single peak in the RF spectrum at the oscillator's repetition rate of 34.083 MHz together with a high signal-to-noise ratio of over 80 dB proves the high stability of the mode-locking operation. We measured the average output power of 78.7 mW, which corresponds to the pulse energy of 2.3 nJ. The autocorrelation function of the chirped pulse of 3.96 ps was measured directly from the oscillator (Fig. 2(c)). However, the chirped pulse was compressed by a diffraction grating compressor down to 98 fs with a temporal Strehl ratio of 0.83, which is very close to the Fourier transform limit (FTL) of 95 fs, as illustrated in Fig. 2(d).

References:

[1] B. Piechal, J. Szczepanek, T. M. Kardaś, and Y. Stepanenko. Journal of Lightwave Technology, 39(2):574–581, 2021.

[2] M. Pielach, B. Piechal, J. Szczepanek, P. Kabaciński, and Y. Stepanenko. IEEE Access, 8:145087–145091, 2020.

[3] M. Yu, Z. Cheng, C. Hong, Y. Shi, Z. Peng, M.Wang, and P.Wang. Opt. Express, 28(22):32764–32776, Oct 2020.

[4] Y. Ma, S. H. Salman, C. Li, C. Mahnke, Y. Hua, S. Droste, J. Fellinger, A. S. Mayer, O. H. Heckl, C. M. Heyl, and I. Hartl. J. Lightwave Technol., 39(13):4431–4438, Jul 2021.

Evaluation of eye accommodation distance in a two-track optical system using a vision-based method

M. PISZCZEK[1], A. KUCHARCZYK[1], K. SUCHECKI[1], M. MACIEJEWSKI[1], M. POMIANEK[1], L. JODŁOWSKI[1], P. KRUKOWSKI[2]
[1]Institute of Optoelectronics, Military University of Technology,
2 Kaliski Str., 00-908 Warsaw, POLAND
[2]RemmedVR sp. z o.o., 47/10 Domaniewska Str., 02-672 Warsaw, POLAND

One of the most important aspects of human vision is the ability to obtain sharp images of objects at different distances in the scene being observed. The occurrence of disorders of this mechanism, as well as the desire to monitor it in therapeutic activities, leads optometrists to prospect tools to study these processes. In this paper, we characterize the proposed measurement system for evaluating the accommodative state using two optical tracks and a vision-based data analysis method. Preliminary experimental results obtained with the presented system are also shown.

Accommodating the eye is achieved through the flexibility of the eye lens which translates into the ability to change its focal length. Assuming the stability of the remaining elements of the optical path of the eye, monitoring the observation distance (the distance to objects in the scene on which the eye is successively focused) comes down to determining the instantaneous focal length value. According to a (simplified) model of the test object (eye) as shown in Figure 1, there are two unknown quantities in it, of which d (the distance between the optics and the retina) is constant and characteristic of a particular eye, and f (the effective focal length of the eye's optics) is functionally dependent on distance (in the range from near to far point).

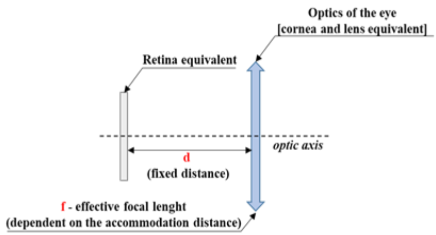

Fig. 1. simplified model of the eye

Theoretically, knowing the value of d and the instantaneous values of f will allow to track the distance to which the eye accommodates according to the formula:

$$L = \left(\frac{d - f}{f * d}\right)$$

Since these quantities cannot be measured directly, the realization of measurements of the value d and f requires the use of indirect measurements using "auxiliary" measurement systems. For this proposed solution has been invented two optical tracks which are used for this purpose. The first track (shown in Fig. 2 - track A) directly observes the retina of the human eye. Measurement with this system is realized by 2D sensor and consists in such modification of f2 focal length to obtain a sharp retinal image on the sensor.

The purpose of the second measurement path (presented in Fig. 2 - track B) is to insert a probe marker and, at the same time, to stimulate the eye to accommodate. This track provided two functions for two different light sources. In the VIS band it is to stimulate the eye to accommodate at a given distance, while in the NIR band it is to project the already mentioned marker onto the retina.

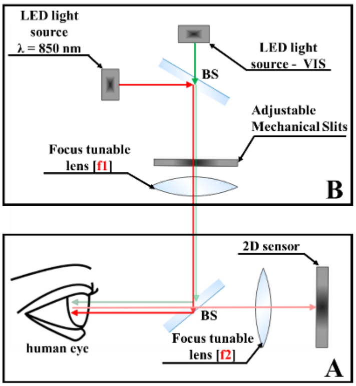

Fig. 2. Idea scheme

Accommodation of the eye with respect to a VIS stimulus and projection of a probe marker are realized by the same optical path, therefore the image registered by the sensor in the first measurement path should show the shape of the reflect measurement marker that illuminates a fragment of the retina. By changing the value of f1 the eye are stimulate to accommodate at different distances. Obviously, changing the distance of accommodative stimulation requires appropriate correction of f2 focal length in the measuring track, which enables obtaining a sharp image on the sensor. Example test results using a real and optoelectronic eye are shown in Figure 3.

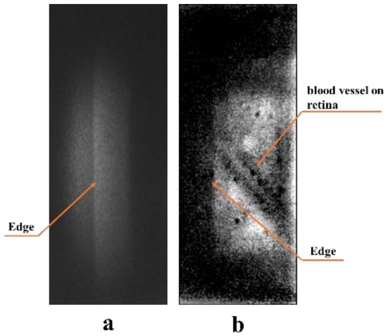

Fig. 3. Result probe marker on retina for: a) optoelectronic eye, b) human eye

The determination of the eye accommodation distance is performed algorithmically based on the values determined previously, and the values of f1 and f2, at which a sharp image was obtained on the sensor.

The designed solution confirmed the possibility of distance measurement to objects synthesized by varifocal optics that produce virtual images (e.g. VR goggles).Further work on the system foresees the separation paths of the accommodation stimulus and the measurement marker, so that it will be possible to evaluate the distance to the object synthesized by computer for VR and to the real objects.

Acknowledgments: This work was supported by Project "RemmedVR device for home vision therapy".

References:

[1] Keeney, Arthur H., Robert E. Hagman, and Cosmo J. Fratello. *Dictionary of Ophthalmic Optics*. Boston: Butterworth-Heinemann, 1995. p. 1 – 345.

Implementation of basic refractive defects into the optoelectronic eye

M. PISZCZEK[1], A. KUCHARCZYK[1], K. SUCHECKI[1], M. MACIEJEWSKI[1], M. POMIANEK[1], L. JODŁOWSKI[1], P. KRUKOWSKI[2]

[1]Institute of Optoelectronics, Military University of Technology, 2 Kaliski Str., 00-908 Warsaw, POLAND
[2]RemmedVR sp. z o.o., 47/10 Domaniewska Str., 02-672 Warsaw, POLAND

The development of new devices for vision diagnosis and therapy often requires the construction of auxiliary equipment. One of such very useful structures turns out to be an optoelectronic eye. Its usefulness comes primarily from its ability to maintain known and stable measurement conditions during various types of testing. Possibility to take into account different variations of the emmetropic eye or to simulate different refractive defects of the eye in the developed device seems desirable. In this paper, the proposed mechano-optical system is characterized and experimental results are presented.

The concept of emmetropic eye does not mean its optical parameters are clearly defined such as the range of effective focal length of cornea or lens and distance between lens and retina. Due to individual differences between people, both an emmetropic eye and an eye with a specific defect value, such as myopia or hyperopia, can have different parameters. The idea of a variant solution for an emmetropic eye and an eye with refractive defects is shown in Figures 1 and 2.

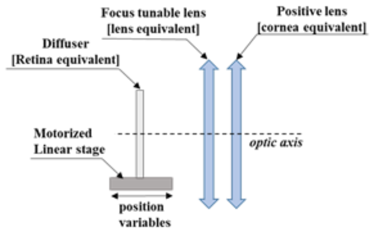

Fig. 1. Schematic diagram for simulating different variants of the emmetropic eye

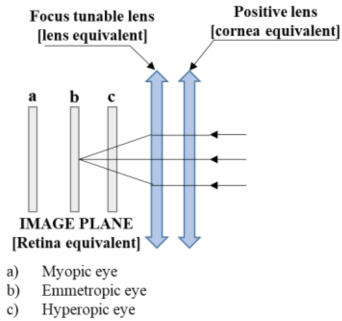

Fig. 2. Schematic diagram for simulating different refractive defect of eye

In the experimental construction, the optics of the eye was modeled using two lenses. The physical implementation was based on a fixed focal length lens (corneal equivalent) and a variable focal length lens (lens equivalent). The optical path is complemented by a focusing screen equivalent to the retina of the human eye. The physical representation of the optoelectronic eye is shown in Figure 3

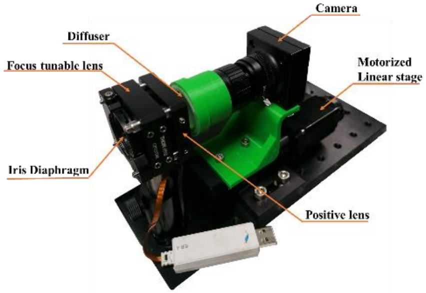

Fig. 3. physical realization of the optoelectronic eye

The proposed mechano-optical system has two control elements. The first, which modifies the distance between the optical system and the image plane, is implemented by a motorized linear stage. The second control is to change the effective focal lens of the optical system realized by the tunable focal lens. Together these two elements allow any configuration of parameters in the optoelectronical eye. Thus, different variations of the emmetropic eye can be obtained. In the system shown, it is possible to change the distance of the focusing screen that simulates the retina from the optic system. From the simulations, obtained the possibility of a variable lens distance from the focusing screen of 0.6 mm with an effective focal range of 21.74 - 27.57 mm. This result is very close to the assumed range of geometry variation in the human eye. [3].

To experimentally verify the ability to simulate refractive defects in the system, tests were performed with a set of lenses used in retinoscopy. The results of the tests are shown in Fig. 4.

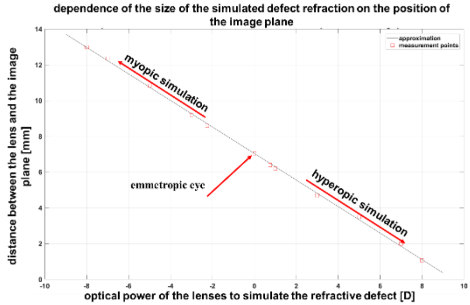

Fig. 4. dependence of the size of the simulated defect refraction on the position of the image plane

The performed tests prove the correctness of the system's operation. The results clearly show the possibility of developing a useful auxiliary device for various tests or calibrations of other optical systems as well as a construction that can be used as a training device for optometrists training e.g. in the use of retinoscope.

Acknowledgments: This work was supported by Project "RemmedVR device for home vision therapy".

References:

[1] Atchison DA, Jones CE, Schmid KL, et al. Eye shape in emmetropiaand myopia. Invest Ophthalmol Vis Sci. 2004;45:3380 –3386.

[2] Lourdes Llorente, Sergio Barbero, Daniel Cano, Carlos Dorronsoro, Susana Marcos; Myopic versus hyperopic eyes: axial length, corneal shape and optical aberrations. Journal of Vision 2004;4(4):5

[3] Lourdes Llorente, Sergio Barbero, Daniel Cano, Carlos Dorronsoro, Susana Marcos; Myopic versus hyperopic eyes: axial length, corneal shape and optical aberrations. Journal of Vision 2004;4(4):5

Field-of-view correction in a VR HMD display with varifocal optics

M. PISZCZEK[1], K. SUCHECKI[1], A. KUCHARCZYK[1], M. POMIANEK[1], M. MACIEJEWSKI[1], L. JODŁOWSKI[1], P. KRUKOWSKI[2]
[1]Institute of Optoelectronics, Military University of Technology, 2 Kaliski Str., 00-908 Warsaw, POLAND
[2]RemmedVR sp. z o.o., 47/10 Domaniewska Str., 02-672 Warsaw, POLAND

Contemporary diagnostics and therapy in optometry is reaching for more advanced tools, including the use of virtual technologies. However, most commercially available VR goggles suffer from the vergence-accommodation conflict (VAC). An HMD with infinitely adjustable distance to the plane of the virtual image is required to ensure the best conditions for vision therapy. The method characterized in this study, assumes the use of variable focal optics. However, the desired change of the plane of accommodation causes unfavorable changes in the field of view. By means of appropriate calibration of the optics and the possibility of programmatic influence on the angular size of the scene synthesized on the display, it is possible to keep the FOV constant for changing parameters of the varifocal optics. In traditional VR goggles, the issue of adjusting visual accommodation to vergence is not involved in spatial image formation. Although some HMDs have non-axial adjustment of the optics,

its purpose is primarily to compensate vision defects.

The way to influence the position of the image plane in the HMD is to change the focal length of the optics while keeping the distance to the display constant. An example of such a solution is shown in the following Figure 1.

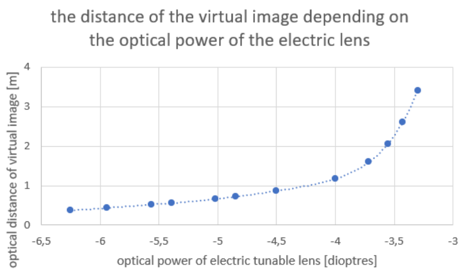

Fig. 1. Measurement of virtual image distance

Based on the above results, we can conclude there is a possibility to obtain a smooth adjustment of the distance to the synthesized image. Unfortunately, while modifying the distance, the angular field of view of the optical system is simultaneously changed. This correlation is shown in Figure 2.

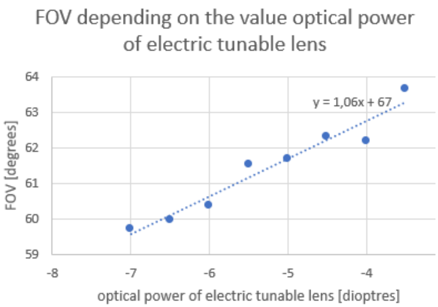

Fig. 2. Graph showing dependence of FOV and optical power

In the case of immersive VR environment perception, this is a very unfavorable effect. Maintaining a constant field of view, in the optical system described above, can be achieved by rescaling the size of the image synthesized on the HMD display. This rescaling must be correlated with changes in the accommodative plane of the eye so as not to cause discomfort to the VR user. VR goggles with adjustable distance of the plane of accommodation and simultaneous maintenance of a constant field of view, require calibration of the system, e.g. calibration by means of optoelectronic eye. In this measuring method the operation of the real eye is well represented. At the same time it is possible to directly measure the geometry of the image formed by the HMD optics. The scheme of the above mentioned measuring system and its physical representation is shown in Fig. 3.

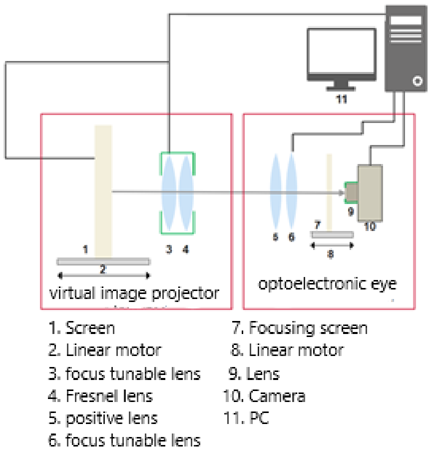

Fig. 3. idea scheme

Based on the analysis of the geometry of the images (recorded by the optoelectronic eye), the dependence of the image scaling as a function of the accommodation distance can be estimated, as shown in Fig. 4

FOR -3 DIPOTERS

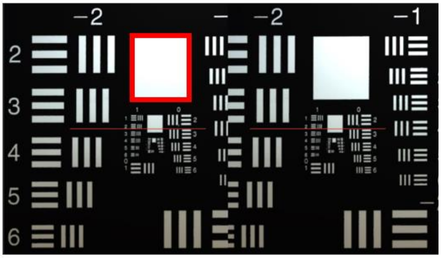

FOR -6 DIOPTERS

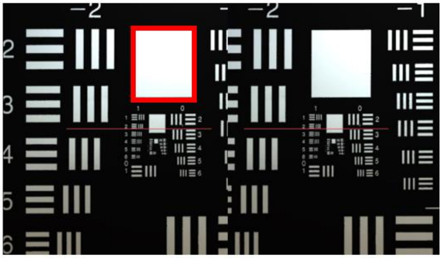

Fig. 4. example of rescaling the image on the display for optical power value of lens: -3 and -6 Red boxes showing the same area of test plate but size of second one is 7.2% greater

The obtained results clearly indicate the possibility of developing VR goggles with desirable properties for vision diagnostics and therapy, especially in the aspect of the possibility of fast and smooth modification of the accommodations plane in the range from near-point to far-point.

Acknowledgments: This work was supported by Project "RemmedVR device for home vision therapy".

References:

[1] G. Kramida, Resolving the vergence-accommodation confict in headmounted displays. (2016)

Room temperature hydrogen sensor based on electropolymerized polycarbazole layers on platinum electrodes

M. PROCEK[1], K. GŁOSZ[2], A. STOLARCZYK[2], T.JAROSZ[2]

[1]Department of Optoelectronics, Silesian University of Technology, 2 Krzywoustego Str. 44-100, Gliwice, Poland
[2]Department of Physical Chemistry and Technology of Polymers, Silesian University of Technology, 9 Strzody Str., 44-100 Gliwice, Poland

e-mail address: marcin.procek@polsl.pl

Hydrogen (H_2) detection and concentration monitoring is extremely important form the safety reasons, because of its high flammability and explosiveness. Hydrogen begins to be one of the most prospective fuel and energy storing medium. In the second hand there is lack of inexpensive electronic hydrogen sensors which are operating at room temperature without any heating requirements. It is also very important to obtain the selectivity of hydrogen sensors to other flammable gases like methane or natural gas.

In this work we are presenting electrochemical (chemo-resistor) hydrogen gas sensor based on electropolymerized polycarbazole deposited on platinum electrodes. The sensing phenomena was reported by the authors first time in [1,2]. In this work more accurate gas sensing properties of the sensor are presented. The sensor shows excellent electrical response to wide range of H_2 concentrations at room temperature. Sensor is also relatively fast and working in wide range of relative humidity. What is more it is also selective to methane and shows good long term stability. The work describes sensor fabrication method, material characterization and gas sensing results. The gas sensing mechanism is also proposed and discussed.

Acknowledgments: This work benefited from facilities and research infrastructure provided by the Department of Optoelectronics Silesian University of Technology, which receives support under project NLPQT – National Laboratory for Photonics and Quantum Technology, POIR.04.02.00-00-B003/18.

References:

[1] A. Stolarczyk et. al., Sensors 19(5), 1098 (2019)
[2] A. Stolarczyk et. al. Polish Pat. pending, P.427906, 1–4 (2018)

The simulation insight into properties of modified nanodiamonds surfaces

K. PYRCHLA[1]

[1]Faculty of Electronics, Telecommunications and Informatics, Gdansk University of Technology, 11/12 Gabriela Narutowicza Street, 80-233Gdansk, Poland
e-mail address: krzpyrch@student.pg.edu.pl

Nanodiamonds with nitrogen-vacancy defects in their structure could be an excellent platform for optical sensing at the microscale. By the analysis of its fluorescence signal, useful physical parameters such as the temperature of the nanodiamond can be measured with high precision even inside the living cells [1]. The high biocompatibility of nanodiamond is an additional advance [2].

However, in cell biology, there is often essential to measure the chemical properties rather than physical. This target could also be achieved by the application of the surficial modification, which mediates the nanodiamonds fluorescence once chemically stimulated. These interactions are complex in nature, so proper modelling is beneficial for both analysis of experimental data and the theoretical description of the problem [3], [4]

In this, the complex simulation study of nanodiamond surface covered by the Ochratoxin A (OTA) was delivered. First, an adequate atomic model of the nanodiamond surface was created. Because the nanodiamonds can vary in size significantly, two different types of modelling are required. The 2D slab of the diamond approximated the very large nanodiamonds (diameter 800 nm) surface. This is a well-known approach when the surface curvature is small.

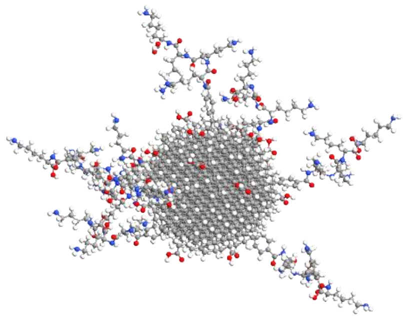

Fig. 1. The ultra-small nanodiamond (diameter 2nm) coated with Ochratoxin A (OTA)

However, the small nanodiamond (few nm diameters) cannot be modelled using this approach; thus, the molecular models of this particle were created (see Fig. 1). Using these slabs models, the optimal concentration of OTA on the surface was found through minimal adsorption energy estimation.

The structures with optimal OTA surface cover were applied to estimate the electrical bandstructure of the diamond-OTA interface. The results achieved during this work simulation correlate with existing experimental data showing fluorescence quenching.

Acknowledgments: This work was supported by the TEAM-NET program of the Foundation for Polish Science co-financed by the European Union under the European Regional Development Fund QUNNA POIR.04.04.00-00-1644/18.

References:

[1] M. Shigeki and S. Ryusuke, “Biological meaning of ‘habitable zone’ in nucleotide composition space,” *Biophys. Physicobiology*, vol. 15, pp. 75–85, 2018.

[2] M. D. Torelli, N. A. Nunn, and O. A. Shenderova, “A Perspective on Fluorescent Nanodiamond Bioimaging,” *Small*, vol. 1902151, pp. 1–20, 2019.

[3] V. This and Á. Gali, “Ab initio theory of the nitrogen-vacancy center in diamond,” *Nanophotonics*, vol. 8, no. 11, pp. 1907–1943, 2019.

[4] M. Kaviani, P. Deák, B. Aradi, T. Frauenheim, J. P. Chou, and A. Gali, “Proper surface termination for luminescent near-surface NV centers in diamond,” *Nano Lett.*, vol. 14, no. 8, pp. 4772–4777, 2014.

Wide-field vector magnetometry using nitrogen-vacancy centers in arbitrarily oriented diamond crystals

S. SENGOTTUVEL[1], M. MRÓZEK[1], M. SAWCZAK[2], M. GŁOWACKI[3], M FICEK[3], W. GAWLIK[1], A. WOJCIECHOWSKI[1]

[1]M. Smoluchowski Institute of Physics, Jagiellonian University in Kraków, Łojasiewicza, 11, 30-348 Kraków, Poland
[2]Polish Academy of Sciences, Szewalski Institute of Fluid-Flow Machinery, 14 Fiszera St., 80-231 Gdansk, Poland
[3]Gdansk University of Technology, 11/12 G. Narutowicza St., 80-233 Gdansk, Poland
e-mail address: saravanan.sengottuvel@doctoral.uj.edu.pl

In recent years, the nitrogen-vacancy (NV) centers embedded in diamond has emerged as a promising magnetic field sensor [1]. Combined with wide-field imaging and continuous wave ODMR technique these centers facilitate measuring magnetic field at high spatial resolution and sensitivity. For mapping the magnetic fields, typically either a bulk diamond with a very thin NV layer or a scanning probe diamond tip is used, which requires a smooth sample surface and the proximity of the probing device, often limiting the sensing capabilities. Here, we determine the three-dimensional orientation of the magnetic field vector [2] and show that NV centers in arbitrarily oriented nanodiamonds (NDs) deposited on a planar surface can be used for sensing the magnetic field. In principle our work can be extended to irregular surfaces which shows a promising path to nanodiamond-based photonic sensors [3].

Acknowledgments: This research was funded by the Foundation for Polish Science under the project Team-NET No. POIR.04.04.00-00-1644/18.

References:

[1] L Rondin et al, Rep. Prog. Phys. 77 056503 (2014).
[2] M. Chipaux et al., The European Physical Journal D volume 69, Article number: 166 (2015).
[3] A. M. Wojciechowski et al., Materials, 12(18), 2951.

Er-doped fluoroindate glasses for sensing applications

B. STARZYK[1], G. L. JIMÉNEZ[1], M. LEŚNIAK[1], M. KOCHANOWICZ[2], M. KUWIK[3], J. ŻMOJDA[2], P. MILUSKI[2], A. BARANOWSKA[2], J. DOROSZ[2], W. PISARSKI[3], J. PISARSKA[3], D. DOROSZ[1]

[1]AGH University of Science and Technology, 30 Mickiewicza Av., 30-059 Krakow, Poland
[2]Bialystok University of Technology, Wiejska 45D Street, 15-351 Bialystok, Poland
[3]Institute of Chemistry, University of Silesia, Szkolna 9, 40-007 Katowice, Poland
e-mail address: starzyk@agh.edu.pl

Low phonon energy (500 cm^{-1}) which characterized the fluoroindate glasses allows to most of the radiative transitions in the lanthanides. Those properties enable many applications of fluoroindate glasses i.a. in industry, defense, medical and as a sensors [1-3].

This work is focused on the Er^{3+} doped fluoroindate glass optimization. The analysis of the structure of prepared glasses was examined by X-Ray diffraction (XRD), mid-infrared (MIR) and Raman measurement techniques. The microstructure of material (composition changes) was examine by SEM-EDS technique. The luminescence of active materials was measured by 976 nm laser excitation. Fig. 1 presents VIS emission of prepared samples where at the 1.6 mol.% concentration of Er^{3+}, the extinction of the luminescence can be observed. The main property of active materials doped with Er^{3+} ions in terms of sensor applications are thermally coupled emission transitions Er^{3+}:$^2H_{11/2}$ and $^4S_{3/2}$. Changes in the intensity of the aforementioned thermally coupled bands with temperature changes will allow the determination of the calibration curve. The calibration curve will be the starting point for the verification of glass as an active low-phonon material for sensing applications.

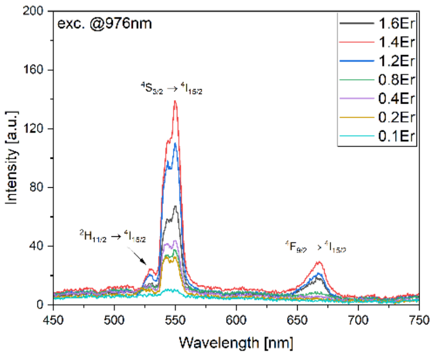

Fig. 1. Luminescence spectra of fluoroindate glasses doped with $xErF_3$ (x=0.1-1.6 mol.%).

Acknowledgments: The research project was funded by the National Science Centre (Poland) granted on the basis of the decision No. 2017/25/B/ST8/0253.

References:

[1] R. Lisiecki et. al., Journal of Non-Crystalline Solids 535, 119965, (2020)
[2] W. Pisarski et. al., Sensors and Actuators A: Physical, 252, 54-58, (2016)
[3] H. Algarni et. al., Optical Materials, 83, 257-262, (2018)

Measuring the refractive index of egg white and yolk according to temperature: a preliminary study

P.SOKOŁOWSKI[1]

[1]Faculty of Electronics, Telecommunications and Informatics, Department of Metrology and Optoelectronics, Gdańsk University of Technology, 11/12 Narutowicza Street, Gdańsk 80-233, Poland.
e-mail address: patsokol@pg.edu.pl

European egg consumption amounts to 240 eggs per person per year [1]. Eggs provides key sources like proteins, fats, vitamins, minerals and bioactive compounds. Eggs compositions and net amount could be influenced by strain, age, hen diet and environmental conditions [2]. Refractive index (RI) could be a potential marker to those factors. The RI of biological cells describes their interaction with light and depends on the concentrations [3].

In this work, we used Fabry-Perot interferometers (FPI) sensor to determine refractive index of egg white and yolk. In order to measure RI of a liquid biological sample like an egg white or yolk, we have setup an measurement setup with FPI sensor as shown in Fig. 1.

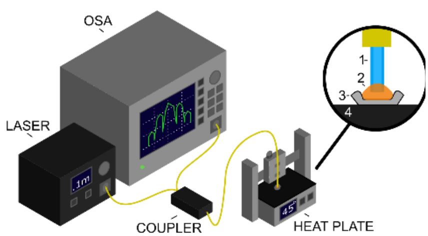

Fig. 1. Measurement setup: (1) Fiber, (2) Sample, (3) Aluminum weighing dish, (4) Heat plate.

FPI have been applied as an optical sensor for measurement of physical parameters due to their high resolution and fast response time [4]. The measurement setup has been made of an optical spectrum analyser (OSA) as the optical signal processor, two superluminescent diodes with wavelengths of 1550nm and 1050nm, single-mode telecommunication fiber (SMF-28), 2:1 fiber coupler and heat plate. Alternative method uses microsphere in FPI configuration instead of clear fiber [5].

In a fiber FPI, the phase of the interference signal is linearly proportional to the optical length of the cavity, defined as the product of the cavity length and the refractive index of the medium filling the cavity [6]. Information about the measurand is encoded in the full spectrum of light reflected from the sensing interferometer [7]. The interference signal and cavity length are used to calculate the refractive index of sample. At first, we estimate cavity length by measurement of air in room temperature with our measurement setup. Then based on estimated cavity length and measured sample interference signal we calculate the refractive index.

Fig. 2 shows a box plot of refractive index as a function of temperature. The straight lines inside the boxes indicate a median value based on all measurement series. The distance between the top and bottom edges of the box is the interquartile range (IQR). Outliers sample represents by symbol 'o' are values that are more than 1.5 IQR away from the box.

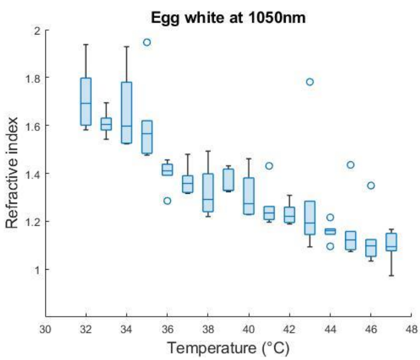

Fig. 2. Refractive index of egg white obtained in 1050 nm and temperature in range (32-47 C).

Summarizing, the measurement setup allows to determine the refractive index. Obtained results are showing that refractive index of egg parts strongly depends on temperature and these changes are relatively fast.

Acknowledgments: This work was supported by DS programs of Faculty of Electronics, Telecommunications and Informatics of Gdańsk University of Technology for the support. Financial support of these studies from Gdańsk University of Technology by the DEC- 11/2020/IDUB/I.3/CC grant under the Curium - Combating Coronavirus, DEC-4/2020/IDUB/III.4.1/Tc grant and DEC-8/2020/IDUB/III.4.1/Tc] grant under the Technetium Talent Management Grants - 'Excellence Initiative - Research University' program is gratefully acknowledged.

References:

[1] Magdelaine P. Egg and egg product production and consumption in Europe and the rest of the world. (2011).

[2]Kuang H, Yang F, Zhang Y, Wang T, Chen G. The Impact of Egg Nutrient Composition and Its Consumption on Cholesterol Homeostasis. *Cholesterol*.

[3]Kim, YJ., Celliers, P.M., Eggert, J.H. Interferometric measurements of refractive index and dispersion at high pressure. *Sci Rep* 11**,** 5610 (2021)

[4] M.R. Islam, M.M. Ali, M. Lai, K. Lim, H. Ahmad, "Chronology of Fabry-Perot Interferometer Fiber-Optic Sensors and Their Applications: A Review", Sensors. 2014, 14(4).

[5] P. Listewnik, M. Hirsch, P. Struk, M. Weber,M. Bechelany, M. Jędrzejewska-Szczerska. Preparation and Characterization of Microsphere ZnO ALD Coating Dedicated for the Fiber-Optic Refractive Index Sensor. Nanomaterials **2019**, 9, 306.

[6] V. Bhatia, K. A. Murphy, R. O. Claus, M. E. Jones, J. L. Grace, T. A. Tran, and J. A. Greene, "Optical fiber based absolute extrinsic Fabry

- Perot interferometric sensing system," Meas. Sci. Technol. 7, 58-61 (1996).
[7] K. Karpienko, M. Wróbel, M. Szczerska. Determination of refractive index dispersion using fiber-optic low-coherence Fabry-Perot interferometer: Implementation and validation. Optical Engineering. 53. (2014).

SPR effect controlled by electric field in the optical fiber device with low refractive index nematic liquid crystal

K. A. STASIEWICZ[1], J. KOREC[1], K. GARBAT[1], L. R. JAROSZEWICZ[1]

[1] New Technologies and Chemistry Faculty, Military University of Technology, gen. S. Kaliskiego 2, 00-908 Warsaw, Poland
e-mail address: karol.stasiewicz@wat.edu.pl

The deposition of a thin metal layer on the surface of tapered optical fiber causes possibilities to obtain surface plasmon effects (SPR) as an effect occurs on a boundary of two different materials metal and dielectric. This phenomenon was widely described in the literature [1]. The phenomenon of SPR is commonly used in sensing techniques because of its simplicity and very high accuracy. In the presented research we show the possibilities to control SPR effects using nematic liquid crystals named 3092A. An optical fiber taper technology allows for direct influence on light propagation inside the structure. Deposition of metal and immersion it in nematic liquid crystal allows to obtain a double clad structure in which the liquid crystal due to their anisotropy allows to change the boundary condition by electric field or temperature [2]. In this research, the three types of liquid crystal cells were under investigation: orthogonal, parallel, and twist. They were differed by rubbing direction of the electrodes in the relation to the fiber axis which determine the initial molecule arrangement inside the cell with taper. For measurement, two kinds of thin metal gold and silver were applied [2,3].

The reason for chosen gold and silver materials were their permittivity parameters like a complex dielectric constant of $\varepsilon = \varepsilon_r + i\varepsilon_i$ and especially connected to the $\varepsilon_r/\varepsilon_i$ ratio which is related with the resonant dip of SPR effect. All measurements were performed at room temperature for different steering voltage U=0-200V, with and without amplitude modulation. In a wide range. As a result, the resonant peaks were obtained, which depend on the liquid crystal cell type, and steering voltage as well. During the measurements, resonant peaks have obtained the position of which can be controlled by the type of liquid crystal cells and the steering voltage, as well. It is possible to modify the light beam propagation properties at the resonant area, which proves the dynamic response visible in the whole spectrum.

Acknowledgments: This work was financed by the Military University of Technology under research project UGB – 888.

References:

[1] B. D. Gupta et al. *Sensors 16*, 1381 (2016).

[2] J. Korec et al. Materials 13(21), 4942 (2020).

[3] J. Korec et al. Molecules, 26, 7553, (2021)

Reduction of nonlinearities by nanodiamond incorporation into glass

G. STĘPNIEWSKI[1,2], M. KLIMCZAK[1], T. KARPATE[1], M. FICEK[3], M. GŁOWACKI[3], A. HEIDT[4], R. BOGDANOWICZ[3], R. BUCZYŃSKI[1,2]

[1] University of Warsaw, Faculty of Physics, Pasteura 5, 02-093, Warsaw, Poland
[2] Łukasiewicz Research Network, Institute of Microelectronics and Photonics, Al. Lotników 32/46, 02-668, Warsaw, Poland
[3] Gdańsk University of Technology, Faculty of Electronics, Telecommunications and Informatics, Narutowicza 11/12, 80-233, Gdańsk, Poland
[4] University of Bern, Institute of Applied Physics, , Sidlerstrasse 5, 3012, Bern, Switzerland
e-mail address: grzegorz.stepniewski@fuw.edu.pl

Nanodiamond (ND) is the allotropic form of carbon in which the atoms are networked through in a tetrahedral crystalline lattice. It is a very interesting material due to the possibility of functionalization by attaching numerous functional groups to its surface, thus changing its electronic and optical properties. An improvement in efficient and controllable fabrication techniques has made possible to apply ND particles as a sensing platform in biology, medicine and physics. One of the most interesting and surprising features of ND is the nonlinear optical response, which is different than in crystalline bulk diamond. For the bulk diamond the nonlinear index of refraction n_2 has been well investigated and its value is positive and varies in the range $n_2 = 4 – 17 \times 10^{-20}$ m^2/W [1]. Whereas the study of nonlinearities in 1 μm thick nanocrystalline diamond membrane shows the negative $n_2 = –2 \times 10^{−17}$ m^2/W at the wavelength of 580 nm [2]. The same behavior was observed in water suspension of detonation nanodiamonds (DND) with particle size of 5-10 nm [3]. The measured value was also negative and equals to $n_2 = −6.0 \times 10^{−19}$ m^2/W.

Negative n_2 of NDs gives the opportunity to shape the nonlinearities of new optical materials containing NDs incorporated into a host matrix. For example optical fibers with NDs in the core would have less nonlinearity, which is very desirable during ultrafast pulses propagation.

We report our results on the study of the influence of NDs on the nonlinear refractive index of water and glass samples with NDs in the volume of the material. Our investigations based on the Z-scan methodology proposed by Sheik-Bahae [5]. The high quality beam ($M^2 < 1.2$) from a femtosecond fiber laser (Fluence Jasper, 1030 nm, 1 kHz, 300 fs) was focused with 200 mm focal length lens on the sample placed on the motorized linear stage (25 mm travel distance). In order to obtain the n_2 we performed the measurement in the closed aperture configuration (variable iris was placed before the power meter), where the normalized transmittance is recording during the sample movement along the *z* axis, near the focus of the lens. As the initial step we check the system accuracy by measuring the self-focusing in the reference sample of fused silica (2 mm thick). We obtained $n_2 = 2.1 – 2.3 \times 10^{-20}$ m^2/W, which is in very good agreement with literature.

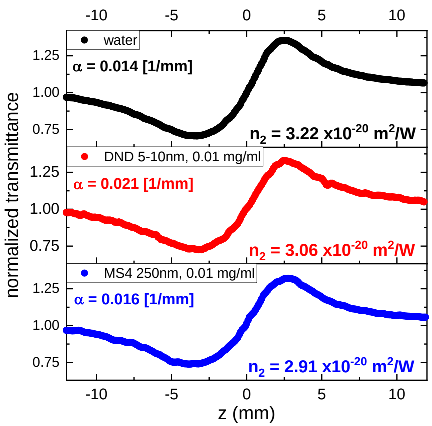

Fig. 1. Z-scan close aperture traces obtained for distilled water (black), water with 5-10 nm ND (red) and for water with 250 nm ND (blue).

To verify negative n_2 of NDs, we prepared two samples of different particle sizes (5-10 nm and 250 nm) suspended in pure water. Both samples have the same concentration of 0.01 mg/ml and were examined in 5 mm thick quartz cuvette. Z-scan normalized transmission traces for pure water and for water with NDs is shown in Fig. 1. For both ND's solutions nonlinear refractive index was lower than for pure water, which suggests negative n_2 of NDs (negative contribution to the total n_2 of the ND suspension).

Similar reduction of n_2 has been observed in the NDs incorporated into glass samples during high power laser vitrification process. In this investigation we compared two 1 mm thick samples flat-parallel polished glass with NDs embedded in the volume. The result of Z-scan measurement is shown in Fig. 2. The ND-functionalized glass has about 7.5% lower nonlinear index of refraction in comparison to pure reference samples.

Our study confirms that NDs incorporated into the glass can reduce optical nonlinearities of the material.

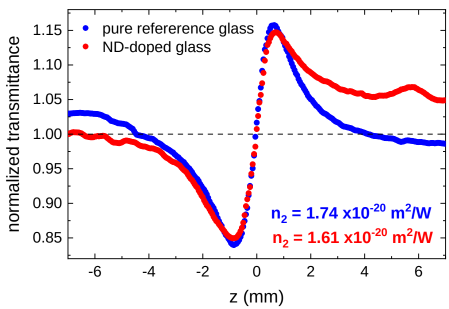

Fig. 2. Closed aperture Z-scan traces recorded for 1 mm thick samples of pure and ND-functionalized glass.

Acknowledgments: This work was supported by Foundation for Polish Science (TEAM NET POIR.04.04.00-00-1644/18)

References:

[1] J.M.P. Almeida et. al., Scientific Reports 7, 14320, (2017)

[2] F. Trojánek et. al., Optics Express 18, 2, (2010)

[3] O. Muller et. al., Scientific Reports 9, 519, (2019)

[4] P. Zao et. al., Optica 5, 5, (2018)

[5] M. Sheik-Bahae et. al., IEEE J. Quantum Electron. 26, (1990)

Integrated photonics structure for sensor applications.

P. STRUK[1]

[1]Department of Optoelectronics, Faculty of Electrical Engineering, Silesian University of Technology, 2 Krzywoustego Str., 44-100 Gliwice, Poland.
e-mail address: Przemyslaw.Struk@polsl.pl

The Author presents concept of sensor structure designed for measurement the blood properties such as hemoglobin concentration and oxidation level. The presented sensor structure is built based on integrated optics circuit which including: input circuit for light based on prism coupler and sensor part with planar waveguide and grating coupler. The principle of operation of presented structure is based on two phenomena: first - evanescence field of propagated waveguide mode in waveguide part of the sensor structure (determination of oxidation level), second: sensing properties of grating coupler, which is used for determination of hemoglobin concentration. In addition the grating coupler pays a role as a output circuit for the light beam. The presented experimental results are focused of numerical optimization of selected geometrical properties of the sensor structure for optimization of sensor efficiency and sensing properties.

References:

[1] P. Struk, Materials, Vol. 12(1), 175, 1-12, 2019.
[2] P. Struk, Photonics Letters Of Poland, Vol. 12 (2), 37-39, 2020.
[3] P.V. Lambeck, Measurement Science and Technology, vol. 17, R93–R116, 2006.

ZnO thin films prepared by sol-gel method and dip-coating technique - optical properties

K. WOJTASIK[1,2], M. ZIĘBA[1], C. TYSZKIEWICZ[1], P. KARASIŃSKI[1]

[1]Silesian University of Technology, Department of Optoelectronics, ul. Krzywoustego 2, 44-100 Gliwice, Poland
[2]Cracow University of Technology, Department of Physics, ul. Podchorążych 1, 30-084 Kraków, Poland
e-mail address: katarzyna.wojtasik@polsl.pl; katarzyna.wojtasik@pk.edu.pl

Zinc oxide (ZnO) is a non-toxic substance with a wide range of applications [1]. It is a transparent, semiconductor oxide of groups II - IV, with a wide energy band gap *Eg* = 3.37 eV at room temperature and high exciton binding energy, about 60 meV [2]. Additionally, it exhibits good chemical and thermal stability. Due to these properties in the form of thin films, it is a attractive for wide application including optoelectronics [3], chemical sensors [4] or as protective coatings for surfaces [5]. ZnO plays an important role in photovoltaic devices, for example in dye-sensitized solar cells (DSSC) [6] or as a transparent conductive electrodes [7].

Many methods of producing ZnO thin films are known. They mainly belong to them atomic layer deposition (ALD) [8], sputtering [9], spray pyrolysis [4] and sol-gel [10]. Depending on the synthetic approach, the obtained ZnO layers differ in morphology and properties, which can be adapted to potential applications [11].

The sol-gel is a chemical method of produced material from a liquid phase. It is characterized by many advantages, including: purity and homogeneity of the material on a nanometric scale, repeatability, high process efficiency and the possibility of shaping the structure at the synthesis stage. The sol-gel is a multi-step method in which the main reactions are hydrolysis and condensation and the end product is sol. The processes progress over time, which is reflected in the properties of the produced layers. Fig. 1 shows a schematic view of the sol-gel method.

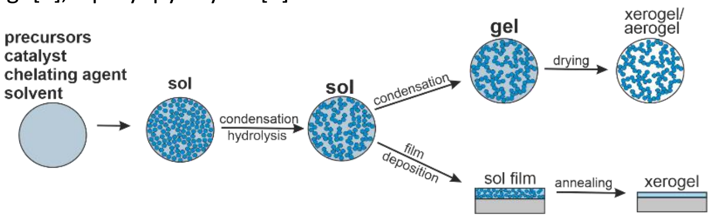

Fig. 1. Scheme of sol-gel method

The sol can be applied to surfaces in a number of ways to obtain thin layers. In laboratory conditions, the most popular are spin-coating and dip-coating method. The dip-coating method (Fig. 2) is characterized by better thickness uniformity and better control of this parameter. The thickness of the layer depends on the speed at which the substrate emerges from the sol. After applying the sol layers on the substrate, the structures are subjected to an annealing process, as a result of which the solvents are evaporated, the material is compacted and the final layer thickness is determined.

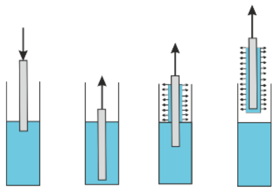

Fig. 2. Scheme of dip-coating method, (a) immersion of the substrate, (b) starting the ascent of the ground, (c) continuing ascent and beginning to evaporate, (d) evaporate

In our technological research, the ZnO precursor used is zinc (II) acetate, the homogenizing agent is ethyl alcohol and the chelating compound - diethanolamine.

In our presentation, we present preliminary studies of the influence of sol aging on the optical properties of ZnO thin layers produced by the sol-gel and dip-coating technique. We present the dependences of the final thicknesses *d* and the refractive indexes *n* of ZnO films on the withdrawal speed v (in the range of 3.23 - 6.61 cm/min) for 2, 26 and 63 days of sol aging. We will also show the effect of sol aging on the transmittance and reflectance of layers in the range of 250 - 1000 nm and on the surface morphology of the produced films (AFM). The layers were applied to soda-lime microscope slides (Menzel Glaser, Thermo Scientific).

The presented results show the attractiveness of the sol-gel method for the production of ZnO thin films.

Acknowledgments: This work was supported by the TEAM-NET project: Hybrid sensor platforms of integrated photonic systems based on ceramic and polymer materials (HYPHa)" from the Foundation for Polish Science. Project no: POIR.04.04.00-00-14D6/18.

References:

[1] O'Brien, S.et al., Thin Solid Films 518 (16), 4515–4519, (2010)
[2] Klingshirn, C., Phys. Status Solidi 71 (2), 547–556, (1975)
[3] Malik, G. et al., Mater. Sci. Semicond. Process. 100, 200–213, (2019)
[4] Yergaliuly, G. et al., Sci. Rep. 12 (1), (2022)
[5] Ennaceri, H. et al., Surf. Coatings Technol. 298, 103–113, (2016)
[6] Jiang, C. Y. et al., Appl. Phys. Lett. 90 (26), 263501, (2007)
[7] Tiwari, A. and Sahay, P. P., Phys. B Condens. Matter 629 (2022)
[8] Szindler, M. et al., Coatings 11 (9), 1–13, (2021)
[9] Kaim, P.et al., Coatings 11 (12), (2021)
[10] Amakali, T. et al., Crystals 10 (2), 132, (2020)
[11] Laurenti, M. and Cauda, V., Coatings 8 (2), 67, (2018)

Time-resolved spectroscopy of nitrogen implanted GaAs

G. WRZESINSKI[1], K. SWITKOWSKI[1]

[1]Faculty of Physics, Warsaw University of Technology, Koszykowa 75, 00-662 Warsaw, Poland
e-mail address: krzysztof.switkowski@pw.edu.pl

The short carrier lifetime semiconductors are crucial for ultrafast optoelectronic devices such as THz photoconductive switches for generation and detection of coherent THz radiation, saturable absorbers for laser mode-locking, and ultrafast photodetectors, to name a few. Low temperature grown (LTG) in Molecular-beam epitaxy (MBE) GaAs is the well-known material used for such devices. We propose an alternative to the MBE method of structural modification of bulk GaAs crystals. The proceeded modification aimed at creation of high-density defects, enabling fast non-radiative relaxation of the photo-carriers through the intentional defect states. The additional, significant, and desirable parameter in the aforementioned THz applications is high dark resistivity of the defected material. To meet this requirement, we proposed the implantation of semi-insulating GaAs by an isoelectronic dopant.

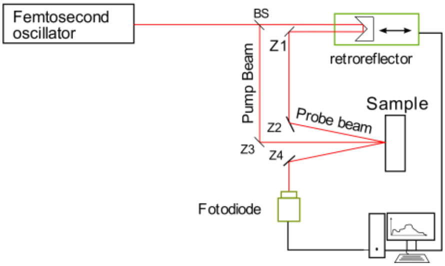

Fig. 1. Scheme of pump and probe method

Nitrogen. Here we present picosecond photo-generated carrier lifetimes in N+ implanted GaAs measured using time-resolved spectroscopy – femtosecond pump and probe method depicted in Fig 1.

Three samples were implanted with high ion kinetic energy (800 keV), with ion doses: 5 × 10^{10}, 1 × 10^{11}, and 5 × 10^{11} ions/cm^2. The measured carrier lifetimes are in the picosecond and sub-picosecond range, which is a requirement to obtain emission spectrum at the THz frequency range. The Nitrogen implantation is a new possibility of obtaining ultrafast carrier lifetimes in GaAs, which could be used for THz photoconductive emitters, detectors, ultrafast photodetectors, and saturable absorbers.

References:

[1] K. Świtkowski et. al., Photonics Letters of Poland 4,1 (2012).

[2] C. Schmuttenmaer et. al., Physical Review B 62, 23 (2000).

Optical properties of erbium-doped TiO_2 films

M. ZIĘBA, K. WOJTASIK, C. TYSZKIEWICZ, P. KARASIŃSKI

Silesian University of Technology, Department of Optoelectronics, ul. Krzywoustego 2, 44-100 Gliwice, Poland

e-mail address: magdalena.zieba@polsl.pl

Lanthanide (Ln^{3+}) doped semiconductors have interesting spectroscopic properties which make them suitable for use in various fields such as electronics, optoelectronics, photonics, displays, optical amplifier, lasers, fluorescent sensing, including medical diagnostics [1,2].

Lanthanide ions show a weakly fluorescent because of the parity forbidden f-f transitions. Therefore to excite the (Ln^{3+}) ions efficiently in a wide spectral range, it is crucial to select an appropriate host material. Various materials such as metal oxides (ZnO, SiO_2, TiO_2, Al_2O_3, Y_2O_3), barium zirconate ($BaZrO_3$) or gallium nitride (GaN) have been investigated as a host material. Titani oxide (TiO_2) has been excellent host material due to its relatively large bandgap (3.2 eV for anatase), chemical and biological inertness, and good thermal, physical, and chemical stability. Furthermore, it has a high refractive index and good transparency in the VIR-NIR spectal range [3]. The presentation presents preliminary results of erbium-doped TiO_2 films. Erbium (Er^{3+}) was chosen as TiO_2 dopant because of favorable electronic configuration with long lifetime excited states, luminescence in the UV-Vis specral range, and inhibition of the increase in crystallite size [4].

Lanthanide doped films can be produced using physical vapor deposition (PVD) or chemical methods, including chemial vapor deposition (CVD) and sol-gel method [5]. The sol-gel is a versatile method of producing materials from a liquid phase that ensures high purity and homogeneity of materials in the nanoscale (Fig. 1).

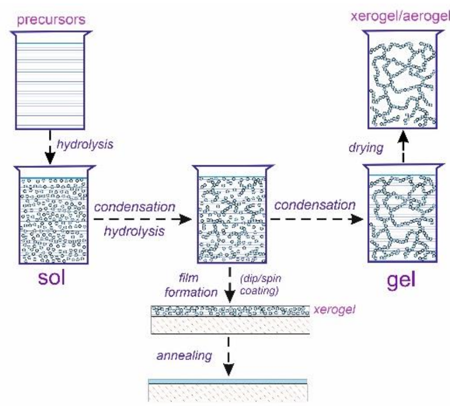

Fig. 1. Scheme of production of thin films *via* sol-gel method.

The sol-gel method has several advantages such as 1) the ability to control the structure of the produced material in a wide range, 2) does not require expensive technological installations, 3) the technological processes are low-temperature, 4) environmentally neutral, 5) the possibility of producing multi-component materials with homogeneity at the molecular level 6) the possibility of shaping physicochemical properties by introducing admixtures.

In typical process, sol is formed from the hydrolysis and polymerization reactions of the precursors, which are usually metal alkoxides or inorganic metal salts. At some point in the formation of the sol, it is suitable for the production of film. Thin films can be applied with different techniques [6]. In our research, we use dip-coating technique to obtained the films into glass substrate [Fig.2].

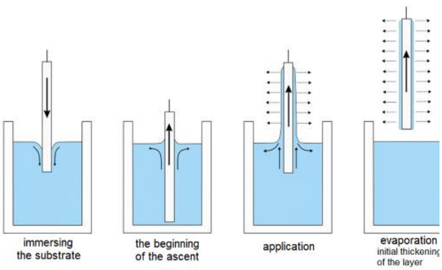

Fig.2. Stages in the dip-coating technique.

Our presentation will show the application of the sol-gel method and dip-coating technique for the fabrication of erbium-doped titania films. In particular, will be presented relationships between a withdrawal speed and film parameters: their thickness and refractive index. The optical properties of erbium-doped silica-titania films will be investigated with aid of UV-Vis spectrophotometry.

Acknowledgments: This research was funded by the TEAM-NET project: "Hybrid sensor platforms of integrated photonic systems based on ceramic and polymer materials (HYPHa)" from the Foundation for Polish Science. Project no: POIR.04.04.00-00-14D6 /18.

References:

[1] M. Pal et. al., Nanoscale Research Letters 7:1 (2012).

[2] J.A. Perez et.al., Vacuum 169, 108873 (2019).

[3] X. Chen et.al., Chem. Rev. 107, 2891-2959 (2007).

[4] S.Obregón et.al. Journal of Catalysis, 299, 298-306 (2013).

[5] J.D.B. Bradley et.al. Laser Photonics Rev 5,3, 368-403 (2011).

[6] P. Karasiński. Prz. Elektrotechniczn. 95, 9 (2019).

Table of contents